

The Dissertation Committee for Syed Ali Certifies that this is the approved version of the following
**Targeting protein: protein interaction sites for drug development against voltage-gated sodium
channels**

Committee:

Fernanda Laezza, MD/PhD

B. Montgomery Pettitt, PhD

Jia Zhou, PhD

Filippo Tempia, MD, PhD

Svetla Stoilova-McPhie, PhD

David Niesel, Ph.D.

Dean, Graduate School

**Targeting protein: protein interaction sites for drug development against voltage-gated sodium
channels**

By

Syed Ali, B.A.

Department of Pharmacology and Toxicology,
University of Texas Medical Branch, Galveston, Texas

Dissertation

Presented to the Faculty of Graduate School of
The University of Texas Medical Branch

In Fulfillment of the Requirements

For the Degree of

Doctor of Philosophy

Approved by the Supervisory Committee

Fernanda Laezza, MD, PhD

B. Montgomery Pettitt, PhD

Jia Zhou, PhD

Filippo Tempia, MD, PhD

Svetla Stoilova-McPhie, PhD

June, 2015

Galveston, Texas

© Copyright by Syed Ali, 2016

All Rights Reserved

Key Words: Voltage-Gated Sodium Channels, Hot-Spots, Short Peptides, Peptidomimetics,
electrophysiology, Luciferase assay, Drug Discovery, Fibroblast Growth Factor 14, FGF14,
Protein:Protein Interaction

DEDICATION

This dissertation is dedicated to my parents, Syed Mansur Ali and Hasina Begum, for their continuous encouragement and support.

ACKNOWLEDGEMENTS

I would like to express my deepest thanks and gratitude to my mentor, Dr. Fernanda Laezza, who constantly supports, encourages, and pushes me to confront new challenges. For the last four years, Dr. Laezza gave me constructive feedbacks and shared her wisdom to improve my research skills. Dr. Laezza has inspired me to look forward to the bigger picture of my research. She not only encourages to do experiments, but she also inspires to think critically. Thank you, Dr. Laezza, for your outstanding mentorship.

I also like to thank Ms. Penny Welsh (retired Pharmacology & Toxicology Student Coordinator). She always supported me during my difficult times. Thank you, Ms. Welsh, for being a great friend to me.

I would like to thank Dr. Kenneth Johnson, the director of the Pharmacology & Toxicology graduate program, who played a critical role to select my lab rotation. In my second year, he sent out emails to the pharmacology & toxicology faculty members to consider me for their labs.

I would like to extend my personal gratitude to present and past lab members, including Drs. Alexander Shavkunov, Neli I. Panova-Elektronova, and Miroslav Nenov, for sharing their knowledge and skills with me.

I also like to acknowledge Mr. Thomas James (Neuroscience Department) and Mardelle Susman (Microbiology & Immunology Department) for editing a number of my manuscripts and my dissertation proposal.

I also like to thank my committee members, Drs. B. Montgomery Pettitt, Jia Zhou, Filippo Tempia, Svetla Stoilova-McPhie, for their valuable feedback in my projects.

I also like to acknowledge our collaborators Dr. Svetla Stoilova-McPhie for her contribution in designing peptide sequences and Dr. Zhiqing Liu from Dr. Zhou's lab for her contribution in synthesizing peptidomimetics respectively.

Last but not least, I would like to thank my parents and my wife for their unconditional support to achieve my goal.

TABLE OF CONTENTS

COMMITTEE.....	I
LIST OF FIGURES.....	viii
LIST OF TABLES.....	x
ABBREVIATIONS.....	xi
ABSTRACT.....	1
CENTRAL HYPOTHESIS AND SPECIFIC AIMS.....	12

CHAPTER 1

Background

<i>Structure and Function Of Voltage-Gated Sodium Channels.....</i>	<i>2</i>
<i>Neurons.....</i>	<i>3</i>
<i>Action Potential.....</i>	<i>4</i>
<i>Depolarization:.....</i>	<i>4</i>
<i>Repolarization</i>	<i>4</i>
<i>Whole-Cell Patch-Clamp Electrophysiology.....</i>	<i>4</i>
<i>Subtypes of Voltage-Gated Sodium Channels.....</i>	<i>4</i>
<i>Relevance of Voltage-Gated Sodium Channels in the Incidence of Brain Disorders.....</i>	<i>6</i>
<i>Current Need to Develop Isoform-Specific Nav Channel Drugs.....</i>	<i>7</i>
<i>Nav1.6 Channels as an Emerging Target for Developing Selective Therapies.....</i>	<i>8</i>
<i>Fibroblast Growth Factor 14 (FGF14) is an Accessory Protein of Nav1.6 Channels.....</i>	<i>9</i>
<i>Targeting the FGF14:Nav1.6 Channel Complex Interaction Sites as a New Strategy For</i>	
<i>Drug Development Against Nav1.6 Channels.....</i>	<i>10</i>

CHAPTER 2

General Experimental Procedures

<i>Materials</i>	14
<i>DNA Construct Preparation</i>	14
<i>Molecular Modeling (for chapter 3)</i>	14
<i>Molecular Modeling (for chapter 4)</i>	15
<i>Peptide Synthesis and Delivery (for chapter 4)</i>	16
<i>Immunoprecipitations</i>	16
<i>Cell Culture and Transient Transfections</i>	17
<i>Split-luciferase Complementation Assay (LCA)</i>	17
<i>Western Blot</i>	18
<i>LCA Data Analysis</i>	18
<i>Protein Over-expression and Purification</i>	19
<i>Intrinsic Fluorescence Spectroscopy</i>	20
<i>Surface Plasmon Resonance Spectroscopy</i>	20
<i>In silico Docking of ZL181</i>	20
<i>In Vitro Electrophysiology Experiments and Data analysis</i>	21
<i>Ex Vivo Electrophysiology Experiments and Data analysis</i>	22

CHAPTER 3

Identification of Amino Acid Residues in the Fibroblast Growth Factor 14 (FGF14) Required For Structure-Function interactions with the Voltage-Gated Sodium Channel Nav1.6

<i>Abstract</i>	26
<i>Keywords</i>	26
<i>Introduction</i>	27
<i>Results</i>	30
<i>Discussion</i>	56

CHAPTER 4

Modulation of the FGF14:FGF14 Homodimer Interaction Through Short Peptide Fragments

<i>Abstract</i>	62
<i>Keywords</i>	62
<i>Introduction</i>	63
<i>Results:</i>	65
<i>Discussion</i>	80

CHAPTER 5

Modulation of the FGF14:Nav1.6 channel interaction through a short peptidomimetic fragment

<i>Abstract</i>	84
<i>Significance</i>	84
<i>Introduction</i>	84
<i>Results:</i>	87
<i>Discussion</i>	95
<i>Supplementary Material</i>	98

CHAPTER 6

<i>Conclusion</i>	103
<i>Future Directions</i>	105

BIBLIOGRAPHY	106
---------------------------	-----

VITA	119
-------------------	-----

LIST OF FIGURES

Figure 1.1: Schematic representation of voltage-gated sodium channel.....	2
Figure 1.2: Voltage-gated sodium channel has three different states.....	3
Figure 1.3: Schematic representation of a neuron.....	3
Figure 1.4: Graphical representation of action potentials.....	4
Figure 1.5: Amino acid sequence similarity and phylogenetic relationships of voltage-gated sodium channel α subunits.....	6
Figure 1.6: Mutations in Nav1.6 channels are linked to a number of brain disorders.....	8
Figure 1.7: Voltage-gated Sodium channels as macromolecular complexes.....	10
Figure 3.1: Homology model-based predicted hot-spots at the PPI interface of FGF14:Nav1.6 and FGF14:FGF14 dimer complex.....	31
Figure 3.2: In-cell LCA characterization of hot-spots at the FGF14:Nav1.6 channel and the FGF14:FGF14 dimer interface.....	35
Figure 3.3: Protein production quantification from Western blots.....	36
Figure 3.4: Differential role of Y158 and V160 at the FGF14:Nav1.6 channel and the FGF14:FGF14 dimer interface assessed by alanine scanning mutagenesis and in-cell LCA.....	39
Figure 3.5: Protein production quantification from Western blots for FGF14 ^{Y158A} , FGF14 ^{V160A} and FGF14 ^{Y158A/V160A}	40
Figure 3.6: Assessing the role of K74 and I76 at the FGF14:Nav1.6 channel and the FGF14:FGF14 dimer interface by alanine scanning mutagenesis by in-cell LCA.....	43
Figure 3.7: Protein production quantification from Western blots for FGF14 ^{K74A} , FGF14 ^{I76A} and FGF14 ^{K74A/I76A}	45
Figure 3.8: The FGF14 ^{V160} residue is required for modulation of Nav1.6 currents.....	47
Figure 3.9: The V160A mutation abolishes FGF14-dependent modulation of biophysical properties of Nav1.6 currents	49

Figure 3.10: Functional validation of K74 and I76 in modulating Nav1.6 currents.....	51
Figure 3.11: Role of K74 and I76 in modulating biophysical properties of Nav1.6 currents.....	53
Figure 3.12: Intrinsic fluorescence emission spectra reveal reduced assembly of FGF14 ^{K74A/I76A} and FGF14 ^{V160A} to Nav1.6 C-tail.....	55
Figure 4.1: In-cell reconstitution of the FGF14:FGF14 homodimer complex using the split-luciferase complementation assay (LCA).....	66
Figure 4.2: Model of the FGF14 homodimer.....	68
Figure 4.3: Peptide mapping on the FGF14 surface.....	69
Figure 4.4: Effect of FGF14 model-based peptides on the FGF14:FGF14 homodimer assembly.....	71
Figure 4.5: Y158N/V160N mutations modify the FGF14:FGF14 homodimer formation.....	74
Figure 4.6: Model of FGF14 ^{Y158N/V160N} hetero- and homodimer.....	76
Figure 4.7: The Y158N and V160N mutations prevent activity of FLPK.....	78
Figure 4.8: FLPK peptide aligns to the FGF14 monomer interface.....	79
Figure 5.1: Validation of peptidomimetics against the FGF14:Nav1.6 complex.....	90
Figure 5.2: ZL181 modulates Nav1.6 channels alone and works synergistically with FGF14 to further modulate Nav1.6 channels.....	92
Figure 5.3: The effect of ZL181 on neuronal firing in medium spiny neurons of nucleus accumbens.....	94
Supplemental Figure S 5.1: Pharmacological inhibition of ZL181 modulates the functional properties of Nav1.1 channels by FGF14.....	98
Supplemental Figure S 5.2: Pharmacological inhibition of ZL181 modulates the functional properties of Nav1.2 channels by FGF14.....	99

LIST OF TABLES

Table 1.1: Mammalian voltage-gated sodium channel α Subunits.....	5
Table 1.2: Specific mutations in Nav channels are linked to neurological, developmental and psychiatric brain disorders.....	7
Table 3.1: Homology model-based hot-spots at the FGF14:Nav1.6 complex and the FGF14:FGF14 dimer PPI interface.....	32
Table 3.2: Impact of Y158 and V160 at the FGF14:Nav1.6 and the FGF14:FGF14 dimer interface.....	38
Table 3.3: Impact of K74 and I76 at the FGF14:Nav1.6 and the FGF14:FGF14 dimer interface.....	44
Table 3.4: Nav1.6-mediated currents in the presence of FGF14 and V160 and Y158 mutants.....	48
Table 3.5: Nav1.6-mediated currents in the presence of FGF14 and K74 and I76 mutants.....	52
Table Supplemental 5.1: Voltage-gated Na ⁺ currents in HEK-Nav1.6.....	100
Table Supplemental 5.2: Voltage-gated Na ⁺ currents in HEK-Nav1.1.....	100
Table Supplemental 5.3: Voltage-gated Na ⁺ currents in HEK-Nav1.2.....	101
Table Supplemental 5.4: Active and passive properties of medium spiny neurons	101

ABBREVIATION

FGF14	= Fibroblast growth factor 14
Nav channel	= Voltage-gated sodium channel
PPI	= Protein: protein interactions
LCA	= Luciferase complementation assay
PBS	= Phosphate buffer saline
N	= Asparagine
Y	= Tyrosine
A	= Alanine
V	= Valine
K	= Lysine
I	= Isoleucine
Ac-FLPK-NH ₂	= Acetyl-Phenyl alanine-Leucine-Proline-Lysine-Amide
Ac-PLEV-NH ₂	= Acetyl-Proline-Leucine-Glutamic acid-Valine-Amide
Ac-EYYV-NH ₂	= Acetyl-Glutamic acid-Tyrosine- Tyrosine-Valine-Amide
HEK293	= Human embryonic kidney 293 cells
SD	= Standard Deviation
SEM	= Standard Error Mean
SP	= Small Peptide
CNS	= Central Nervous System
PNS	= Peripheral Nervous System

COMMITTEE

Fernanda Laezza, M.D., Ph.D., Associate Professor, Department of Pharmacology and Toxicology,
University of Texas Medical Branch at Galveston

Monte Pettitt, Ph.D., Professor, Sealy Center for Structural Biology and Molecular Biophysics,
University of Texas Medical Branch at Galveston

Jia Zhou, Ph.D., Associate Professor, Department of Pharmacology and Toxicology,
University of Texas Medical Branch at Galveston

Svetla Stoilova-McPhie, Ph.D., Assistant Professor, Department of Neuroscience & Cell Biology,
University of Texas Medical Branch at Galveston

Filippo Tempia, M.D., Ph.D., Professor, Department of Neuroscience,
University of Turin, Italy

ABSTRACT

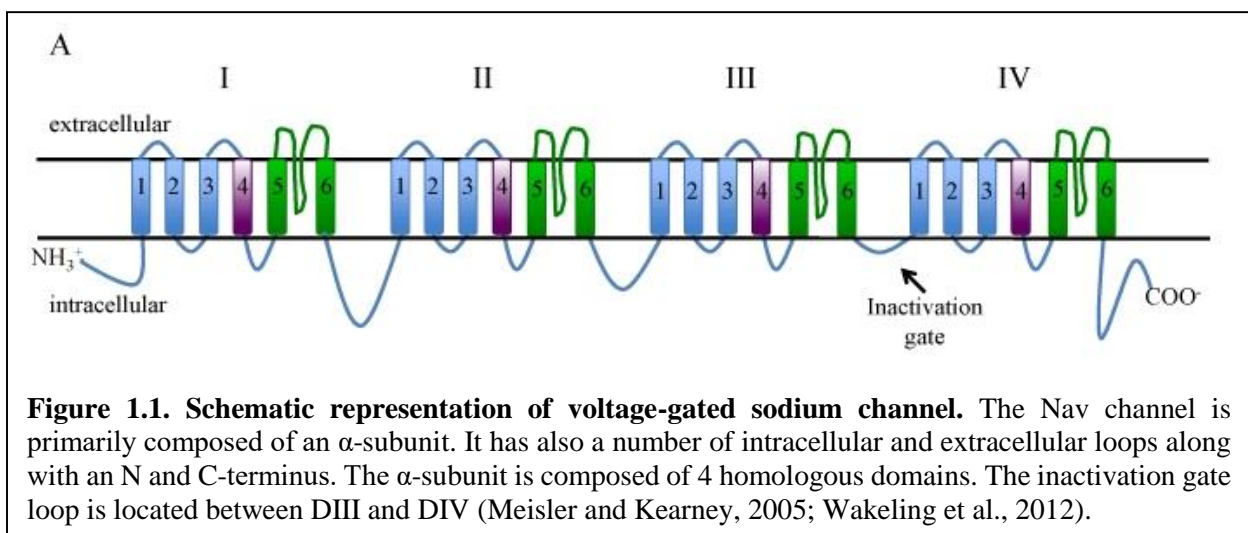
Voltage-gated sodium (Nav) channels are responsible for initiation and propagation of action potentials, which contribute to control of neuronal excitability. Malfunction of specific Nav channel isoforms is associated with a wide range of brain disorders including psychological, neurological and developmental disorders. Unfortunately, currently available drugs targeting Nav channels are directed against highly conserved domains of the α -subunit of all Nav channels, and as such they have severe side effects, including cardiac malfunction. Fortunately, the macromolecular complex of Nav channels is a source of less conserved protein-protein interaction (PPI) interfaces that represent a novel opportunity for designing isoform-specific chemical leads targeting Nav channels. The macromolecular complex of Nav channels is regulated by a number of accessory proteins. Very few proteins regulate the functional properties of Nav channels as potently as the intracellular fibroblast growth factor 14 (FGF14). FGF14 is a biologically relevant accessory protein of the neuronal Nav channel complex controlling gating, stability, and trafficking of native Nav channels. Through a monomeric interaction with the intracellular C-terminal tail of Nav channel α subunits, FGF14 binds and modulates the activity of Nav channels in an isoform-specific manner. By applying luciferase-based assays, patch clamp electrophysiology, and intrinsic fluorescence studies, we have identified the β 9 loop at the interface of FGF14 as critical for binding to Nav1.6 channels. Based on this information, we have identified a short sequence on FGF14 and designed a peptidomimetic (ZL181) fragment as an effective probe for modulating Nav1.6 channels as measured by luciferase-based assay. This peptidomimetic was further evaluated with purified proteins, *in silico* docking, and whole-cell patch clamp electrophysiology in both *in vitro* and *ex vivo* systems. Overall, our data demonstrated that a novel peptidomimetic (ZL181) can modulate the functional properties of Nav1.6 channels and can suppress neuronal excitability in nucleus accumbens medium spiny neurons. The new knowledge gained from this study might be useful for the treatment of Nav1.6 channel-related brain disorders such as epilepsy, schizophrenia and cognitive disorders.

Chapter 1

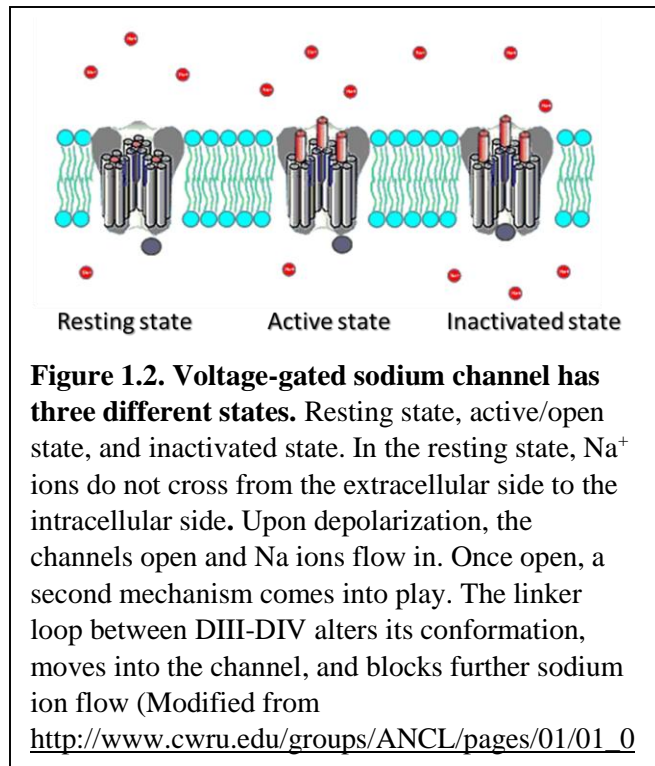
BACKGROUND

Structure and Function of Voltage-Gated Sodium Channels

Voltage-gated sodium (Nav) channels are the primary instigator for generating action potentials in excitable cells. The Nav channel consists of a pore forming α -subunit which is approximately 260 kDa. Although the α -subunit of the Nav channel is sufficient for the function and expression of Nav channels, the kinetics and voltage dependence of channel gating are modified by auxiliary β subunits (22-26 kDa) (Goldin et al., 2000). Nav channels located in the heart and adult central nervous system contain $\beta 1$ - $\beta 4$ subunits, whereas adult skeletal muscles have only $\beta 1$ subunits (Kaplan et al., 2001). Structurally, the α -subunit of the Nav channel is composed of four homologous domains (I-IV), each of which consists of six transmembrane segments (S1-S6) (**Fig. 1.1**). Transmembrane segments S1 to S4 in domain I-IV form voltage sensors which are responsible for channel opening, whereas transmembrane segments S5 to S6 from each of four domains form the central pore which allows Na^+ ions to permeate from the extracellular side to the intracellular side (Bosmans et al., 2008; Chanda and Bezanilla, 2002; Sheets et al., 1999). The



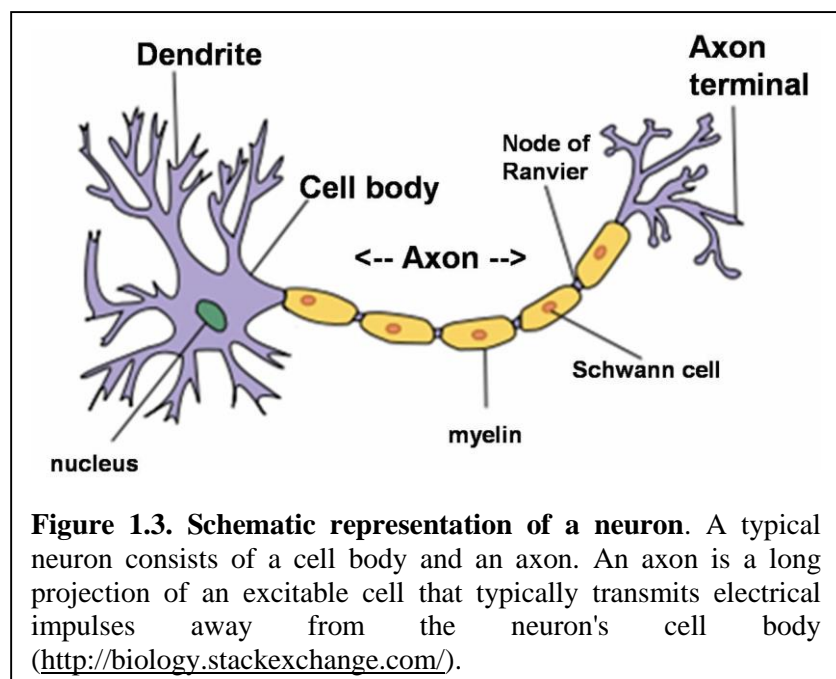
Nav channel has three different states: resting, active, inactivate (**Fig. 1.2**). The voltage-gated Na^+ channels are sensitive to changes in membrane potential through the S4 transmembrane segments. Upon depolarization, the four S4 segment alpha helices translocate toward the outer layer of the lipid bilayer, leading to a series of molecular events that open the channel pore, allowing sodium ions to enter. Once open, a second mechanism comes into play. The linker loop between DIII-DIV alters its conformation, moves into the channel and blocks further sodium ion flow. The linker loop between DIII-DIV alters its conformation, moves into the channel and blocks



further sodium ion flow; this mechanism is known as the inactivated state. Subsequently the channel closes, and repolarization starts.

Neuron

A neuron is an excitable nerve cell which is the basic foundation of the nervous system. The human brain has approximately 100 billion neurons. Neurons are specialized nerve cells that are responsible for communicating information in both chemical and electrical forms. A neuron is primarily



composed of a cell body and an axon (**Fig. 1.3**). Through the axon, action potentials travel down the axon in one direction only to the axon terminal where the signal is transferred to other neurons.

Action Potential:

An action potential is a short- lasting alteration of the membrane potential in an excitable cell generated by the activity of voltage-gated ion channels embedded in the membrane (**Fig. 1.4**).

Depolarization

Stimulus causes voltage-gated sodium channels to open and sodium ions rush into the cell. The cell becomes positive on the inside and negative on the outside.

Repolarization

When the cell becomes positive on the inside and negative on the outside, the sodium channel closes very quickly, while voltage-gated potassium channels open, allowing potassium ions to flow out rapidly. The cell returns to positive on the outside and negative on the inside, and, subsequently, the potassium channels close.

Whole Cell Patch-clamp Electrophysiology

With whole-cell patch-clamp electrophysiology, an electrical connection between the cell interior and a bath solution is established through a recording pipette connected to an amplifier. With this configuration, membrane voltage can be controlled through the amplifier and rapid inward Na^+ currents can be recorded under various stimulatory protocols. This allows us to study absolute ion flux as well as the kinetics of transition among close, open and inactivate states of ion channels.

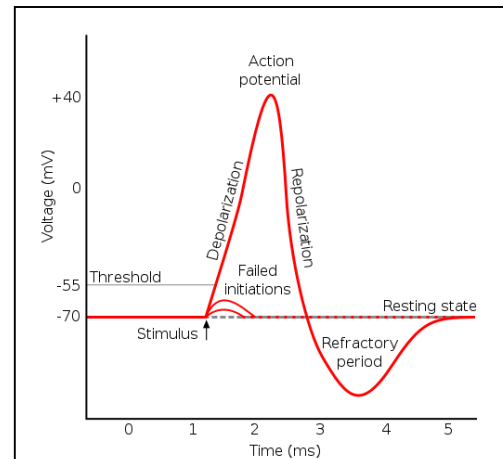


Figure 1.4. Graphical representation of action potentials. Estimated plot of a typical action potential which consists of depolarization (opening of Nav channels), repolarization (gradual closing of Nav channels), and a refractory period (modified from <http://www.innovateus.net>).

Subtype of Voltage-Gated Sodium Channels

There are nine isoforms of voltage-gated sodium channels (Nav1.1-Nav1.9), plus an atypical sodium channel that is designated Nav_x which has a greater than 50% sequence identity to other Nav channels as shown in **Fig.1.5** (Lai and Jan, 2006). The distribution of different isoforms of Nav channels is shown in **Table 1.1**.

Table 1.1. Expression of mammalian voltage-gated sodium channel α subunits (modified from Nomenclature of Voltage-Gated Sodium Channels) (Goldin et al., 2000).

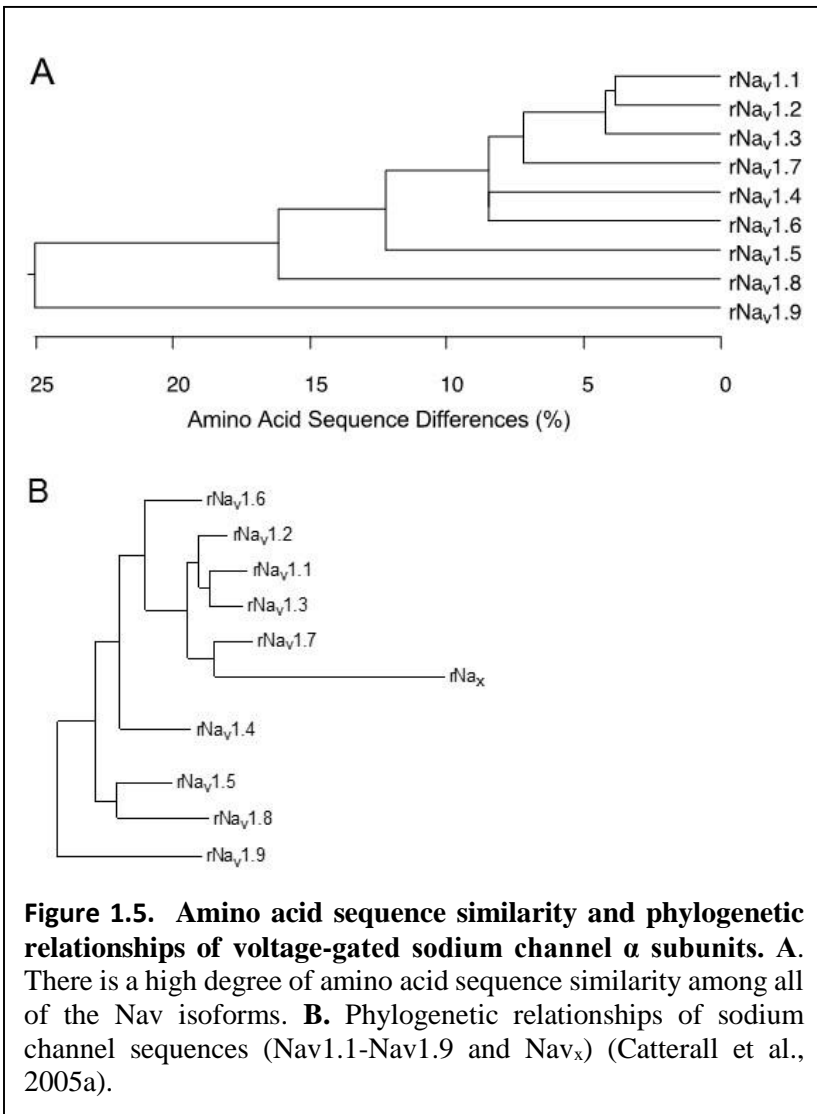
Type	Gene Symbol	Primary Tissues
Nav1.1	SCN1A	CNS, PNS
Nav1.2	SCN2A	CNS
Nav1.3	SCN3A	CNS
Nav1.4	SCN4A	Muscle
Nav1.5	SCN5A	Muscle and heart
Nav1.6	SCN8A	CNS, PNS
Nav1.7	SCN9A	PNS, and Schwann cells
Nav1.8	SCN10A	DRG
Nav1.9	SCN11A	PNS
Nax	SCN7A, SCN6Ab	DRG, heart, and uterus,

There are similarities among all isoforms of Nav channels in terms of amino acid sequence (**Fig. 1.5 A**). According to the phylogenetic tree (**Fig. 1.5 B**), Nav1.1, Nav1.2, Nav1.3, Nav1.6 and Nav1.7 are closely related to each other, and these Nav channels are highly tetrodotoxin (TTX)-sensitive. On the other hand, Nav1.5, Nav1.8, and Nav1.9 are closely related to each other, and they are tetrodotoxin (TTX)-resistant. Amino acid sequence and phylogenetic relationships support the notion that all nine Nav channels have been functionally evolved from a single family of protein.

Besides the nine isoforms of Nav channels, a new sodium channel has been identified and is known as Nav_x. Although this isoform is significantly different from the other Nav channel isoforms in its voltage sensors, inactivation gate, and pore region, it has around 50% similarity to typical Nav channel isoforms in terms of amino acid sequence (Catterall et al., 2005a).

Relevance of Voltage-Gated Sodium Channels in the Incidence of Brain Disorders

A number of neurological and psychiatric disorders is linked to Nav1.1, Nav1.2, and Nav1.6 channels (Chahine et al., 2008; Eijkelkamp et al., 2012). Both gain of function and loss of function of Nav channels due to mutations are related to a number of brain



disorders (**Table 1.2**). For example: Loss of function mutations of Nav1.1 channels can lead to a homeostatic compensatory upregulation of Nav1.6 channels which results in epilepsy (Catterall et al., 2010). Moreover, gain of functions of Nav1.6 channels can lead to epilepsy, and ataxia. Furthermore, multifunction of specific Nav channel isoforms is related to dravet syndrome, congenital insensitivity to pain, primary erythromelalgia, paroxysmal extreme pain disorder, cardiac arrhythmias, brugada Syndrome, and autism (Birch et al., 2004; Catterall et al., 2010; Papale et al., 2010; Savio-Galimberti et al., 2012).

Table 1.2. Specific mutations in Nav channels are linked to a number of neurological, developmental, and psychiatric brain disorders (Catterall et al., 2008; Catterall et al., 2010; Yu and Catterall, 2003).

	Gain of function (+)	Loss of function (-)	Unknown (?)
Epilepsy	Nav1.1 ^{D188V,W1204R,R1648H,I1656M,R1657C,A1685V,M1841T,R1916G} Nav1.6 ^{N1768D,N984K,T1716I}	Nav1.1 ^{R859C,T875M,V1353L,D1866Y} Nav1.6 ^{G1451S}	Nav1.6 ^{R662C,L1331V,R1872Q}
Autism			Nav1.1 ^{R542Q,I1034T,F1038L,T1067A,I1955} Nav1.2 ^{R19K,V755I,R1902L} Nav1.3 ^{G1813S}
Mental retardation/ Cerebellar atrophy		Nav1.6 ^{P1719R}	
Ataxia	Nav1.6 ^{A1327T}		
Migraine		Nav1.1 ^{Q1489K}	
Erythromel algia (pain)	Nav1.7 ^{Q875E} , Nav1.7 ^{V400M}		

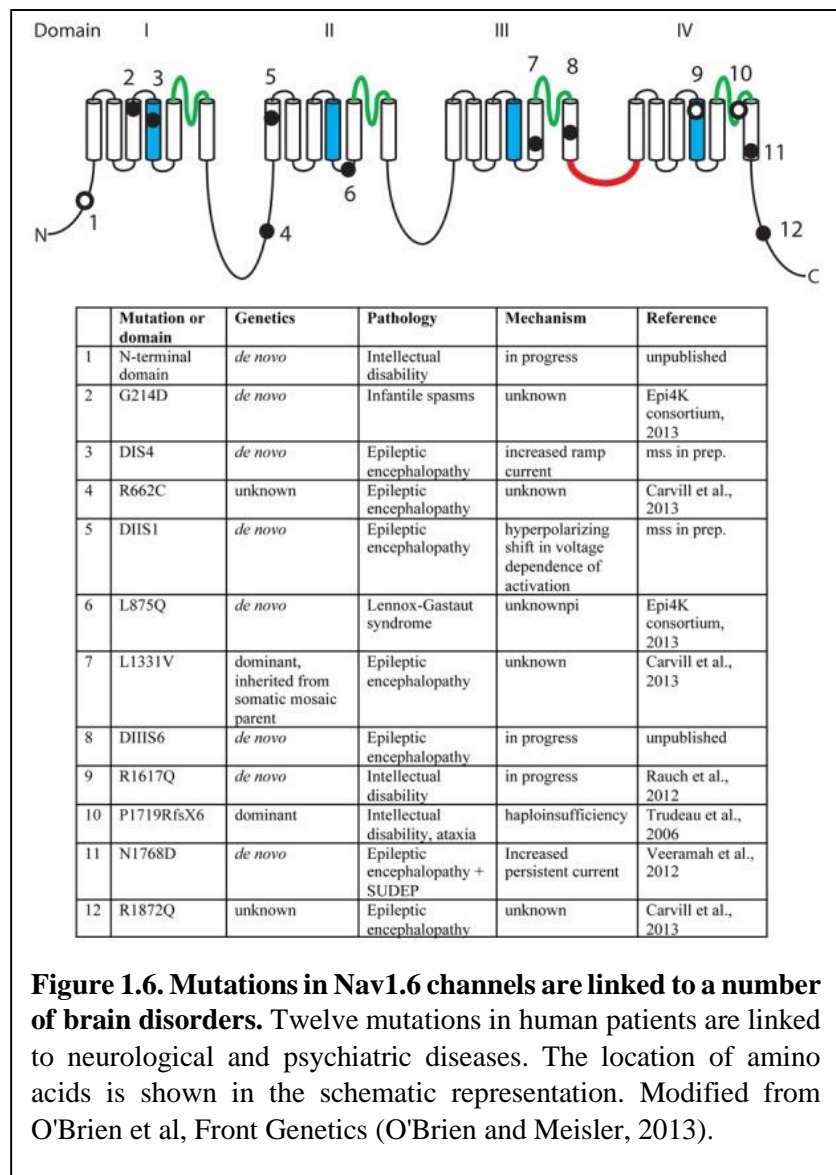
Current Need to Develop Isoform-specific Nav Channel Drugs

Common Nav channel blockers, lidocaine, lamotrigine, carbamazepine, benzocaine, and phenytoin, are used to treat human diseases such as epilepsy or pain (Denac et al., 2000). Two mechanisms have been proposed to explain how these drugs work. In one model, drugs might directly bind to the pore of a channel. In the other model, drugs might access the channel through fenestration pores at the lipid bilayer interface (Yang et al., 2010). In most cases, Nav channel blockers bind to domain IV transmembrane segment 6 and shift the steady-state inactivation toward more negative values (Denac et al., 2000). Since the drug binding site of Nav channels is highly conserved across all Nav channels, all currently available therapeutic drugs

targeting Nav channels lack subtype selectivity. Lack of specificity results in unwanted side effects such as irritability, sleep disturbances, hyperactivity and cardiac malfunction (Bath and Scharfman, 2013). Although there has been some progress in developing isoform specific drugs like molecules targeting Nav1.1, Nav1.2, Nav1.3, Nav1.6, Nav1.7 and Nav1.8 channels (Bagal et al., 2013; Crestey et al., 2015; Rivara et al., 2008; Rivara et al., 2012), there is still a need for more research in this area to develop selective drugs.

Nav1.6 channels as an emerging target for developing selective therapies

Among different isoforms of Nav channels, the Nav1.6 channel is an emerging target due to its critical role in controlling neuronal excitability. These channels are expressed in the cerebral cortex, cerebellar granule cell layer, brainstem, hippocampus, cerebellum, spinal cord, astrocytes, schwann cells, dorsal root ganglion, nodes of ranvier of sensory, motor axons in the peripheral nervous system (PNS), and the central nervous system (CNS). Nav1.6 channels play critical role in generating and transmitting action potentials. Additionally, Nav1.6 has a significant contribution in resurgent current, persistent current, and repetitive neuronal



firing (O'Brien and Meisler, 2013). Both loss of function or gain of function mutations in Nav1.6 channel is related to a malfunction in neuronal excitability in the brain circuitry. In animal models, kindling is associated with higher expression of Nav1.6 sodium channels in hippocampal CA3 neurons (Blumenfeld et al., 2009). Furthermore, mouse *Scn8a* (med) mutants shows dystonia, tremor, movement disorders, pain (Xie et al., 2015), traumatic brain injury, (Mao et al., 2010) and sleep disorder. Additionally, the abnormal expression or function of Nav1.6 channels due to mutations has been linked to epilepsy (G214D, DIS4, R662C, DIIS1, L1331V, L875Q, N1768D, R1872Q) and cognitive disorders (R1617Q, P1719R) (12-15) as shown in **Fig.1.6**. This evidence suggests that the targeting of Nav1.6 channels might contribute significantly to the development of Nav1.6 isoform-specific therapeutic drugs as potential therapies for epilepsy and cognitive brain disorders.

Fibroblast Growth Factor 14 (FGF14) is an Accessory Protein of Nav1.6 Channels

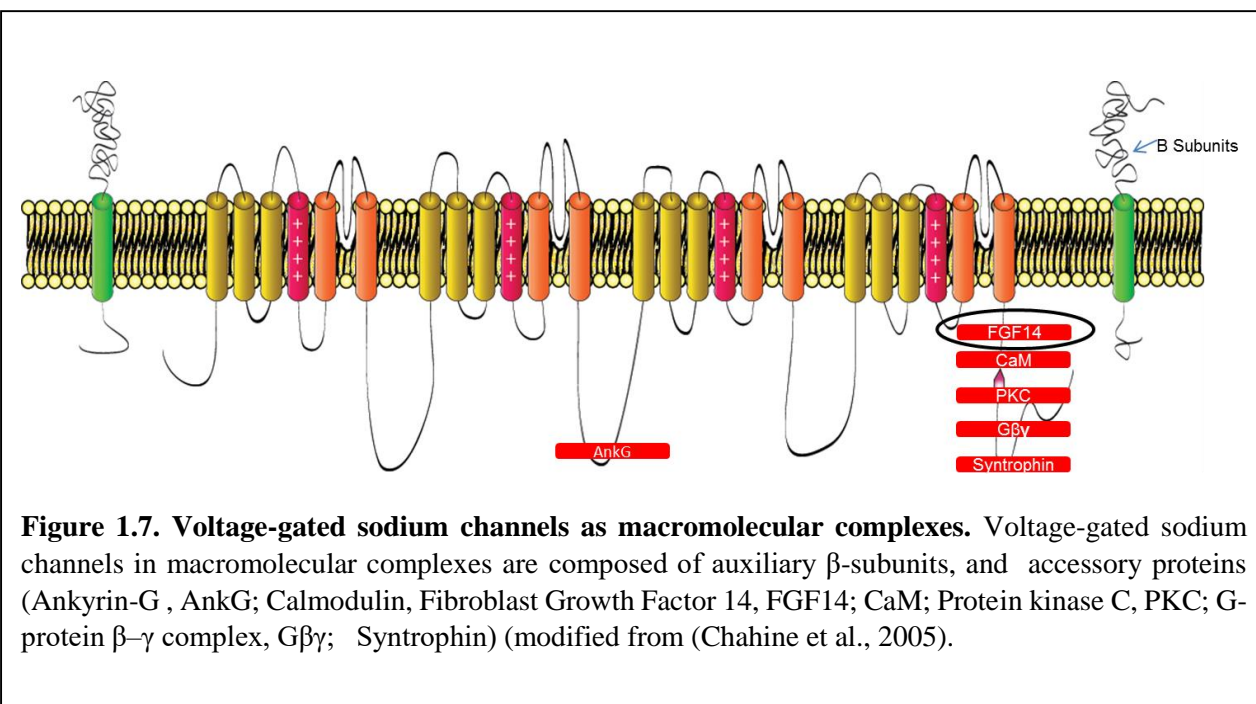
Native Nav channels are regulated by a number of accessory proteins such as caveolin-3, connexin-43, telethonin, CaMKII, plakophilin, ankyrins, NEDD4, SAPs, syntrophin/dystrophin complex, and intracellular fibroblast growth factors (iFGFs) (Liu et al., 2001; Liu et al., 2003a; Musa et al., 2015; Olsen et al., 2003; Savio-Galimberti et al., 2012; Schoorlemmer and Goldfarb, 2001; Wittmack et al., 2004). Although most of these proteins interact with the C-tail of Nav1.6 channels (**Fig. 1.7**), only a few of these accessory proteins produce functional outcomes on Na⁺ currents and neuronal firing. One of the important accessory proteins of Nav1.6 channels is intracellular fibroblast growth factor 14 (FGF14). FGF14 is highly abundant in the CNS, and this protein is required for action potential firing and synaptic plasticity of neurons (Xiao et al., 2013). Furthermore, FGF14 is a physiologically relevant accessory protein of Nav1.6 channels that has been associated with neurological disorders such as ataxia (van Swieten et al., 2003), schizophrenia (Rodriguez-Murillo et al., 2014) and depression (Verbeek et al., 2012). FGF14 differentially modulates Nav1.1, Nav1.2, and Nav1.6 channels, and its phenotype is distinct from that of other iFGFs (Ali et al., 2014; Goetz et al., 2009; Liu et al., 2001; Liu et al., 2003a; Rush et al., 2006; Tempia et al., 2015; Wittmack et al., 2004). In addition to forming a high-affinity monomeric complex with the Nav1.6 channel C-tail,

FGF14 monomers can interact with other FGF14 monomers and form an FGF14 homodimer (Ali et al., 2014; Ali et al., 2016b).

Targeting the FGF14:Nav1.6 Channel Complex Interaction Sites as a New Strategy for Drug Development Against Nav1.6 Channels

There is an ongoing effort both in industry and academia to develop isoform specific inhibitors targeting Nav1.6 channels based on the 2, 4 (1H)-Diarylimidazoles molecule. Although this strategy has shown some success in the discovery of subtype specific Nav1.6 channel blockers (Rivara et al., 2012), novel approaches are required to develop subtype specific compounds targeting Nav1.6 channels.

In search of new strategies to develop novel compounds targeting Nav1.6 channels, we have explored the interaction sites of FGF14:Nav1.6 complex to discover novel compounds. This rich macromolecular complex of Nav1.6 channel introduces specific protein:protein interaction (PPI) sites that could serve as novel targets for drug development (Stoilova-McPhie et al., 2013). In searching for the



FGF14:Nav1.6 surfaces that could lead to the development of potential probes and drug-like molecules targeting Nav1.6 channels, we have investigated hot-spots at the interface of this complex.

Although the FGF14 directly interacts with the C-tail of Nav1.6 channel, not all residues at the FGF14:Nav1.6 complex interface are involved in the PPI. The FGF14:Nav1.6 PPI interaction is mediated by specific amino acid residues known as “hot spots.” The hot spots of PPI can be determined by substituting a particular amino acid residue with an alanine amino acid residue, a methodology known as alanine-scanning mutagenesis. (Guo et al., 2014). By this approach, the critical amino acids at the interface of FGF14:Nav1.6 complex could be identified, and the interface could be utilized to design peptides that could modulate this complex.

To do this, we have implemented an integrative approach comprised of molecular modeling, LCA, biochemical assays, and patch-clamp techniques to investigate the FGF14:Nav1.6 interaction sites as a new drug development target for discovering small molecules. After extensive studies, we have identified a FGF14 β 9 loop as a potential druggable site by validating hot spots at the interface of FGF14:Nav1.6 complex. Based on this information, we have designed short peptide fragments that align with pockets defined by the FGF14 β 9 loop. For one peptide, FLPK, we have applied medicinal chemistry efforts to generate novel peptidomimetics that target the FGF14:Nav1.6 channels complex. After performing different biochemical assays, we have identified a peptidomimetic (ZL181) and validated its functional activity against the Nav1.6 channel. These breakthrough results identify the FGF14 β 9 as part of potential druggable pockets against the FGF14:Nav1.6 complex and indicate that the peptidomimetics targeting these pockets might give rise to a new class of unconventional PPI-based modulators of Nav channels that could restore malfunction of neuronal excitability and plasticity in brain disorders. In the future, our work might contribute significantly to the development of Nav1.6 isoform-specific therapeutic drugs for the treatment of Nav1.6 channels associated brain disorders such as epilepsy, depression, and schizophrenia.

Central Hypothesis

Targeting FGF14-Nav1.6 interaction “Hotspots” is a novel druggable interface that can be modulated by small peptides

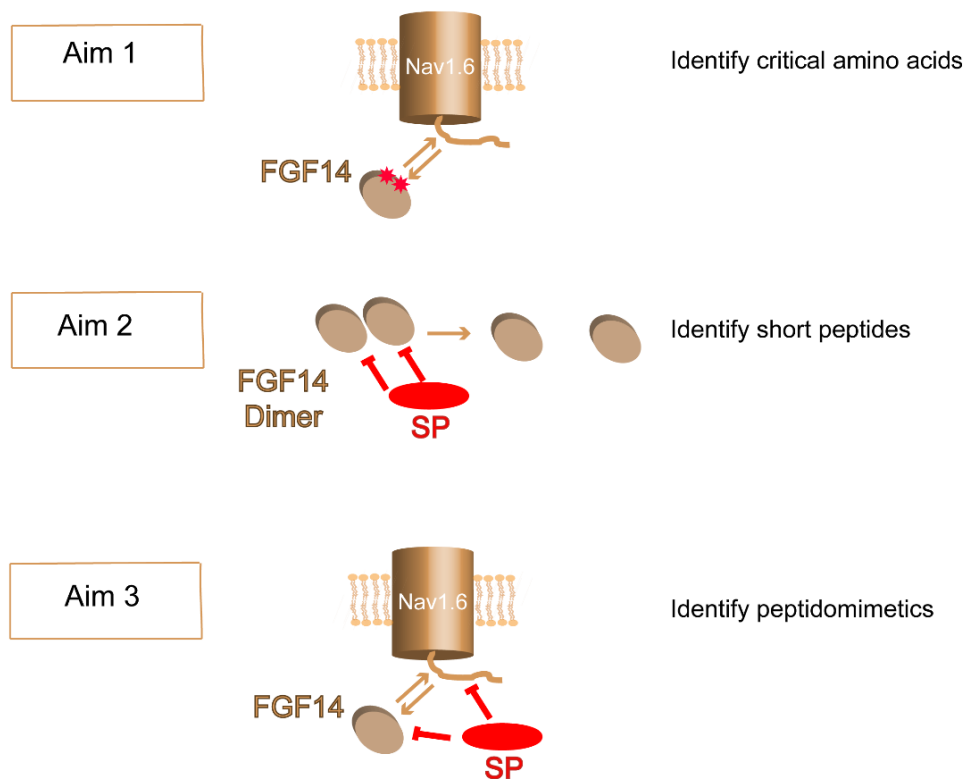
Specific aims

Aim 1 (chapter 3). *To identify critical amino acids at the FGF14:Nav1.6 complex interface*

Aim 2 (chapter 4). *To modulate the FGF14:FGF14 homodimer interaction through short peptide fragments*

Aim 3 (chapter 5). *To validate optimized peptidomimetics as novel modulators of the FGF14:Nav1.6 complex*

Graphical Representation



Chapter 2

The following experimental procedures are published in the following journals:

1. **Ali S.**, Singh A., Laezza F. (2016) Identification of Amino Acid Residues in the Fibroblast Growth Factor 14 (FGF14) Required for Structure-Function interactions with the Voltage-Gated Sodium Channel Nav1.6. *The journal of biological chemistry*, jbc.M115.703868.
2. **Ali S.**, Shavkunov A., Panova-Elektronova N., Stoilova-McPhie S., Laezza F. (2014) Modulation of the FGF14:FGF14 homodimer interaction through short peptide fragments. *CNS Neurol Disord Drug Targets* 13(9): 1559-1570.
3. Shavkunov A., **Ali S.**, Panova-Elektronova N., Laezza F. (2015) Split-luciferase complementation assay to detect channel-protein interactions in live cells. *Methods in molecular biology* 1278:497-514. doi:10.1007/978-1-4939-2425-7_33.
4. **Ali S.**, Liu Z., Nenov M., Scala F., James T., Singh A., Panova-Elektronova N., Chen H., Zhou J., and Laezza F. Modulation of the FGF14: Nav channels interaction through short peptide fragments (*in preparation*).

Written permission was taken from these publishers to use the material as a chapter in my dissertation.

GENERAL EXPERIMENTAL PROCEDURES

Materials—D-luciferin was purchased from Gold Biotechnology (St. Louis, MO) and prepared as a 30 mg/ml stock solution in phosphate-buffered saline (PBS) and stored in a -20° freezer. Anti-luciferase antibodies against the C- (251-550) and N-terminus (1-107) were purchased from Santa Cruz (Dallas, TX) and NovusBio (Littleton, CO), respectively.

DNA Construct Preparation—Plasmid DNA with cloned inserts encoding for FGF14^{K74F/I76R}, FGF14^{L116K/R117F}, FGF14^{N157D/Y1159H}, FGF14^{L202R/K204M/P205S/V208S}, FGF14^{Y158A}, FGF14^{V160A}, and FGF14^{Y158A/V160A}, FGF14^{Y158N/V160N} were synthesized by DNA2.0 (Menlo Park, CA), and transferred from the pJ204 shuttle vectors into mammalian expression vectors as previously described (Shavkunov et al., 2015; Shavkunov et al., 2013b). The FGF14-GFP was generated and characterized as described previously (Lou et al., 2005a). DNA with cloned inserts encoding for FGF14^{Y158A/V160A} was synthesized by DNA2.0 (Menlo Park, CA) and transferred into the GFP plasmid (pQBI-fC2; Quantum Biotechnology Inc., Montreal, Canada). FGF14^{K74A}-GFP, FGF14^{I76A}-GFP, FGF14^{K74A/I76A}-GFP, and FGF14^{V160A}-GFP constructs were generated using FGF14^{WT}-GFP as a template with Agilent Technologies QuikChange Lightning kits (Santa Clara, CA). CLuc-FGF14^{K74A}, CLuc-FGF14^{I76A}, CLuc-FGF14^{K74A/I76A} constructs were generated using CLuc-FGF14^{WT} as a template while FGF14^{K74A}-NLuc, FGF14^{I76A}-NLuc, FGF14^{K74A/I76A}-NLuc constructs were generated using FGF14^{WT}-NLuc as a template with Agilent Technologies QuikChange Lightning kits (Santa Clara, CA).

Molecular Modeling (chapter 3) —The FGF14:Nav1.6 homology model was generated using the FGF13:Nav1.5: CaM ternary complex crystal structure (4DCK) as a template. The FGF14 (amino acids 71-218) and Nav1.6 (amino acids 1790-1917) sequences were aligned with the crystal structure of the FGF13:Nav1.5 (4DCK) and a project PDB file was created by Deepview/swiss pdb viewer (Guex et al., 2009). This file was submitted to the Swiss-model server (QMEAN is 0.808 out of 1); subsequently the model was improved by energy minimization in the Chiron web server (Ramachandran et al., 2011), and validated by the Molprobit web server (Chen et al., 2010) (MolProbit score is 1.56, 94th percentile).

Similarly, the FGF14:FGF14 dimer model was generated using the FGF13:FGF13 dimer crystal structure (3HBW) as a template. The FGF14 target sequence (amino acids 71-218) and the FGF13 crystal structure were aligned using the DeepView/Swiss PDB viewer. The resulting PDB file (QMEAN is 0.652 out of 1) was submitted to the Swiss-Model web server to generate the FGF14 dimer homology model. The model obtained from Swiss-Model web server was further improved by energy minimization by the Chiron web server (Ramachandran et al., 2011), and subsequently, validated by MolProbity (MolProbity score is 1.47, 96th percentile). FGF14^{K74A/I76A}:Nav1.6, FGF14^{V160A}:Nav1.6 C-tail, FGF14^{K74A/I76A}:FGF14^{K74A/I76A} and FGF14^{Y158A/V160A}:FGF14^{Y158A/V160A} *in silico* mutations in FGF14 were generated by the USCF-Chimera molecular modeling suite (Pettersen et al., 2004) and the best rotamers were selected according to their side-chain torsion as well as probability values in the rotamers library. Subsequently, energy minimization of the models was done by Chiron web server (Ramachandran et al., 2011).

Molecular Modeling (chapter 4)- The FGF14:FGF14 homodimer model was built with the FGF13 dimer crystal structure (3hbw) as a template (Goetz et al., 2009) by aligning the sequence and structure of the FGF14 monomer model (van Swieten et al., 2003) to the FGF13 monomers in the FGF13 dimer crystal structure. The Y158N/V160N mutations were carried *in silico* within the USCF-Chimera molecular modeling suite (Pettersen et al., 2004). The sequence alignment of the FGF14 model (van Swieten et al., 2003) to the FGF13 monomers in the FGF13 dimer crystal structure (3hbw) was performed with the MatchMaker algorithm (Meng et al., 2006) by superimposing both structures created with a pairwise sequence alignment using the Needleman-Wunsch and BLOSUM-62 algorithms. The structure of the FGF14 homodimer, as well as of the FGF14^{Y158N/V160N} hetero- and homodimer mutant structures were energy minimized with the Amber's Antechamber module implemented in UCSF-Chimera (Wang et al., 2006; Wang et al., 2004). Before minimizing the FGF14 homodimer structure, the FGF14 monomer:monomer interface was optimized with the DockPrep algorithm (Lang et al., 2009; Moustakas et al., 2006), also implemented in the UCSF Chimera suite.

Peptide Synthesis and Delivery (chapter 4) -Custom made peptides (acetylated group on the N-terminal and amide group on the C-terminal) were synthesized by the American Peptide Company (Sunnyvale, CA). Peptides were dissolved in phosphate buffer saline (PBS) at a concentration of 10 mM and delivered to HEK293 cells in conjunction with cDNA during transient transfection to a final concentration of 10 μ M. Mixtures of peptides (40 μ M) along with cDNA plasmids (1-2 μ g) or Lipofectamine 2000 alone were first incubated each in 50 μ l DMEM+ F12 media for 5-6 min, and then combined and allowed to stand for 20 minutes. The combined 100 μ l mixtures were then gently vortexed for 30 seconds and dispensed into individual wells of a 24-well plate containing 4.5×10^5 cells/well seeded with 100 μ l DMEM+F12 media for 6 hours. The final concentration of the peptides for the time of transfection was 10 μ M into a 200 μ l final volume of DMEM+F12 media. Six hours later, 800 μ l media (DMEM+F12+FBS+antibiotics) was added to maintain cells in culture. PBS alone mixed with cDNA and Lipofectamine 2000 was used as a negative control.

Immunoprecipitations-HEK293 cells were transiently transfected with pQBI-FGF14-6xmyc and pQBI-FGF14-GFP plasmids (5ug per plasmid). The following day, cells were washed twice with PBS and lysed in lysis buffer (20 mM Tris-HCl, 150 mM NaCl, 1% NP-40), and protease inhibitor mixture (set #3, Calbiochem, Billerica, MA) was added immediately before cell lysis. Cell extracts were collected and sonicated for 20 s and centrifuged at 4°C, at $13,000 \times g$ for 15 min. Supernatants were collected and mixed with rabbit anti-myc agarose beads (Sigma), treated with 10 μ M FLPK peptide and incubated overnight at 4°C with agitation. After washing five times with lysis buffer, 2 \times sample buffer (Bio-Rad, Hercules, CA) containing 50 mM TCEP “tris (2-carboxyethyl) phosphine” was added. Lysates were then heated for 10–15 min at 70 °C and resolved on 7.5% or 4–15% polyacrylamide gradient gels (Bio-Rad, Hercules, CA). Resolved proteins were transferred to PVDF membranes (Millipore, Bedford, MA) for 2 h at 4°C and blocked in blocked in tris-buffered saline (TBS) with 3% nonfat dry milk and 0.1% Tween-20. Membranes were then incubated in blocking buffer containing an anti-GFP (1:1000) or monoclonal mouse anti-myc (1:1000; Santa Cruz Biotechnology, Santa Cruz, CA) antibody overnight at 4°C. Washed membranes were incubated with secondary goat anti-mouse or goat anti-rabbit-HRP (1:5000) and visualized with ECL

Advance Western Blotting Detection kit (GE Healthcare, Piscataway, NJ); protein bands were imaged using FluorChem® HD2 System and analyzed with AlphaView 3.1 software (ProteinSimple, Santa Clara, CA).

Cell Culture and Transient Transfections—HEK-293 cells and HEK293 stably expressing Nav1.6 were maintained in medium composed of equal volumes of DMEM and F-12 (Invitrogen, CA) supplemented with 0.05% glucose, 0.5 mM pyruvate, 10% fetal bovine serum, 100 units/ml penicillin, 100 µg/ml streptomycin, and 80 µg/ml G418 (Invitrogen, Carlsbad, CA) for selection of Nav1.6 stably transfected cells, and incubated at 37°C with 5% CO₂. Transfections were performed in 24-well CELLSTAR® tissue culture plates (Greiner Bio-One, Monroe, NC) at 4.5x10⁵ cells per well and incubated overnight to produce monolayers at 90%-100% confluence. The cells were then transiently transfected or co-transfected with the appropriate plasmids using Lipofectamine 2000 (Invitrogen). For co-transfections the DNA concentration of plasmid pairs was adjusted, based on previous studies, to achieve an equal ratio of protein production (Ali et al., 2014; Shavkunov et al., 2012; Shavkunov et al., 2015).

Split-luciferase Complementation Assay (LCA) —Twenty-four hours after transfection, cells were replated from the 24-well plate using a 0.04% Trypsin: EDTA mixture dissolved in PBS. Suspended cells were centrifuged and seeded in white, clear-bottom CELLSTAR® µClear® 96-well tissue culture plates (Greiner Bio-One) in 200 µl of medium. The cells were incubated for 24 h and then the growth medium was replaced with 100 µl of serum-free, phenol red-free DMEM/F12 medium (Invitrogen). The bioluminescence reaction was initiated by automatic injection of 100 µl of D-luciferin substrate (1.5 mg/mL dissolved in PBS) using a Synergy™ H4 Multi-Mode Micro plate Reader (Biotech, Winooski, VT). Luminescence readings were initiated after 3 s of mild plate shaking and performed at 2 min intervals for 20 min with integration times of 0.5 s. Cells were maintained at 37°C throughout the measurements. Detailed methods for LCA can be found in previous studies (Shavkunov et al., 2015).

Western Blot—Transfected HEK293 cells were washed with cold PBS. Subsequently, 50 µl of lysis buffer (20 mM Tris-HCl, 150 mM NaCl, 1% NP-40) and 1 µl Protease inhibitor cocktail (set #3, Calbiochem, Billerica, MA) were added. Cell extracts were collected, sonicated for 16 sec and centrifuged at 4°C, 13,000

x g for 15 min adding 4x sample buffer containing 50 mM tris (2-carboxyethyl) phosphine (TCEP). Mixtures were heated for 10 min at 60°C and resolved on 7.5% polyacrylamide gels (BioRad, Hercules, CA). Resolved proteins were transferred to PVDF membranes (Millipore, Bedford, MA) for 2 hours at 4°C and blocked in tris-buffered saline (TBS) with 3% nonfat dry milk and 0.1% Tween-20. Membranes were then incubated overnight in blocking buffer containing the anti-luciferase (251-550) mouse polyclonal antibody (Santa Cruz, Dallas, TX) and anti-luciferase antibody (1-107) mouse monoclonal antibody (NovusBio, Littleton, CO) or anti-calnexin rabbit polyclonal antibody (Cell Signaling Technology, Danvers, MA). Washed membranes were incubated with goat anti-mouse or goat anti-rabbit-HRP (1:5000) and visualized with ECL Advance Western Blotting Detection kit (GE Healthcare, Piscataway, NJ). Protein bands were visualized using the FluorChem® HD2 System and analyzed with AlphaView 3.1 software (ProteinSimple, Santa Clara, CA).

LCA Data Analysis-Relative luminescence values (RLU) measured by Synergy H4™ Multi-Mode Microplate Reader were tabulated by well position and time point into Microsoft Excel. Signal intensity for each well was calculated as a mean value of peak luminescence measured at three adjacent time points; the calculated values were expressed as percent of mean signal intensity in the control samples from the same experimental plate. Statistical values were calculated as mean and standard error of the mean (mean \pm SEM), unless otherwise specified. The statistical significance (* $p < 0.05$) of different groups was determined by Student's t-test, one-way ANOVA with *post-hoc* Bonferroni's method or Kruskal-Wallis one-way ANOVA on ranks with *post-hoc* Dunn's method using Sigma Stat (San Jose, CA) and Graph Prism^R (La Jolla, CA) software. Graphs were plotted in Origin 8.6 Software (Origin Lab Corporation, Northampton, MA).

The statistical significance (* $p < 0.05$) of different groups was determined by Student's t-test, one-way ANOVA with *post-hoc* Bonferroni's method or Kruskal-Wallis one-way ANOVA on ranks with *post-hoc* Dunn's method using Sigma Stat (San Jose, CA) and Graph Prism^R (La Jolla, CA) software. Dose- response modulation was determined by

$$y = \text{START} + (\text{END} - \text{START}) * x^n / (k^n + x^n)$$

where k, Michaelis constant; n, cooperative sites; x, independent variable; y, dependable variable.

Graphs were plotted in Origin 8.6 Software (Origin Lab Corporation, Northampton, MA).

Protein Over-expression and Purification- cDNAs encoding FGF14^{WT} (accession number NP_787125; aa 64-252) or the C-terminal domain of Nav1.6 (accession number #NP_001171455; aa 1756-1939) were sub-cloned into suitable pET bacterial expression vectors (pET28a-FGF14; pET30a-Nav1.6) with a 6X His-tag at the N-terminal site; these plasmids were a gift of Drs. Regina Goetz and Moosa Mohammadi (Goetz et al., 2009). The mutation coding for FGF14^{K74A/I76A}, FGF14^{V160A} was generated by site-directed mutagenesis and PCR using FGF14 as a template. Upon transformation with corresponding cDNA clones, recombinant proteins FGF14^{WT}, FGF14^{K74A/I76A}, FGF14^{V160A} and Nav1.6 C-tail were expressed in the bacterial strain *E. coli* BL21 (DE3) pLys (Invitrogen)) after induction with 0.2 mM isopropyl thio-β-D-galacto-pyranoside (IPTG) for 8 h at 15°C. After induction with IPTG, bacterial cells were harvested and lysed by lysozyme and sonication at 4°C in lysis/binding buffer containing sodium phosphate 10 mM (prepared from 1M of Na₂HPO₄ and NaH₂PO₄) + CHAPS 0.1% pH 7.0 (for FGF14 proteins), HEPES 25 mM + NaCl 150 mM + glycerol 10% (Nav1.6) pH 7.5 containing 0.1 mM phenyl methyl sulphonyl fluoride (PMSF). The respective proteins were centrifuged at 18000 x g for 30 min at 4°C. For purification of FGF14^{WT}, FGF14^{K74A/I76A} and FGF14^{V160A}, the supernatant was applied to pre-equilibrated heparin and the proteins were then eluted with NaCl 0.2-2.0 M in the lysis/binding buffer. For purification of the Nav1.6 C-tail, the supernatant was applied first to Ni²⁺ NTA column and eluted with imidazole (200 mM). The Nav1.6 C-tail was further purified using HiTrap QFF-sepharose column (GE Healthcare) with a buffer containing Tris-HCl 50 mM and eluted with NaCl (10-500 mM) at pH 7.5. Finally, all concentrated proteins were purified on an AKTA purifier using Superdex 200 Hiload 16 x 60 columns (both products from GE Healthcare Bio-Sciences, Pittsburg, PA) and equilibrated in Tris-HCl 50 mM + NaCl 150 mM, pH 7.5.

Intrinsic Fluorescence Spectroscopy-Intrinsic fluorescence emission spectra of protein samples were recorded on a Spex FluoroMax (Spex Industries, Inc. Edison N.J. USA) in Tris-HCl 25 mM + NaCl 150 mM, pH 7.5. The spectra (300–450 nm) were recorded at an excitation wavelength of 295 nm in the proper spectrum mode of the instrument using excitation and emission band passes of 5 nm each. The binding affinity of FGF14^{WT}, FGF14^{K74A/I76A} and FGF14^{V160A} with the Nav1.6-Ctail was determined by titrating the protein solutions with standard 5.5 μ M concentration aliquots.

Surface Plasmon Resonance Spectroscopy- SPR experiments were performed on a Biacore T100 instrument (Biacore GE), and the interaction between FGF14 to Nav1.6 channel was studied at 25 °C. To analyze the effects of ZL181 on channel binding, FGF14^{WT} and Nav1.6 C-tail were immobilized using acetate 5.5 with amine coupling kit on CM5 sensor chip, and obtaining RU 3000 and 4500 respectively. No protein was coupled to the control flow channel of the chip. ZL181 (5–200 μ M) in HBS-P+ (50 μ l/min) buffer (100 mM HEPES, 150 mM NaCl, 0.005% (v/v) P20), pH7.4 were injected over the chip for 180 s. Next, HBS-P+ buffer without protein were passed over the chip for 180 s to monitor dissociation, and the chip surface was then regenerated with NaCl (200 mM). For each injection of ZL181 binding to the FGF14^{WT} or the Nav1.6, the nonspecific responses were subtracted from the responses obtained for control prior to data analysis. Maximal equilibrium responses were plotted against the concentrations of ZL181, and the equilibrium dissociation constant (KD) was calculated from the fitted saturation binding curve. Fitted binding curves were judged to be accurate based on the distribution of the residuals (even and near zero). Graphs were plotted in GraphPad Prism 6 Software (La Jolla, CA).

In silico Docking of ZL181- Docking was performed with Schrödinger Small-Molecule Drug Discovery Suite using the FGF14:Nav1.6 homology model. ZL181 was prepared with LigPrep, and the FGF14:Nav1.6 complex was prepared with Protein Preparation Wizard. Grids on docking surface were generated with Glide Grid Generator. The docking center was selected at the coordination of X = 14.566, Y = -11.536, Z = -12.008. Docking was performed with Glide Ligand Docking using SP- Peptide mode and the top pose with a docking score of -2.223 was selected.

Electrophysiology Experiments and Data Analysis-HEK-Nav1.6 cells transfected with GFP or FGF14-GFP or FGF14^{V160A}-GFP or FGF14^{Y158A/V160A}, or FGF14^{Y158N/V160N}-GFP were plated at low density on glass cover slips for 3-4 hours and subsequently transferred to the recording chamber. Recordings were performed at room temperature (20-22°C) 24 h post-transfection using a MultiClamp 700B amplifier (Molecular Devices, Sunnyvale, CA). The composition of recording solutions consisted of the following salts: extracellular (mM): 140 NaCl, 3 KCl, 1 MgCl₂, 1 CaCl₂, 10 HEPES, 10 glucose, pH 7.3; intracellular (mM): 130 CH₃O₃SCs, 1 EGTA, 10 NaCl, 10 HEPES, pH 7.3. Membrane capacitance and series resistance were estimated by the dial settings on the amplifier and compensated for electronically by 70–80%. Data were acquired at 20 kHz and filtered at 5 kHz prior to digitization and storage. All experimental parameters were controlled by Clampex 9.2 software (Molecular Devices) and interfaced to the electrophysiological equipment using a Digidata 1200 analog-digital interface (Molecular Devices). Voltage-dependent inward currents for HEK-Nav1.6 cells were evoked by depolarizations to test potentials between –100 mV and +60 mV from a holding potential of –70 mV followed by a voltage pre-step pulse of –120 mV (Nav1.6). Steady-state (fast) inactivation of Nav channels was measured with a paired-pulse protocol. From the holding potential, cells were stepped to varying test potentials between –120 mV (Nav1.6) and +20 mV (pre-pulse) prior to a test pulse to –20 mV.

Current densities were obtained by dividing Na⁺ current (I_{Na}) amplitude by membrane capacitance. Current–voltage relationships were generated by plotting current density as a function of the holding potential. Conductance (G_{Na}) was calculated by the following equation:

$$G_{Na} = I_{Na} / (V_m - E_{rev})$$

where I_{Na} is the current amplitude at voltage V_m , and E_{rev} is the Na⁺ reversal potential.

Steady-state activation curves were derived by plotting normalized G_{Na} as a function of test potential and fitted using the Boltzmann equation:

$$G_{Na} / G_{Na,Max} = 1 + e[(V_a - E_m) / k]$$

where $G_{Na,Max}$ is the maximum conductance, V_a is the membrane potential of half-maximal activation, E_m is the membrane voltage and k is the slope factor. For steady-state inactivation, normalized current amplitude ($I_{Na}/I_{Na,Max}$) at the test potential was plotted as a function of prepulse potential (V_m) and fitted using the Boltzmann equation:

$$I_{Na}/I_{Na,Max} = 1 / [1 + e^{[(V_h - E_m)/k]}]$$

where V_h is the potential of half-maximal inactivation, E_m is the membrane voltage, and k is the slope factor.

Transient I_{Na} inactivation decay was estimated with standard exponential equation. Inactivation time constant (τ , τ_1) was fitted with the following equation:

$$f(x) = A_1 e^{-x/\tau_1} + C,$$

where A_1 and τ_1 are the amplitude and time constant, respectively. The variable C is a constant offset term along the Y axis. The goodness of fitting was determined by correlation coefficient (R), and the cutoff of R was set at 0.85.

Data analysis was performed using Clampfit 9 software (Molecular Devices) and Origin 8.6 software (OriginLab Corporation, Northampton, MA). Results were expressed as mean \pm SEM. The statistical significance of observed differences among groups was determined by Student's t-test, one-way ANOVA with *post-hoc* Bonferroni or Dunnett; $p < 0.05$ was regarded as statistically significant.

***Ex vivo* Electrophysiology Experiments and Data Analysis.** Coronal nucleus accumbens slices were prepared from wild type mice (C67/BL6) either treated with ZL181 or vehicle control. Evoked action potentials were recorded in regular ASCF solution at 30–31°C using Axopatch 200B and 700B amplifiers (Molecular Devices, Union City, CA). Recordings were filtered at 2 kHz and digitized at 10–20 kHz using a Digidata 1320 analog-to-digital interface and pClamp9 acquisition software (Molecular Devices, Union City, CA). Patch pipettes (4–6 M Ω) were prepared from borosilicate glass using a Narishige PC-10 vertical

puller (Narishige International Inc., East Meadow, NY). The extracellular bath solution contained (in mM) 130 NaCl, 3.5 KCl, 10 glucose, 1.5 MgCl₂, 1.4 CaCl₂, 23 NaHCO₃, 1.25 NaH₂PO₄, osmolarity 300-310, pH 7.4, and the intracellular recording solution contained (in mM) 120 CH₃KO₃S, 10 KCl, 10 HEPES, 10 glucose, 2 MgCl₂, 0.5 EGTA, 2 MgATP, and 0.5 NaGTP, , osmolarity 280-290, pH 7.3. Upon forming a whole-cell connection, artificial cerebrospinal fluid containing 10μM bicucilline, 30μM NBQX, and 100μM D-APV was perfused into the bath solution in order to block synaptic transmission. After seal formation and membrane rupture, action potential trains were evoked with a current step protocol injections of 10pA increment.

Chapter 3

The following chapter was published to the Journal of Biological Chemistry (March, 2016) under the title **“Identification of Amino Acid Residues in the Fibroblast Growth Factor 14 (FGF14) Required For Structure-Function interactions with the Voltage-Gated Sodium Channel Nav1.6.”**

“It is the policy of the American Society for Biochemistry and Molecular Biology to allow reuse of any material published in its journals (the Journal of Biological Chemistry, Molecular & Cellular Proteomics and the Journal of Lipid Research) in a thesis or dissertation at no cost and with no explicit permission needed. Please see our copyright permissions page on the journal site for more information”.

Identification of Amino Acid Residues in the Fibroblast Growth Factor 14 (FGF14) Required For Structure-Function interactions with the Voltage-Gated Sodium Channel Nav1.6

Syed R. Ali^{1,2}, Aditya K. Singh¹ and Fernanda Laezza^{1,3,4,5,6*}

Department of Pharmacology & Toxicology¹, Pharmacology and Toxicology Graduate Program², Mitchell Center for Neurodegenerative Diseases³, Center for Addiction Research⁴, Center for Environmental Toxicology⁵, Center for Biomedical Engineering⁶, The University of Texas Medical Branch, Galveston, TX 77555, USA

***Corresponding Author:**

Dr. Fernanda Laezza, M.D., Ph.D.

Department of Pharmacology & Toxicology

The University of Texas Medical Branch

301 University Boulevard

Galveston, 77555, Texas, USA

Phone: 001:409:772:9672

Fax: 001:409:772:9642

Email: felaezza@utmb.edu

ABSTRACT:

The voltage-gated Na⁺ (Nav) channel provides the basis for electrical excitability in the brain. This channel is regulated by a number of accessory proteins including fibroblast growth factor 14 (FGF14), a member of the intracellular FGFs family. In addition to forming homodimers, FGF14 binds directly to the Nav1.6 channel C-tail regulating channel gating and expression, properties that are required for intrinsic excitability in neurons. Seeking amino acid residues with unique roles at the PPI interface of the FGF14:Nav1.6, we engineered model-guided mutations of FGF14 and validated their impact on the FGF14:Nav1.6 and FGF14:FGF14 complex formation using luciferase assay. Divergence was found in the β -9 sheet of FGF14 where alanine (A) mutation of V160 impaired binding to Nav1.6, but had no effects on FGF14:FGF14 dimer formation. Additional analysis revealed also a key role of residues K74/I76 at the N-terminal of FGF14 in the FGF14:Nav1.6 complex and the FGF14:FGF14 dimer formation. Using whole cell patch-clamp electrophysiology we demonstrate that either the FGF14^{V160A} or the FGF14^{K74A/I76A} mutations are sufficient to abolish FGF14-dependent regulation of peak transient Na⁺ currents and voltage-dependence of activation and steady-state inactivation of Nav1.6, but that only V160A with a concomitant alanine mutation at Y158 can impede FGF14-dependent modulation of the channel fast inactivation. Intrinsic fluorescence spectroscopy of purified proteins confirmed stronger binding reduction of FGF14^{V160A} to the Nav1.6 C-tail compared to FGF14^{K74A/I76A}. Altogether these studies indicate that the β -9 sheet and the N-terminus of FGF14 are well-positioned targets for drug development of PPI-based allosteric modulators of Nav channels.

KEYWORDS:

Fibroblast growth factor 14 (FGF14), hot-spots, protein:protein interaction, split-luciferase complementation assay, voltage-gated sodium channels, Nav1.6, ion channels, amino acid

INTRODUCTION:

Voltage-gated sodium (Nav) channels are responsible for initiation and propagation of the action potential in excitable cells. Nine isoforms of Nav channels (Nav1.1-Nav1.9) have been functionally characterized and evidence for a tenth (Nav_x) has been provided (Catterall, 2012, 2014; Catterall et al., 2005a; Chahine et al., 2008; Cusdin et al., 2008; Denac et al., 2000; Goldin et al., 2000; Leterrier et al., 2010; Marban et al., 1998; Savio-Galimberti et al., 2012; Yu and Catterall, 2003). Nav channels are differentially expressed in organs with Nav1.1, 1.2, 1.3 and 1.6 primarily in the central and peripheral nervous systems, Nav1.4 in the adult skeletal muscle, Nav1.5 in cardiac muscle, and Nav1.7, 1.8 and 1.9 primarily in the peripheral nervous system (Catterall et al., 2005a; Chahine et al., 2008; Goldin et al., 2000; Laedermann et al., 2014; Yu and Catterall, 2003). With such widespread expression, it is not surprising that numerous diseases have been ascribed to mutations of specific Nav channel isoforms (Chahine et al., 2008; Mantegazza et al., 2010). These include the Dravet syndrome and other types of epilepsy (Claes et al., 2001; Mantegazza et al., 2005; Mullen and Scheffer, 2009); pain-related syndromes, such as congenital insensitivity to pain (Woods et al., 2015; Wright, 2015), primary erythromelalgia (Tang et al., 2015), and paroxysmal extreme pain disorder (Dib-Hajj et al., 2009a; Lampert et al., 2010); cardiac arrhythmias with congenital long QT syndrome (LQTS) type 3 (Musa et al., 2015; Wang et al., 1995), and Brugada Syndrome (Probst et al., 2003). Furthermore, SNPs and/or copy variants within Nav channel genes have been recently associated with autism (Nav1.2) (Emmett et al., 2014). Nav channels blockers are currently used in combined therapy for bipolar disorder (Farber et al., 2002; Post et al., 1998), depression (Papale et al., 2010; Prakriya and Mennerick, 2000) and schizophrenia (Large et al., 2011), extending the role of Nav channels to virtually all brain disorders both neurological and psychiatric (Eijkelkamp et al., 2012; Emmett et al., 2014; Mantegazza et al., 2010). Their centrality in the pathophysiology of so many disruptive diseases has made Nav channels key pharmacological target sites for antiepileptic, analgesic, antiarrhythmic, and psychiatric drugs (Clare et al., 2000; Dib-Hajj et al., 2009b; Mantegazza et al., 2010; Savio-Galimberti et al., 2012). Unfortunately, current Nav channel blockers lack specificity as they are directed against molecular domains conserved across all Nav isoforms. As such, therapies based on these medications can result in severe side

effects, such as Steven-Johnsons syndrome, blood dyscrasias, and ataxia (Bath and Scharfman, 2013). While some success has been achieved in developing more targeted therapeutics against Nav channels (Theile and Cummins, 2011), there is still an unmet need to develop safe and potent Nav isoform-specific compounds.

The pore-forming α subunit of Nav channels is composed of four homologous domains (I–IV), each consisting of six transmembrane α -helices (S1–S6) and an additional pore loop located between the S5 and S6 segments (Catterall et al., 2005a). The S5 and S6 transmembrane segments from each domain make up a central pore when assembled within a tetrameric configuration. Upon depolarization, the pore of the channel allows Na^+ to rapidly enter the cell; subsequently the channel inactivates and then closes (Catterall, 2014). When expressed in heterologous systems, the α subunit is sufficient to recapitulate the basic functional properties of the channel, but kinetics, voltage-dependence, gating, cellular targeting and trafficking of the channel are modified by the many accessory proteins that compose the channel macromolecular complex in native conditions. Besides the β subunits, other relevant regulatory proteins have been identified. As yet, caveolin-3, CaMKII, connexin-43, telethonin, plakophilin, ankyrins, NEDD4, SAPs, syntrophin/dystrophin complex, and intracellular fibroblast growth factors (iFGFs) have been identified as Nav channel accessory proteins (Liu et al., 2001; Liu et al., 2003a; Musa et al., 2015; Olsen et al., 2003; Savio-Galimberti et al., 2012; Schoorlemmer and Goldfarb, 2001; Wittmack et al., 2004). Some of these interactors have been confirmed as components of the proteome of native Nav1.2 in the brain (Wildburger et al., 2015). This rich macromolecular complex of native Nav channels offers a unique source of specific protein:protein interaction (PPI) sites that could serve as targets for drug development (Stoilova-McPhie et al., 2013); a new direction in pharmacology that has paid off in cancer (Pitteri and Hanash, 2010) and cardiovascular fields (Teiwes and Toto, 2007), but it is still at a nascent stage in neuroscience. In searching for PPI surfaces that could lead to the development of probes and drug-like molecules targeting Nav channels, we have identified FGF14, a member of the iFGF family, as a physiologically relevant accessory protein with implications for brain function and pathology in both animal models and humans

(Rodriguez-Murillo et al., 2014; Verbeek et al., 2012; Xiao et al., 2007). FGF14 is an emerging disease-relevant protein that was initially associated with neurological disorders such as ataxia (van Swieten et al., 2003), and from more recent GWAS studies as a potential risk factor for schizophrenia (Rodriguez-Murillo et al., 2014) and depression (Verbeek et al., 2012). Binding of FGF14 to Nav1.1, Nav1.2 and Nav1.6 exerts powerful effects on Na⁺ currents producing phenotypes that are Nav isoform-dependent and distinct from those associated with other iFGFs (Ali et al., 2014; Goetz et al., 2009; Liu et al., 2001; Liu et al., 2003a; Rush et al., 2006; Tempia et al., 2015; Wittmack et al., 2004).

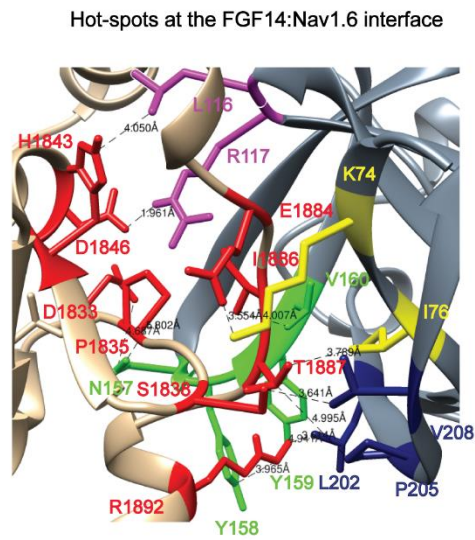
In addition to binding to Nav channels, iFGF can form dimers. Previous structural studies have proposed the existence of a common interface of all iFGF responsible for both iFGF:Nav complexes and iFGF:iFGF dimer formation (Ali et al., 2014; Goetz et al., 2009). However, this hypothesis has never been tested systematically and might not hold for FGF14 given its unique primary sequence (at the N-terminus) and modulation of Nav channels (Laezza et al., 2009; Shavkunov et al., 2013b).

To search for differences at the FGF14:Nav1.6 complex and the FGF14:FGF14 dimer interface, we engineered model-guided mutations at the predicted FGF14 surface and applied the in-cell split-luciferase complementation assay (LCA) to evaluate the effects of these mutants on FGF14:FGF14 dimer formation and monomer binding to the Nav1.6 C-tail. Through patch-clamp electrophysiology we then show that either a single alanine mutation at V160 or a double alanine mutation at K74/I76 are sufficient to abolish previously described functional modulations of Nav1.6 currents by FGF14 (Laezza et al., 2009; Lou et al., 2005a) but full functional activity of FGF14 requires intact V160. Complementary studies using intrinsic fluorescence spectroscopy of purified proteins confirmed that V160 and K74/I76 are required for FGF14 binding to the Nav1.6 C-tail, but that a single alanine mutation at V160 is structurally more disruptive. Overall, K74/I76 and V160 might be part of druggable pockets to be utilized for drug development against Nav channels.

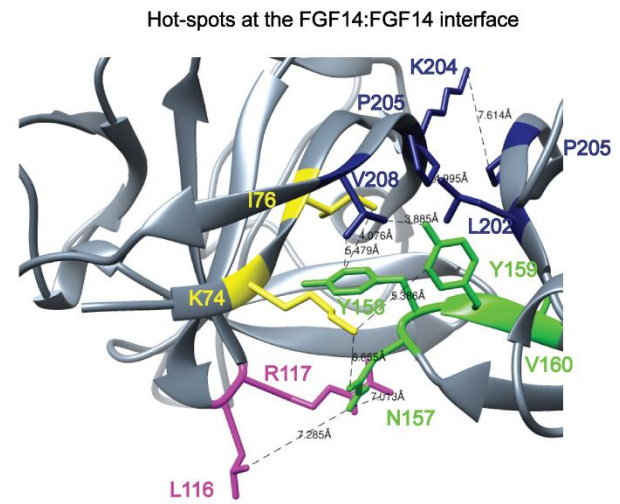
RESULTS

Homology Model-based Characterization of putative FGF14 PPI Surface Hot-spots – To compare putative amino acid residues at the FGF14 PPI interface of FGF14:Nav1.6 and FGF14:FGF14 dimer complex, homology models based on other iFGFs (either in their dimeric form or in complex with the Nav1.5 channel C-tail) were created (**Fig. 3.1, A-B**). Inspection of the FGF14:Nav1.6 homology model revealed that in FGF14, residues K74/I76 (located at the N-terminal), L116/R117 (located at the β -5), N157/Y158/Y159/V160 (located at the β 9), and L202/P205/V208 (located at the β -12) were within a distance $< 8\text{\AA}$ from (Cohen et al., 2009; Tobi and Elber, 2000) the closest neighboring amino acid of the Nav channel consistent with putative hot-spots (**Fig. 3.1, C and Table 3.1**). While most of these residues seemed to exert a similar role in the FGF14:FGF14 dimer complex, K204 and V160 appeared to structurally diverge (**Fig. 3.1, C and Table 3.1**). K204 interacted with the neighboring P205 in FGF14, but had no close neighbors in Nav1.6, while V160 interacted with residue I1886 in Nav1.6, but had no putative interactors in the FGF14:FGF14 dimer. Thus, homology modeling predicts some conserved residues at the FGF14 surface, but potential structural differences depending on the local microenvironment.

A



B



C

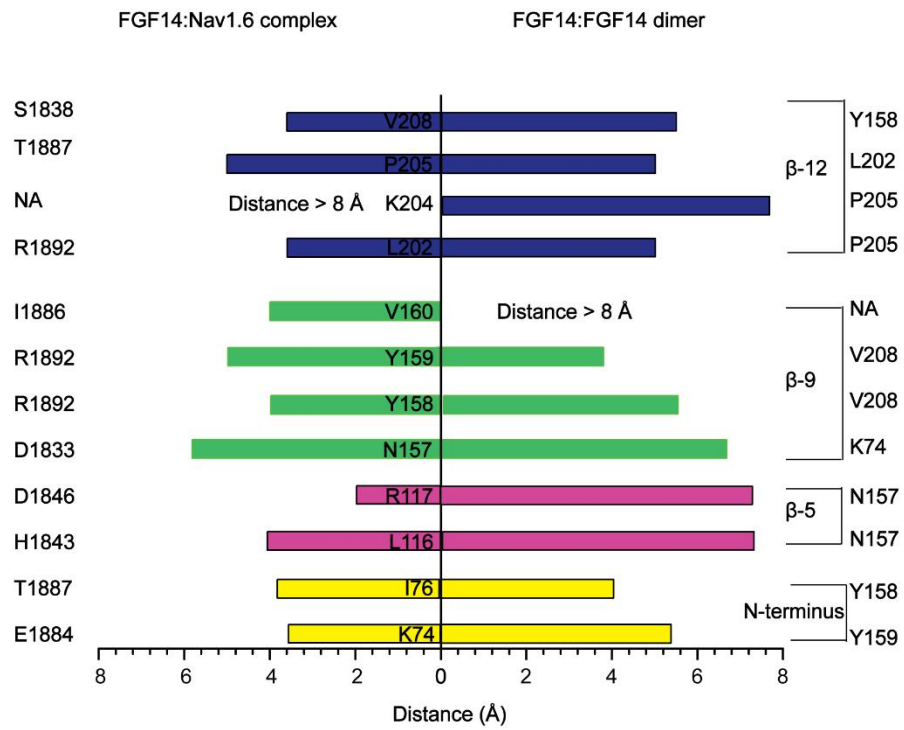


Figure 3.1. Homology model-based predicted hot-spots at the PPI interface of FGF14:Nav1.6 and FGF14:FGF14 dimer complex. *A*, the FGF14:Nav1.6 complex homology model (zoom view) was generated by FGF13:Nav1.5 (PDB: 4DCK) crystal structure as a template. The C-tail of the Nav1.6 channel and FGF14 are shown as tan and gray color, respectively. The critical amino acids K74/I76 (yellow), L116/R117 (magenta), N157/Y158 /Y159/V160 (green), L202/K204/P205/V208 (blue) are located at N-terminal, β 5, β 9, and β 12 strand of FGF14. Critical amino acids of the C-tail of Nav1.6 channel are shown as red color. *B*, the FGF14:FGF14 dimer homology model (zoom view) was generated by FGF13:FGF13 (PDB: 3HBW) dimer crystal structure as a template. *C*, the distance (less than 8 Å) between each critical amino acid of FGF14 to neighboring critical amino acid of FGF14 or to neighboring critical amino acid of C-tail of Nav channels is determined by UCSF-Chimera software from homology models of the FGF14:FGF14 dimer and the FGF14:Nav1.6 complex.

Table 3.1: Homology model-based hot-spots at the FGF14:Nav1.6 complex and the FGF14:FGF14 dimer PPI interface

Location	FGF14:Nav1.6	FGF14:FGF14
N-terminus	K74, I76	K74, I76
β -5	L116, R117	L116, R117
β -9	N157, Y158, Y159, V160	N157, Y158, Y159
β -12	L202, P205, V208	L202, K204, P205, V208

In-cell Validation of Hot-spots at the FGF14:Nav1.6 and the FGF14:FGF14 Dimer Interface –To experimentally evaluate the role of these model-based predicted hot-spots, we engineered double/quadruple mutations in the FGF14 protein and examined their impact on the FGF14:Nav1.6 complex and FGF14:FGF14 dimer formation using our previously validated in-cell split-luciferase complementation assay (LCA) (Ali et al., 2014; Hsu et al., 2015; Shavkunov et al., 2012; Shavkunov et al., 2015; Shavkunov et al., 2013b). The FGF14 mutations were essentially grouped by β -sheet and/or N-terminus location as in previous studies on FGF13 (Goetz et al., 2009) and engineered to carry FGF14^{mutant} proteins fused with either CLuc (fused to the 5' terminal end of the cDNA of interest) or NLuc fragments (fused to the 3' terminal end of the cDNA of interest) of the *Photinus pyralis* firefly enzyme to allow for in-cell reconstitution of FGF14:Nav1.6 C-tail and/or FGF14:FGF14 protein pairs. Mutations of the FGF14 protein considered in this study were: FGF14^{K74F/I76R}, FGF14^{L116K/R117F}, FGF14^{N157D/Y159H}, FGF14^{Y158N/V160N} and FGF14^{L202R/K204M/P205S/V208S}. Combinations of FGF14 wild type (FGF14^{WT}) or/and FGF14^{mutant} constructs (tagged with either CLuc- or NLuc fragments) were transiently co-expressed with either CD4-Nav1.6-C-tail-NLuc (a chimeric construct that allows the membrane presentation of the Nav1.6 C-tail) (Ali et al., 2014; Hsu et al., 2015; Shavkunov et al., 2012; Shavkunov et al., 2015) or with the same corresponding FGF14^{mutant} proteins in HEK293 cells (**Fig. 3.2**); this latter set of experiments was designed to reconstitute hetero- and homodimer forms of each FGF14^{mutant}. Upon binding of the respective protein pairs, the enzymatic activity of the luciferase enzyme was reconstituted by complementation of the full enzyme giving rise to a robust luminescence response in the presence of the D-luciferin substrate. Representative luminescence responses of the assembly of CLuc-FGF14:CD4-Nav1.6-NLuc, CLuc-FGF14^{K74F/I76R}:CD4-Nav1.6-NLuc and CLuc-FGF14^{Y158N/V160N}:CD4-Nav1.6-NLuc are shown in Fig. 2A. For each construct pair, the maximum luminescence response of the CLuc-FGF14^{mutant}:CD4-Nav1.6-NLuc complex was normalized to the CLuc-FGF14^{WT}:CD4-Nav1.6-NLuc complex (**Fig. 3.2, B**). One way ANOVA with *post-hoc* Dunnett's analysis over a large data set (N=6-9 independent experiments, n=4 repetitions) revealed that the strength of interaction of all protein complexes carrying mutations within the FGF14 protein was significantly reduced (p<0.001) compared to the CLuc-FGF14^{WT}:Nav1.6-NLuc complex (**Fig. 3.2, B**). LCA

studies for both FGF14^{mutant} homo- and heterodimer complexes with representative traces and cumulative normalized luminescence responses are shown in **Fig. 3.2, C-D**. Importantly, as summarized in **Fig. 3.2 E**, FGF14 mutations within the N-terminus, $\beta 5$, and $\beta 12$ led to a relative decrease in PPI binding compared to control (yellow, pink, and blue in **Fig. 3.2, B-D**). Mutations of V160 and Y158 resulted in reduced binding to the Nav1.6 C-tail (**Fig. 3.2, B**), but had either no significant effect (Y158N/V160N heterodimer) or augmented Y158N/V160N homodimer) relative binding strength when examined in the context of the FGF14 dimer (**Fig. 3.2, D**). Furthermore, mutations at the K74/I76 residues had the greatest effect on both the FGF14:Nav1.6 complex and the FGF14 dimer, likely due to a strong interaction with neighboring amino acids as predicted our molecular modeling. Western blot analysis of total cell lysates derived from cells transfected with each pair of plasmids confirmed that the protein production across the experimental groups was comparable, confirming the validity of the LCA results (**Fig. 3.3, A-D**). Altogether, these data support our homology model predictions suggesting structural divergence at the FGF14 $\beta 9$ sheet with mutations of Y158/V160 and structural conservation at the FGF14 N-terminus with mutations of K74A/I76 having a significant role in both the FGF14:Nav1.6 complex and the FGF14:FGF14 dimer formation.

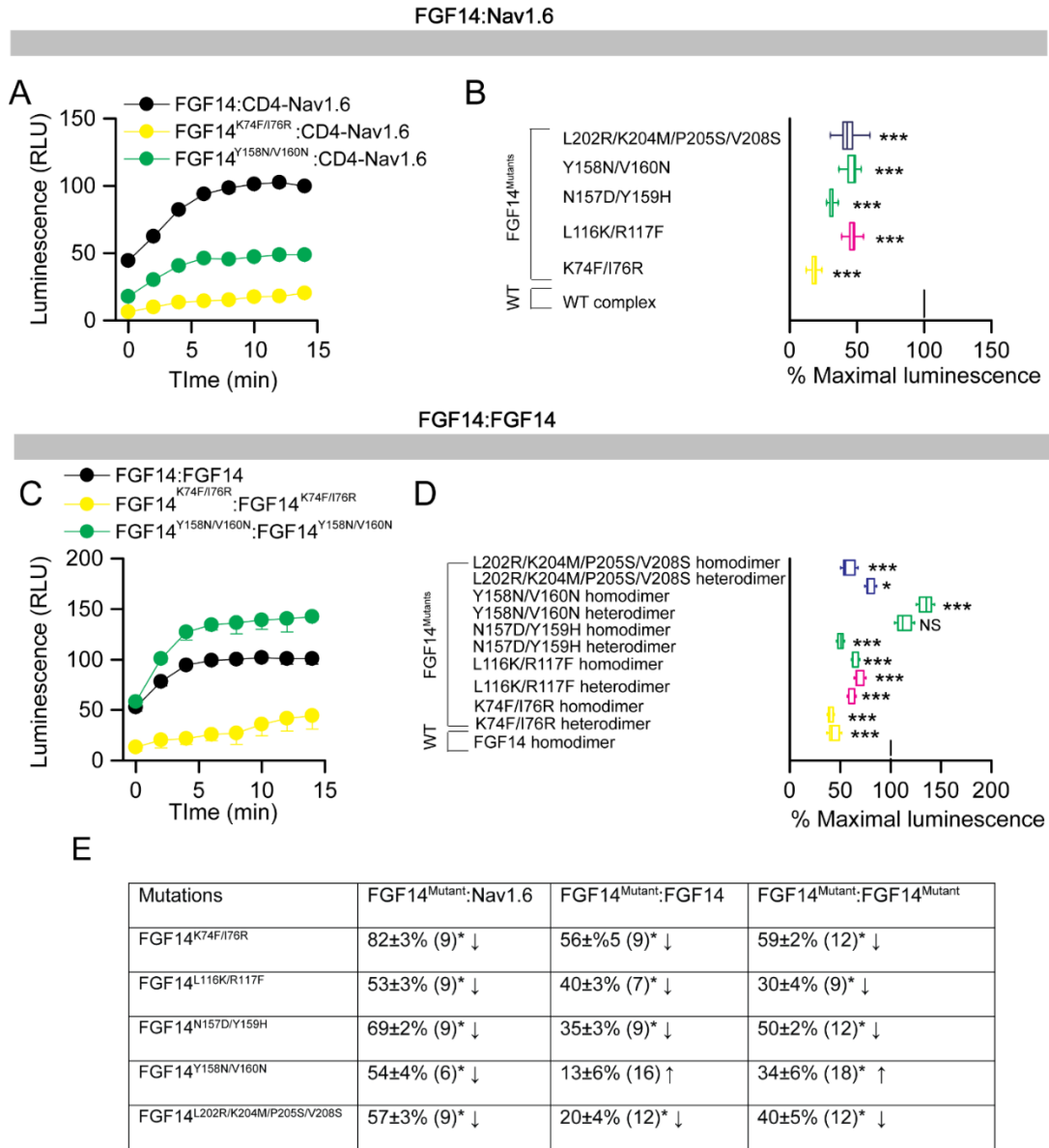


Figure 3.2. In-cell LCA characterization of hot-spots at the FGF14:Nav1.6 channel and the FGF14:FGF14 dimer interface. A, representative luminescence response (RLU) corresponding to the assembly of CLuc-FGF14:CD4-Nav1.6-NLuc (black) and respective mutants (Y158N/V160N, green-circle; K74F/I76R, yellow-circle). B, box plot represents % maximal luminescence response of relative mutants normalized to the CLuc-FGF14: CD4-Nav-NLuc control (black). C, representative luminescence response (RLU) corresponding to the assembly of CLuc-FGF14:FGF14-NLuc (black) and respective mutants (Y158N/V160N, green-circle; K74F/I76R, yellow-circle). D, box plot represents % maximal luminescence response of relative mutants normalized to the CLuc-FGF14:FGF14-NLuc (black) homodimer response. Data are mean ± SEM. The statistical significance between the three groups was assessed using Kruskal-Wallis one-way ANOVA on ranks with post-hoc Dunn's method. ***p<0.001 or *p<0.05. E, data summary of the modulation of hot-spots in FGF14 to form the FGF14:Nav1.6 complex and the FGF14:FGF14 dimer is shown.

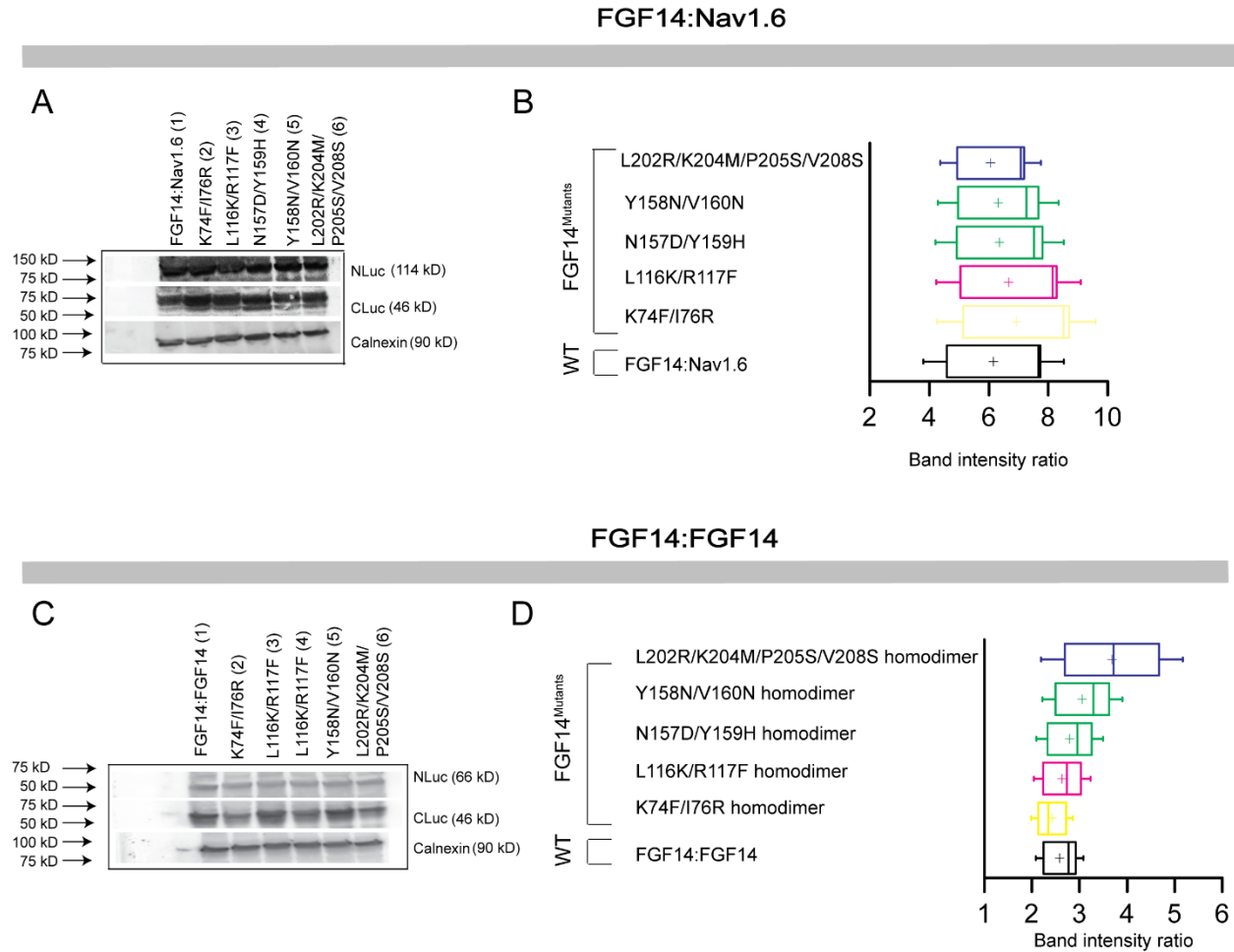


Figure 3.3. Protein production quantification from Western blots. *A*, Western blots of whole-cell extracts from cells transfected with the indicated CLuc-FGF14 and CD4-Nav1.6-NLuc constructs. *B*, summary graph of densitometry analysis of CLuc and NLuc band intensity ratio of the respective protein products. *C*, Western blots of whole-cell extracts from cells transfected with the indicated CLuc-FGF14 and FGF14-NLuc constructs. *D*, Summary graph of densitometry analysis as described in panel *C*. Membrane were probed with anti-luciferase antibodies that recognize either the CLuc or the NLuc fragments (~46 kD and ~66/114 kD, respectively); immunodetection of calnexin was used as loading control.

Alanine Scanning Mutagenesis of Y158 and V160 at the FGF14:Nav1.6 and FGF14:FGF14 Dimer Complexes – These results prompted us to investigate the impact of size and polarity at the Y158 and V160 residues in the two PPI complexes. To this end, we engineered single and double Ala (A) mutations of Y158 and V160 (FGF14^{Y158A}, FGF14^{V160A} and FGF14^{Y158A/V160A} in both the CLuc- and the NLuc format) and continued our screening evaluation with LCA for both the FGF14:Nav1.6 and the FGF14:FGF14 dimer complex. Representative traces and maximal luminescence signal of the FGF14^{mutant}:CD4-Nav1.6 complex (normalized to FGF14^{WT}:CD4-Nav1.6 complex) are shown in **Fig. 3.4, A-B** and **Table 3.2**. One way ANOVA with *post-hoc* Dunnet's revealed that one single A mutation at Y158 was not sufficient to disrupt binding (CLuc-FGF14^{Y158A}:CD4-Nav1.6-NLuc; 95.80± 5.246 %, n=21, p>0.05), but a single V160 to A disrupted the complex (CLuc-FGF14^{V160A}:CD4-Nav1.6-NLuc; 67.11± 3.701 %, n=21, p<0.001). However, the double mutant exhibited a much lower relative binding (CLuc-FGF14^{Y158A/V160A}:CD4-Nav1.6-NLuc; 33.63 ± 2.0%, n=6) when compared to the FGF14^{WT}:Nav1.6 complex (p<0.001) or to the single V160A mutation (p<0.001). The expression of all single and double A mutant proteins was confirmed across all groups by Western blot analysis (**Fig. 3.5, A-B**). Corresponding homology models of the FGF14^{WT}:Nav1.6 and FGF14^{V160A}:Nav1.6 complexes were built (**Fig. 3.4, C-D**) to inspect the role of V160 at the corresponding PPI interfaces. In the FGF14^{WT}:Nav1.6 complex, V160 interacts with I1886 (distance 4.1 Å) of Nav1.6 through hydrophobic interaction (**Fig. 3.4 C**). In the FGF14^{V160A}:Nav1.6 model, the V160A mutation (orange) of FGF14 was further (red, 5.3 Å) from the I1886 of Nav1.6 (**Fig. 3.4, D**), suggesting fewer opportunities for interaction with Nav1.6 (Gregoret and Sauer, 1998).

When examined in the FGF14:FGF14 dimer context (**Fig. 3.4, E-F** and **Table 3.2**), neither the Y158A (CLuc-FGF14^{Y158A}:FGF14^{WT}-NLuc, 111.18 ± 4.89%, n=25, p>0.05; CLuc-FGF14^{Y158A}:FGF14^{Y158A}-NLuc, 93.69± 6.12%, n=18, p>0.05) nor the V160A mutation (CLuc-FGF14^{V160A}:FGF14^{WT}-NLuc, 83.19± 9.87 %, n=15, p>0.05; CLuc-FGF14^{V160A}:FGF14^{V160A}-NLuc, 85.46± 9.23%, n=18, p>0.05) alone had a significant impact on complex stability. On the other hand, the FGF14^{Y158A/V160A} double mutant (both in the hetero- and homodimers) exhibited reduced relative binding (CLuc-FGF14^{Y158A/V160A}:FGF14^{WT}, 49.04 ± 4.0%, n=6, p<0.01; CLuc-FGF14^{Y158A/V160A}:FGF14^{Y158A/V160A}-

NLuc, $49.85 \pm 2.05\%$, $n=12$, $p<0.01$). The expression of all single and double alanine mutant proteins was validated across all groups by Western blot analysis (**Fig. 3.5, C-D**). These results indicate that V160 alone is not sufficient to mediate PPI in the FGF14:FGF14 complex, but that it might work synergistically with Y158 to stabilize it. Corresponding homology models of FGF14^{WT}:FGF14^{WT} and FGF14^{Y158A/V160A}:FGF14^{Y158A/V160A} dimers were built (Fig. 4, G-H). The model predicts that Y158 and V160 are within protruding β -9 loops that connect the two monomers in the intertwined dimer (**Fig. 3.4, G**). Notably, Y158 in each monomer appears to interact with V208 of the neighboring monomer through hydrogen bonding, while V160 had no predicted interactions. Simultaneous replacement of Y158 and V160 with a neutral alanine residue might disrupt hydrogen bonding, weakening the stability of the β -9 loop (Fig. 4H).

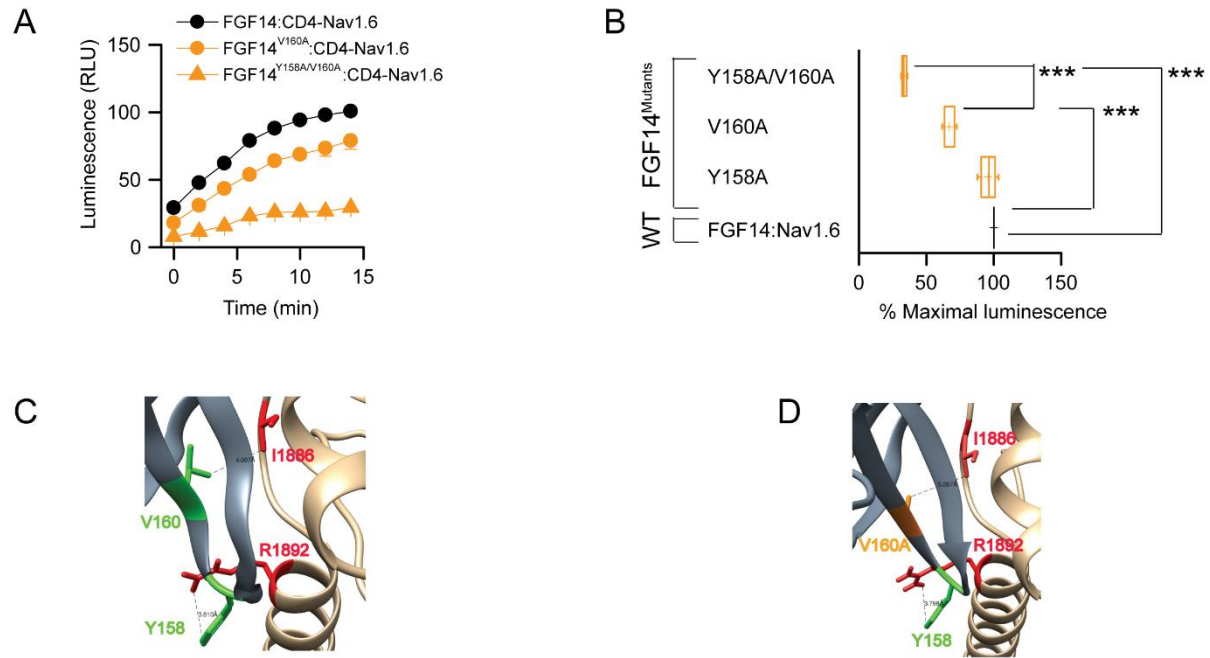
Homology modeling predictions and LCA results together suggest that the PPI interface of the FGF14:Nav1.6 complex is controlled by V160 through hydrophobic interactions, while the FGF14:FGF14 dimer requires the synergistic action of Y158 and V160 through hydrogen bonding.

Table 3.2: Impact of Y158 and V160 at the FGF14:Nav1.6 and the FGF14:FGF14 dimer interface

Mutations	FGF14 ^{Mutant} :Nav1.6	FGF14 ^{Mutant} :FGF14	FGF14 ^{Mutant} :FGF14 ^{Mutant}
FGF14 ^{Y158A}	$95 \pm 5\%$ (21) ↓	$111 \pm 7\%$ (15) ↑	$93 \pm 6\%$ (18) ↑
FGF14 ^{V160A}	$67 \pm 4\%$ (21)*** ↓	$83 \pm 9\%$ (15) ↓	$85 \pm 9\%$ (18) ↓
FGF14 ^{Y158A/V160A}	$33 \pm 2\%$ (6)*** ↓	$49 \pm 4\%$ (6)** ↓	$49 \pm 2\%$ (12)** ↓

*** $p < 0.001$, One way ANOVA with *post-hoc* Dunnett's multiple comparisons test compared with either FGF14^{WT}:Nav1.6 or FGF14^{WT}:FGF14^{WT}.

FGF14:Nav1.6



FGF14:FGF14

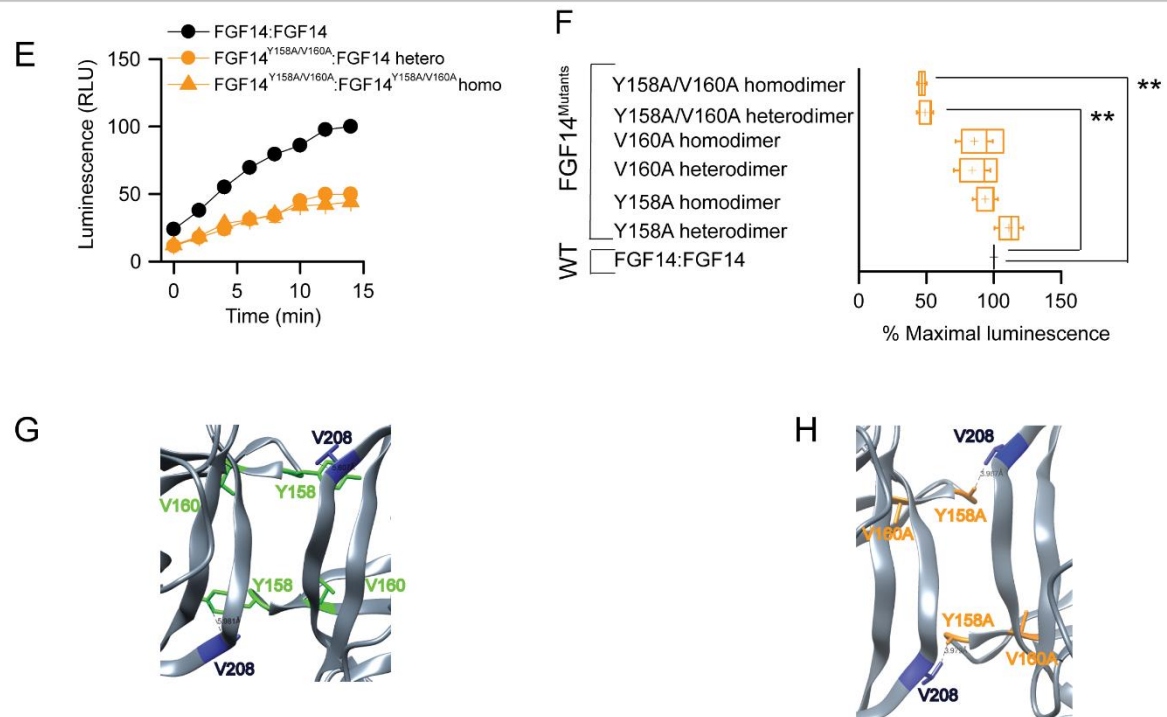


Figure 3.4. Differential role of Y158 and V160 at the FGF14:Nav1.6 channel and the FGF14:FGF14 dimer interface assessed by alanine scanning mutagenesis and in-cell LCA. *A*, representative luminescence response (RLU) corresponding to the assembly of CLuc-FGF14:CD4-Nav1.6-NLuc (black-circle) and respective mutants (V160A, orange-circle; Y158A/V160A, orange-triangle). *B*, box plot represents % maximal luminescence response of relative mutants normalized to the CLuc-FGF14: CD4-Nav1.6-NLuc control (black). *C*, homology model of the FGF14:Nav1.6 complex (zoom view) in which FGF14 is shown as gray and C-tail of Nav1.6 is shown as tan. Y158 (green) and V160 (green) interact respectively with R1892 and I1886 of C-tail of Nav1.6. *D*, interaction between V160A (orange) of FGF14 with I1886 (red) of C-tail of Nav1.6 is shown in the FGF14^{V160A}:Nav1.6 homology model. *E*, representative luminescence response (RLU) corresponding to the assembly of CLuc-FGF14:FGF14-NLuc (black) and respective mutants (Y158A/V160A heterodimer, orange-circle; Y158A/V160A homodimer, orange-triangle). *F*, box plot represents % maximal luminescence response of relative mutants normalized to the CLuc-FGF14:FGF14-NLuc (black) homodimer response. Data are mean \pm SEM. The statistical significance between the three groups was assessed using Kruskal-Wallis one-way ANOVA on ranks with post-hoc Dunn's method; *** $p < 0.001$ or ** $p < 0.01$. *G*, homology model of the FGF14:FGF14 homodimer (zoom view) in which Y158 (green) from one FGF14 monomer interacts with V208 of neighboring FGF14. *H*, interaction between Y158A (orange) of FGF14 with V208 (blue) of neighboring FGF14 monomer is shown in the FGF14^{Y158A/V160A}:FGF14^{Y158A/V160A} homodimer model.

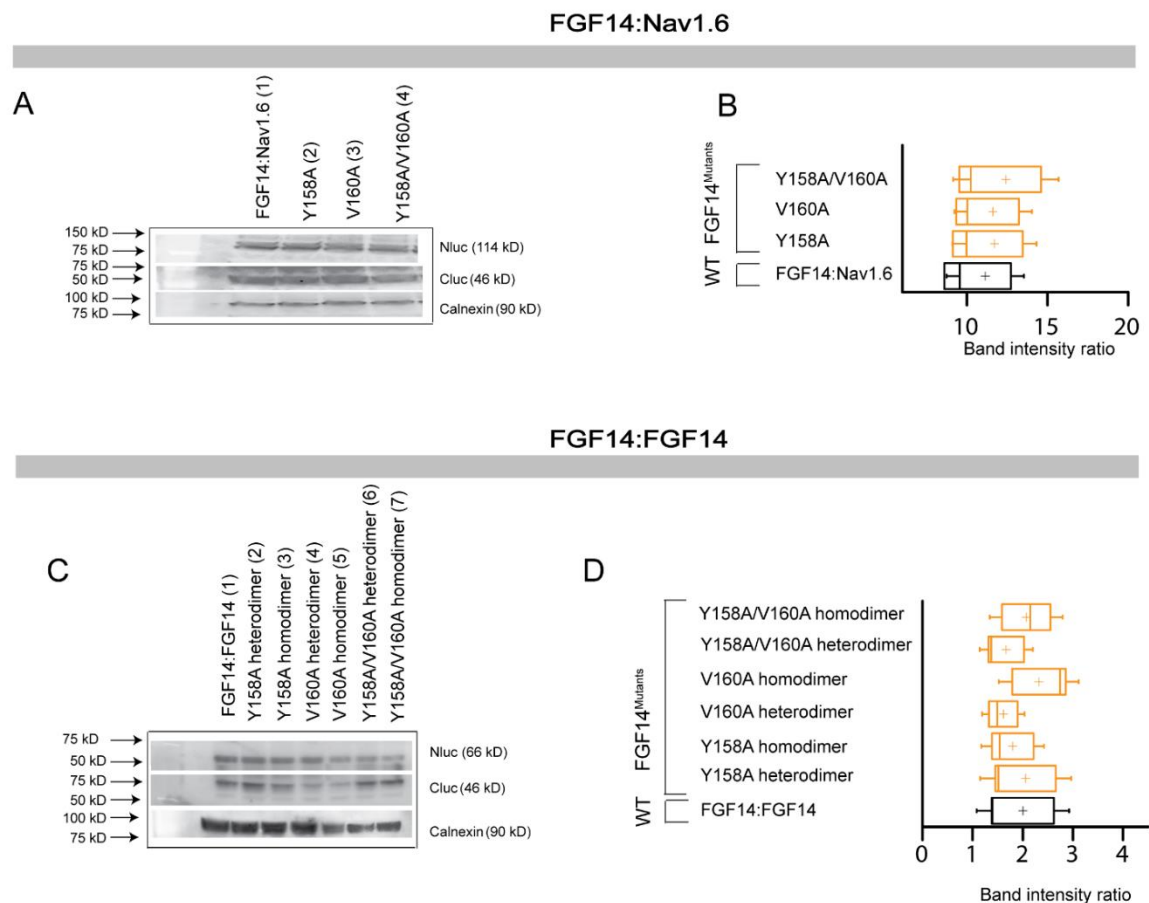


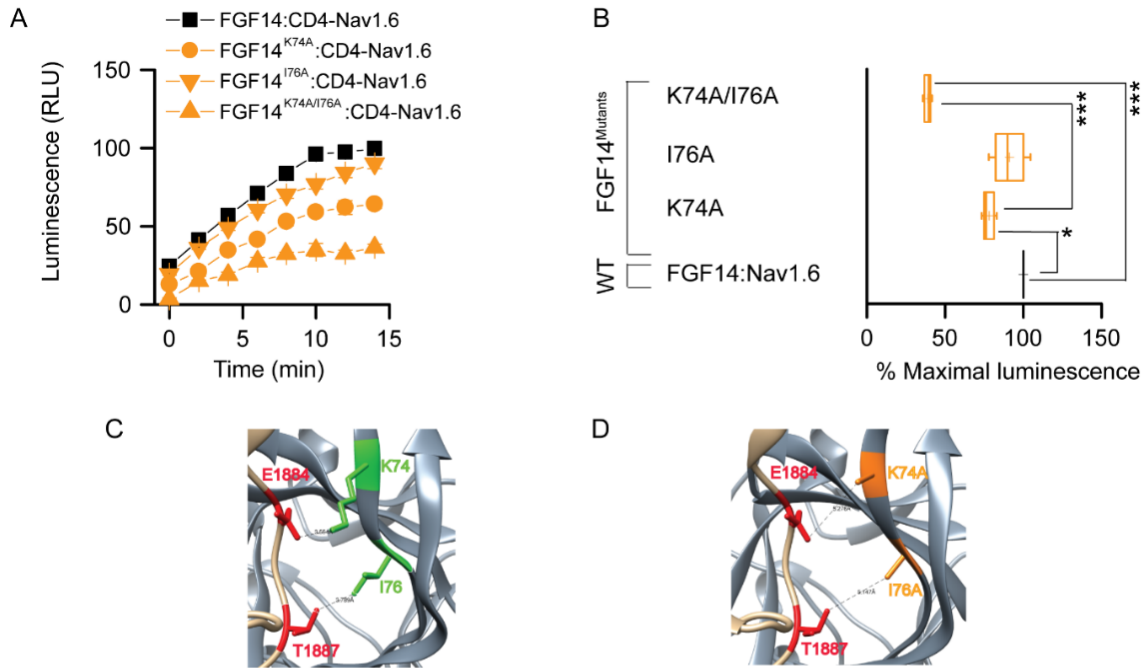
Figure 3.5. Protein production quantification from Western blots for FGF14^{Y158A}, FGF14^{V160A} and FGF14^{Y158A/V160A}. *A*, Western blots of whole-cell extracts from cells transfected with the indicated CLuc-FGF14 and CD4-Nav1.6-NLuc constructs. *B*, summary graph of densitometry analysis of CLuc and NLuc band intensity ratio of the respective protein products. *C*, Western blots of whole-cell extracts from cells transfected with the indicated CLuc-FGF14 and FGF14-NLuc constructs. *D*, Summary graph of densitometry analysis as described in panel. *C*, Membrane were probed with anti-luciferase antibodies that recognize either the CLuc or the NLuc fragments (~46 kD and ~66/114 kD, respectively); immunodetection of calnexin was used as loading control.

Alanine Scanning Mutagenesis of K74 and I76 at the FGF14:Nav1.6 and FGF14:FGF14 Dimer Complexes

– The key role of K74/I76 in both the FGF14:Nav1.6 complex and the FGF14:FGF14 dimer (**Fig. 3.2**) prompted us to investigate the role of these amino acid residues with single and double alanine mutations. To this end, FGF14^{K74A}, FGF14^{I76A} and FGF14^{K74A/I76A} in both the CLuc- and the NLuc format were engineered and evaluated with LCA. Representative traces and maximal luminescence signal of the FGF14^{mutant}:Nav1.6 complex (normalized to FGF14^{WT}:Nav1.6 complex) are shown in **Fig. 3.6, A-B** and **Table 3.3**. One way ANOVA (Kruskal-Wallis) with *post-hoc* Dunn's multiple comparisons test revealed that a single A mutation at I76 was not sufficient to disrupt binding (CLuc-FGF14^{I76A}:CD4-Nav1.6-NLuc; 91.80± 8.8 %, n=12, p>0.05), but a single A mutation at K74 moderately disrupts the complex (CLuc-FGF14^{K74A}:CD4-Nav1.6-NLuc; 78.13± 3.22 %, n=12, p<0.05). However, the double mutant showed a significant lower relative binding affinity (CLuc-FGF14^{K74A/I76A}:CD4-Nav1.6-NLuc; 38.08 ± 2.01%, n=6) when compared to the FGF14^{WT}:CD4-Nav1.6 complex (p<0.001) or to the FGF14^{K74A}:CD4-Nav1.6 complex (p<0.001). The expression of all single and double alanine mutant proteins was confirmed across all groups by Western blot analysis (**Fig. 3.7, A-B**). Corresponding homology models of the FGF14^{WT}:Nav1.6 and FGF14^{K74A/I76A}:Nav1.6 complexes were built (**Fig. 3.6, C-D**) to inspect the role of K74 and I76 at the corresponding PPI interfaces. In the FGF14^{WT}:Nav1.6 complex, K74 and I76 interact with E1884 (distance 3.5 Å) and T1887 (distance 3.71 Å) of Nav1.6, respectively, through a salt-bridge and hydrophobic interactions (**Fig. 3.6, C**). In the FGF14^{K74A/I76A}:Nav1.6 model the K74A and I76A mutations (orange) of FGF14 were further from the E1884 and T1887 residues of Nav1.6 (**Fig. 3.6, D**), suggesting disruption of salt-bridge and hydrophobic interactions.

When examined in the FGF14:FGF14 dimer context (**Fig. 3.6, E-F** and **Table 3.3**), K74A alone or in combination with I76A was found to have the strongest impact on the complex stability in the hetero and the homo dimer formation; I76A alone, on the other hand, was relatively inactive. Corresponding homology models of FGF14^{WT}:FGF14^{WT} and FGF14^{K74A/I76A}:FGF14^{K74A/I76A} dimers were built (**Fig. 3.6, G-H**). The model predicts that K74 and I76 interact with Y159 and Y158 of neighboring FGF14 through salt-bridge and hydrogen bonding respectively. These interactions are both disrupted upon alanine mutation, though K74A appears to have a stronger impact at the PPI interface (**Fig. 3.6, H**). Overall, both LCA and homology modeling support that K74 at N-terminus in FGF14 plays a more significant role in the FGF14:FGF14 dimer formation compared to I76. The expression of all single and double alanine mutant proteins was validated across all groups by Western blot analysis (**Fig. 3.7, C-D**).

FGF14:Nav1.6



FGF14:FGF14

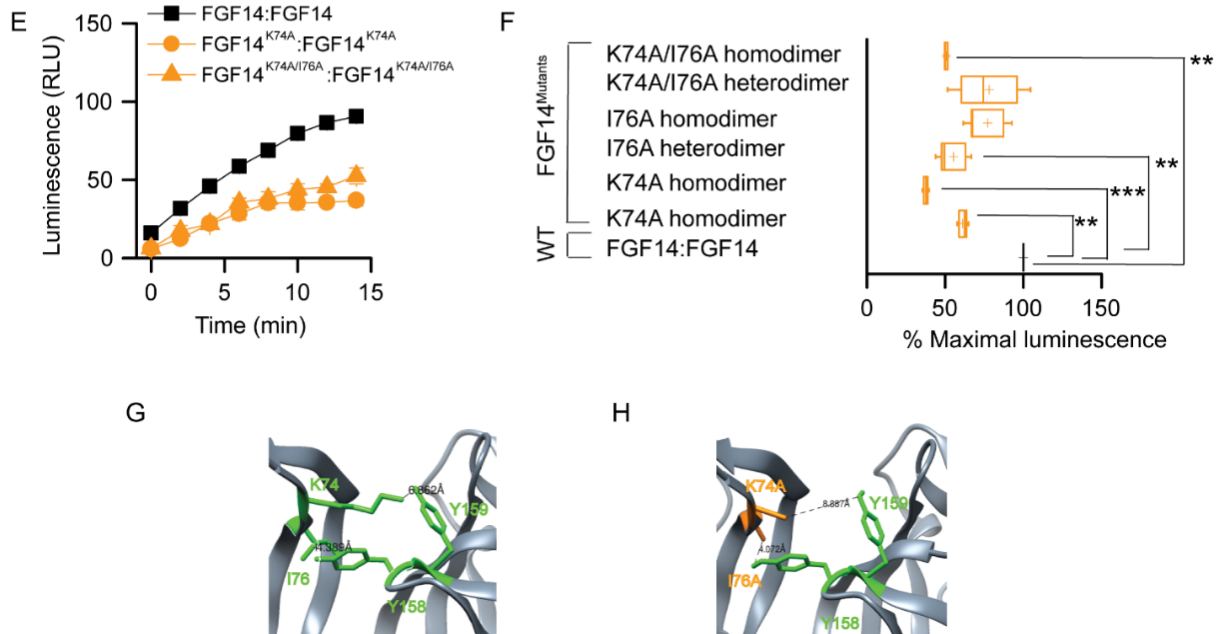


Figure 3.6. Assessing the role of K74 and I76 at the FGF14:Nav1.6 channel and the FGF14:FGF14 dimer interface by alanine scanning mutagenesis by in-cell LCA. *A*, representative luminescence response (RLU) corresponding to the assembly of CLuc-FGF14:CD4-Nav1.6-NLuc (black-square) and respective mutants (K74A, orange-circle; I76A, orange-inverted triangle; K74A/I76A, orange- triangle). *B*, box plot represents % maximal luminescence response of relative mutants normalized to the CLuc-FGF14:CD4-Nav1.6-NLuc control (black). *C*, homology model of the FGF14:Nav1.6 complex (zoom view) in which FGF14 is shown as gray and the C-tail of Nav1.6 is shown as tan. K74 (green) and I76 (green) interact with E1884 and T1887 of the C-tail of Nav1.6, respectively. *D*, interaction of K74A (orange) and I76A (orange) of FGF14 with E1884 (red) and T1887 (red) of the C-tail of Nav1.6 is shown in the FGF14^{K74A/I76A}:Nav1.6 homology model. *E*, representative luminescence response (RLU) corresponding to the assembly of CLuc-FGF14:FGF14-NLuc (black) and respective mutants (K74A homodimer, orange-circle; K74/I76A homodimer, orange-upper triangle). *F*, box plot represents % maximal luminescence response of relative mutants normalized to the CLuc-FGF14:FGF14-NLuc (black) homodimer response. Data are mean \pm SEM. The statistical significance between the three groups was assessed using Kruskal-Wallis one-way ANOVA on ranks with post-hoc Dunn's method; *** p <0.001 or ** p <0.01. *G*, homology model of the FGF14:FGF14 homodimer (zoom view) in which K74 (green) and I76 (green) from one FGF14 monomer interacts with Y159 and Y158 respectively with neighboring FGF14. *H*, interaction between K74A (orange) and I76A (orange) of FGF14 with Y158 and Y159 respectively with neighboring FGF14 monomer is shown in the FGF14^{K74A/I76A}:FGF14^{K74A/I76A} homodimer model.

TABLE 3.3: Impact of K74 and I76 at the FGF14:Nav1.6 and the FGF14:FGF14 dimer interface

Mutations	FGF14 ^{Mutant} :Nav1.6	FGF14 ^{Mutant} :FGF14	FGF14 ^{Mutant} :FGF14 ^{Mutant}
FGF14 ^{K74A}	78 \pm 3% (12)* \downarrow	62 \pm 2% (6)** \downarrow	36 \pm 2% (6)*** \downarrow
FGF14 ^{I76A}	91 \pm 8% (12) \downarrow	61 \pm 8% (6)** \downarrow	82 \pm 9% (6) \downarrow
FGF14 ^{K74A/I76A}	38 \pm 2% (6)*** \downarrow	78 \pm 17% (3) \downarrow	50 \pm 1% (3)*** \downarrow

*** p < 0.001 or ** p < 0.01 or * p < 0.05, One way ANOVA with *post-hoc* Dunn's/Dunnett's multiple comparisons test compared with either FGF14^{WT}:Nav1.6 or FGF14^{WT}:FGF14^{WT}.

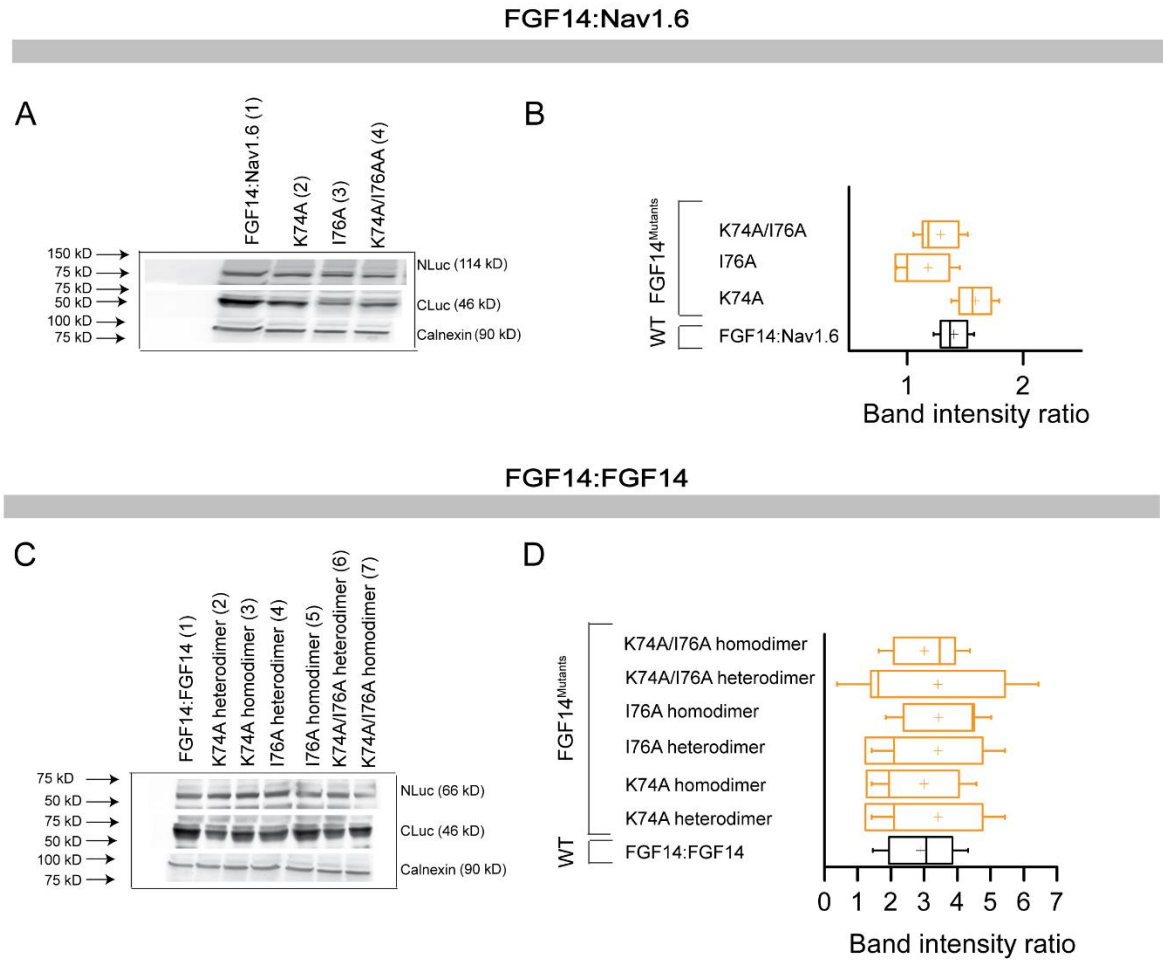


Figure 3.7. Protein production quantification from Western blots for FGF14^{K74A}, FGF14^{I76A} and FGF14^{K74A/I76A}. *A*, Western blots of whole-cell extracts from cells transfected with the indicated CLuc-FGF14 and CD4-Nav1.6-NLuc constructs. *B*, summary graph of densitometry analysis of CLuc and NLuc band intensity ratio of the respective protein products. *C*, Western blots of whole-cell extracts from cells transfected with the indicated CLuc-FGF14 and FGF14-NLuc constructs. *D*, Summary graph of densitometry analysis as described in panel *C*. Membrane were probed with anti-luciferase antibodies that recognize either the CLuc or the NLuc fragments (~46 kD and ~66/114 kD, respectively); immunodetection of calnexin was used as loading control.

V160 is Required for Modulation of Nav1.6 Currents – Abundant evidence exists for a role of FGF14 in regulating current amplitude and biophysical properties of Nav1.6-mediated currents (Laezza et al., 2009; Lou et al., 2005a). To investigate the functional impact of single V160 and combined Y158/V160 mutations on the FGF14-dependent modulation of Nav1.6-encoded currents, we applied whole-cell patch-clamp electrophysiology to HEK293 cells stably expressing Nav1.6 (HEK-Nav1.6 cells), that were transiently expressing GFP, FGF14-GFP, FGF14^{V160A}-GFP, FGF14^{Y158A/V160A}-GFP, and/or FGF14^{Y158N/V160N}-GFP constructs. The purpose of generating FGF14^{V160A}, FGF14^{Y158A/V160A}, and FGF14^{Y158N/V160N} was to investigate the role of single amino acid, polarity and size of Y158 and V160 in modulating Na⁺ currents and to match our LCA studies. In agreement with previous studies (Laezza et al., 2009; Shavkunov et al., 2013b), we found that HEK-Nav1.6 cells expressing FGF14-GFP show significantly lower peak I_{Na+} densities (-9.8±1.5 pA/pF, *n* = 14, *p* < 0.001, Kruskal-Wallis, *post-hoc* Dunn test) than cells expressing GFP (-58.6±13.4 pA/pF, *n* = 16; **Fig. 3.8, A-B and Table 3.4**). Yet, we found that replacing the V160 residue with alanine mutation led to no significant changes in peak I_{Na+} densities, resulting in values comparable to GFP control (-44.14±12.4 pA/pF, *n*=10 for FGF14^{V160A}-GFP, **Table 3.4**). Similar phenotypes were observed also for FGF14 double mutants (-59.3±14.1, *n*=15 for FGF14^{Y158A/V160A} and -58.5±8.5 pA/pF, *n*=11 for FGF14^{Y158N/V160N} compared to GFP control). Further analysis revealed that the decay time constant (τ) of transient I_{Na+} (which reflects the kinetics of open channel entry into the fast inactivation state) was significantly slower in FGF14-GFP (1.7±0.2 ms, *n* = 10, *p* < 0.05) compared to GFP control (1.1±0.1, *n*=14). This phenotype persisted in the FGF14^{V160A}-GFP group (1.7±0.3, *n*=10, *p* < 0.05), but was abolished in the FGF14^{Y158A/V160A}-GFP (0.8±0.1, *n* = 15, *p* > 0.05) or FGF14^{Y158N/V160N}-GFP group (0.8±0.1, *n*=13, *p* > 0.05; **Fig. 3.8, C-D and Table 4**). We also examined other basic biophysical properties of Nav1.6 channels in the presence of these FGF14 mutant proteins that were previously reported as targets of FGF14 modulation (Laezza et al., 2009; Shavkunov et al., 2013b). The voltage-dependences of I_{Na+} activation and steady-state inactivation were determined by plotting normalized conductance (activation) or normalized current amplitudes (inactivation) as a function of the test potential (activation) or the pre-pulse potential (inactivation) following previously described stimulation protocols (Laezza et al., 2009; Shavkunov et al.,

2013b). In agreement with previous studies (Laezza et al., 2009; Shavkunov et al., 2013b) we found that expression of FGF14-GFP led to a significant depolarizing shift in both the voltage-dependence of activation ($p<0.05$) and steady-state inactivation of *Nav1.6* ($p<0.05$). Notably, we found that none of these parameters were significantly affected when cells expressed FGF14^{V160A}-GFP, FGF14^{Y158A/V160A}-GFP and/or FGF14^{Y158N/V160N}-GFP (**Fig. 3.9, A- D** and **Table 3.4**). Thus, we conclude that V160, alone or in cooperation with Y158, is required for FGF14-dependent functional modulation of Nav1.6 currents.

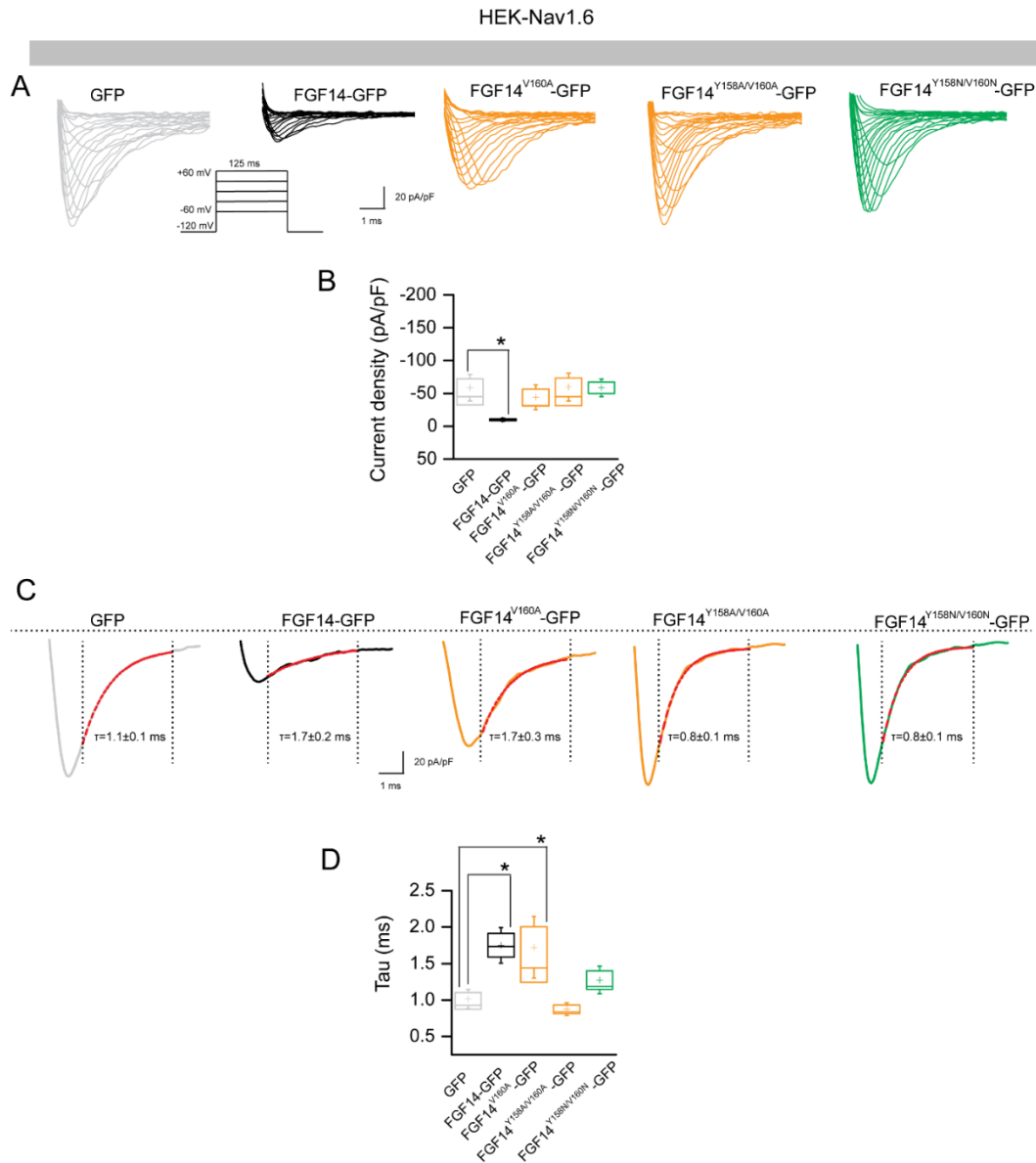


Figure 3.8. The FGF14^{V160} residue is required for modulation of Nav1.6 currents. *A*, representative traces of voltage-gated Na⁺ currents (I_{Na+}) recorded from HEK-Nav1.6 cells transiently expressing GFP (gray), FGF14-GFP (black), FGF14^{V160A}-GFP (orange), FGF14^{Y158A/V160A}-GFP (orange) and FGF14^{Y158N/V160N}-GFP (green) in response to voltage steps from -120 mV to +60 mV from a holding potential of -70 mV (inset). *B*, box plot represents peak current densities measured in individual HEK-Nav1.6 cells expressing GFP, FGF14, FGF14^{V160A}-GFP, FGF14^{Y158A/V160A}-GFP, and FGF14^{Y158N/V160N}. *C*, representative traces of experimental groups described in Panel A in which tau (τ) of I_{Na+} was estimated from a one-term exponential fitting function (red dotted line). Values are plotted as a function of amplitude and time constant. *D*, summary box plot of tau calculated at the peak current density (-10 mV) in the indicated experimental groups. Data are mean \pm S.E. * $p < 0.05$.

TABLE 3.4: Nav1.6-mediated currents in the presence of FGF14 and V160 and Y158 mutants

Condition	Peak density	Activation	K _{act}	Inactivation	K _{inact}	τ
	pA/pF	mV	mV	mV	mV	ms
GFP	-58.6 \pm 13.4 (16)	-20.4 \pm 1.6 (12)	5.3 \pm 0.3 (12)	-58.9 \pm 0.8(14)	5.8 \pm 0.3 (12)	1.1 \pm 0.1 (14)
FGF14-GFP	-9.8 \pm 1.5 (14) ^a	-15.4 \pm 1.1(11) ^b	6.3 \pm 0.5 (11) ^c	-54.4 \pm 1.4 (10) ^d	6.3 \pm 0.7 (10)	1.7 \pm 0.2 (10) ^e
FGF14 ^{V160A} -GFP	-44.14 \pm 12.4 (10)	-22.4 \pm 1.6 (10)	4.6 \pm 0.6 (10)	-58.8 \pm 1.3(10)	6.4 \pm 0.5 (10)	1.7 \pm 0.3 (10) ^f
FGF14 ^{Y158A/V160A} -GFP	-59.3 \pm 14.1 (15)	-21.5 \pm 1.6 (15)	4.6 \pm 0.5 (15)	-62.2 \pm 1.6(15)	7.8 \pm 0.9 (15)	0.8 \pm 0.1 (15)
FGF14 ^{Y158N/V160N} -GFP	-58.5 \pm 8.5 (11)	-21.5 \pm 1.5 (9)	4.2 \pm 0.4 (9)	-62.11 \pm 1.3(9)	7.4 \pm 0.6 (9)	0.8 \pm 0.1 (13)

^a $p < 0.001$, Kruskal-Wallis, post hoc Dunn test compared with GFP; data are mean \pm S.E.

^b $p < 0.05$, one-way ANOVA, post hoc Dunnett's multiple comparisons test compared with GFP; data are mean \pm S.E.

^c $p < 0.05$, one-way ANOVA, post hoc Dunnett's multiple comparisons test compared with GFP; data are mean \pm S.E.

^d $p < 0.001$, Kruskal-Wallis, post hoc Dunnett's multiple comparisons test compared with GFP; data are mean \pm S.E.

^e $p < 0.01$, one-way ANOVA, post hoc Dunn's multiple comparisons test compared with GFP; data are mean \pm S.E.

^f $p < 0.05$, one-way ANOVA, post hoc Dunn's multiple comparisons test compared with GFP; data are mean \pm S.E.

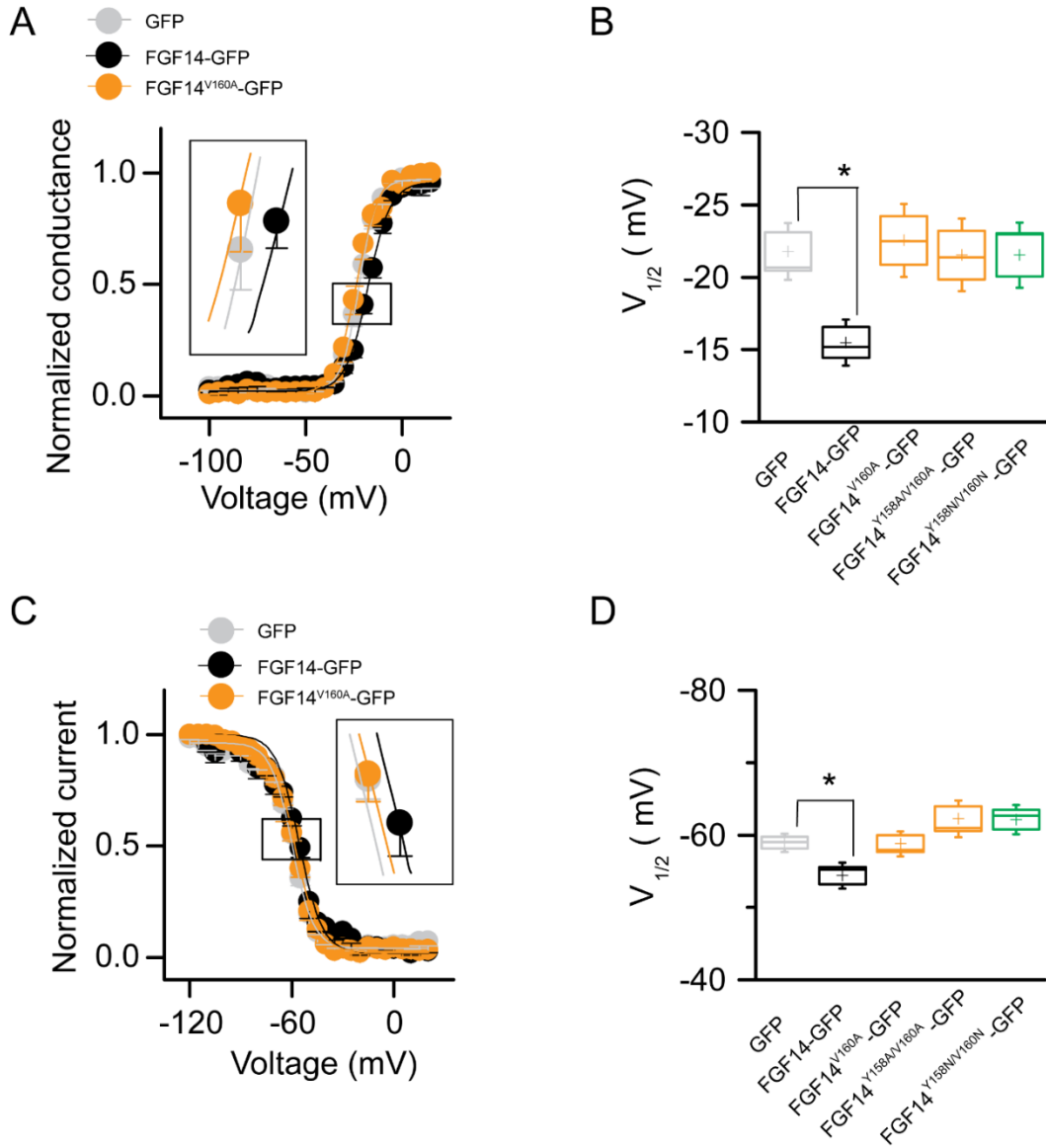


Figure 3.9. The V160A mutation abolishes FGF14-dependent modulation of biophysical properties of Nav1.6 currents. *A*, voltage-dependence of I_{Na} activation is plotted as a function of the membrane potential (mV); data (GFP, FGF14-GFP, and FGF14^{V160A}-GFP) were fitted with the Boltzmann function as indicated in the experimental section. *B*, box plot summary of $V_{1/2}$ for voltage-dependence activation (voltage at which 50% channels are opened) in the indicated experimental groups. *C*, steady-state inactivation is measured using a two-step protocol and values plotted as a function of the membrane potential (mV); data (GFP, FGF14-GFP, FGF14^{V160A}-GFP) were fitted with the Boltzmann function as indicated in the experimental section. The shift of voltage-dependence activation and steady-state inactivation is shown in the two insets in panel *A* and *C*, respectively. *D*, box plot summary of $V_{1/2}$ for voltage-dependence of steady-state inactivation (voltage at which 50% channels are closed) in the indicated experimental groups. Data are mean \pm S.E.; * $p < 0.05$.

K74 and I76 are Required for Modulation of Nav1.6 Currents – We extended our whole-cell patch clamp studies to evaluate the impact of FGF14^{K74A}-GFP, FGF14^{I76A}-GFP, and/or FGF14^{K74A/I76A}-GFP constructs on FGF14-dependent modulation of Nav1.6 currents. We found that while the FGF14^{I76A} mutant behaved similar to FGF14-GFP (-10.9 ± 2.4 pA/pF, $n = 7$; **Fig. 3.10, A-B** and **Table 3.5**), the FGF14^{K74A} single or FGF14^{K74A/I76A} double mutant rescues peak I_{Na+} densities to GFP control values either partially (-21.2 ± 2.5 pA/pF, $n=8$ for FGF14^{K74A}-GFP, **Table 3.5**) or completely (-46.8 ± 13.6 , $n=10$ for FGF14^{K74A/I76A}, **Table 3.5**). However, none of the mutant combinations were effectively rescuing τ of transient I_{Na+} (**Fig. 3.10, C-D** and **Table 3.5**). Additional studies revealed that in the presence of these FGF14 mutants voltage-dependence of activation and steady-state inactivation of Nav1.6 currents were either indistinguishable from GFP control or exhibited a gain-of-function phenotype (voltage-dependence of steady-state inactivation in the presence of FGF14^{I76A}-GFP), suggesting a complex and cooperative interaction of K74 and I76 in regulating biophysical properties of Nav1.6 (**Fig. 3.11, A- D** and **Table 3.5**).

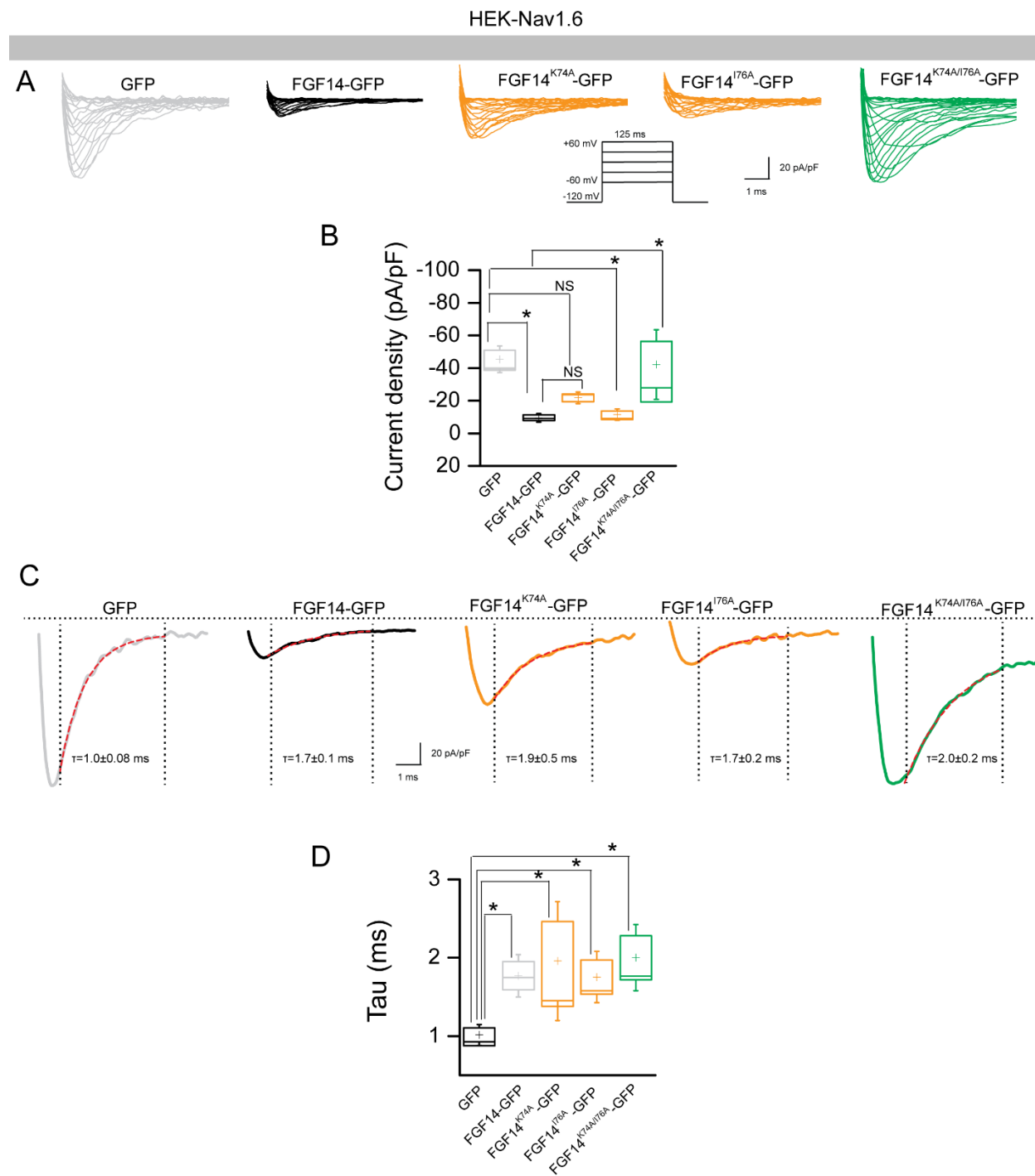


Figure 3.10. Functional validation of K74 and I76 in modulating Nav1.6 currents. *A*, representative traces of voltage-gated Na⁺ currents (I_{Na+}) recorded from HEK-Nav1.6 cells transiently expressing GFP (gray), FGF14-GFP (black), FGF14^{K74A}-GFP (orange), FGF14^{I76A}-GFP (orange) and FGF14^{K74A/I76A}-GFP (green) in response to voltage steps from -120 mV to +60 mV from a holding potential of -70 mV (inset). *B*, box plot represents peak current densities measured in individual HEK-Nav1.6 cells expressing GFP, FGF14, FGF14^{K74A}-GFP, FGF14^{I76A}-GFP, and FGF14^{K74A/I76A}. *C*, representative traces of experimental groups described in Panel A in which tau (τ) of I_{Na+} was estimated from a one-term exponential fitting function (red dotted line). Values are plotted as a function of amplitude and time constant. *D*, summary box plot of tau calculated at the peak current density (-10 mV) in the indicated experimental groups. Data are mean ± S.E. *p<0.05.

TABLE 3.5: Nav1.6-mediated currents in the presence of FGF14 and K74 and I76 mutants

Condition	Peak density	Activation	K _{act}	Inactivation	K _{inact}	τ
	pA/pF	mV	mV	mV	mV	ms
GFP	-43.2±5.1 (21)	-20.8±0.9 (19)	4.7±0.2 (19)	-62±1.4(15)	6.3±0.3 (15)	1.0±0.08 (14)
FGF14-GFP	-9.3±1.8 (12) ^a	-15.7±0.9(11) ^c	6.2±0.4 (11) ^d	-56.0±1.0 (10) ^d	7.1±1.1 (10)	1.7±0.18 (10) ^h
FGF14 ^{K74A} -GFP	-21.2±2.5 (8)	-19.4±1.1 (8)	4.8±0.2 (8)	-71.9±5.9(8)	11.2±1.1 (8)	1.9±0.5 (8) ⁱ
FGF14 ^{I76A} -GFP	-10.9±2.4 (7) ^b	-18.6±1.2 (7)	6.2±0.3 (7) ^e	-86.6±3.5(7) ^f	15.7±1.0 (7) ^g	1.7±0.2 (7) ^j
FGF14 ^{K74A/I76A} -GFP	-46.8±13.6 (10)	-27.4±2.9 (8)	3.9±0.7 (8)	-62.5±3.0(9)	8.8±1.2 (9)	2.0±0.2 (9) ^k

^a $p < 0.001$, one-way ANOVA, post hoc Dunn's multiple comparisons test compared with GFP; data are mean ± S.E.

^b $p < 0.01$, one-way ANOVA, post hoc Dunn's multiple comparisons test compared with GFP; data are mean ± S.E.

^c $p < 0.01$, one-way ANOVA, post hoc Dunn's multiple comparisons test compared with GFP; data are mean ± S.E.

^{d,e} $p < 0.05$, one-way ANOVA, post hoc Dunnett's multiple comparisons test compared with GFP; data are mean ± S.E.

^f $p < 0.05$, student-t test compared with GFP; data are mean ± S.E.

^g $p < 0.01$, one-way ANOVA, post hoc Dunn's multiple comparisons test compared with GFP; data are mean ± S.E.

^{h,i,j,k} $p < 0.05$, one-way ANOVA, post hoc Dunn's multiple comparisons test compared with GFP; data are mean ± S.E.

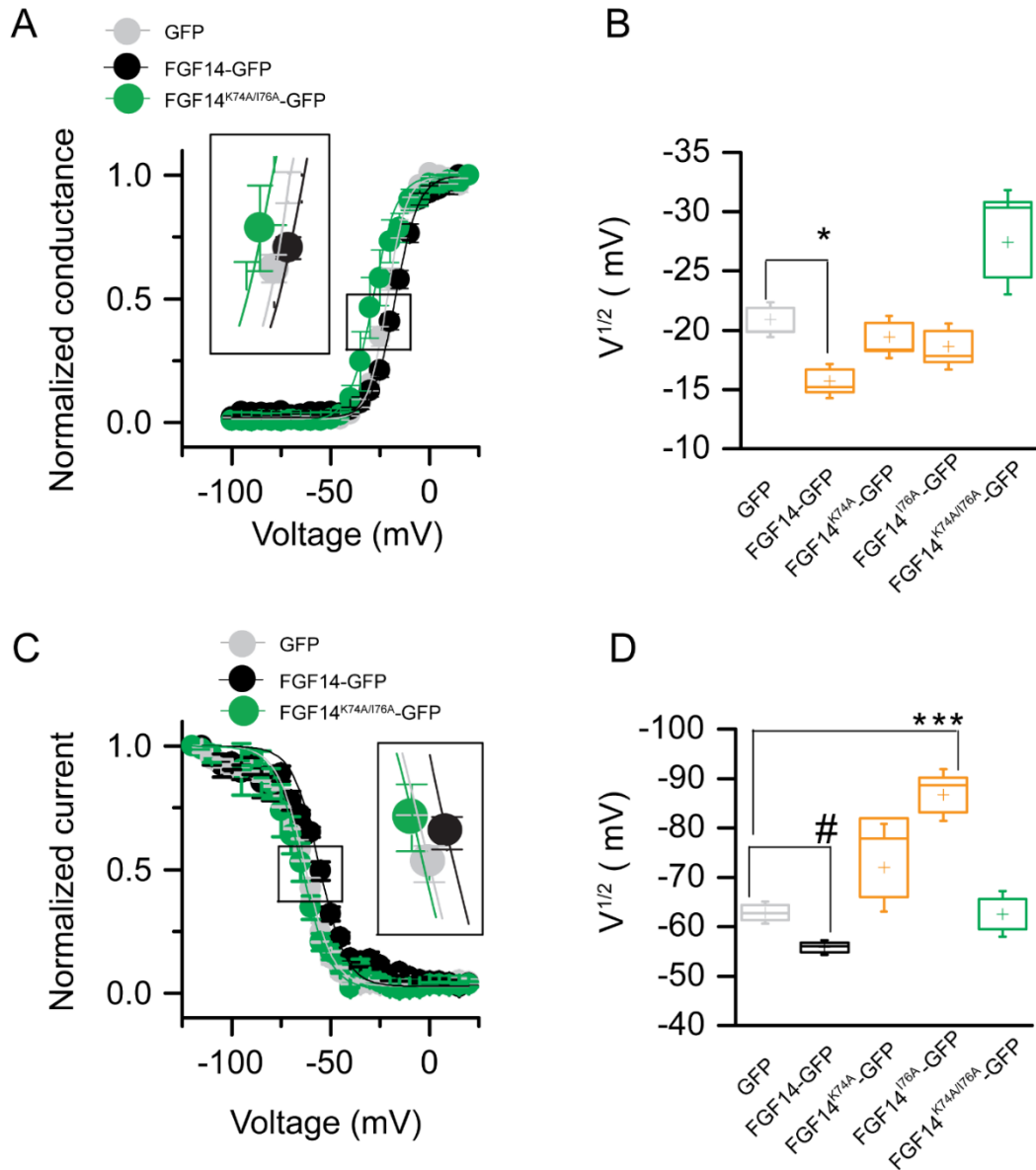


Figure 3.11. Role of K74 and I76 in modulating biophysical properties of Nav1.6 currents. *A*, voltage-dependence of I_{Na} activation is plotted as a function of the membrane potential (mV); data (GFP, FGF14-GFP, and FGF14^{K74A/I76A}-GFP) were fitted with the Boltzmann function as indicated in the experimental section. *B*, box plot summary of $V_{1/2}$ for voltage-dependence activation (voltage at which 50% channels are opened) in the indicated experimental groups. *C*, steady-state inactivation is measured using a two-step protocol and values plotted as a function of the membrane potential (mV); data (GFP, FGF14-GFP, FGF14^{K74A/I76A}-GFP) were fitted with the Boltzmann function as indicated in the experimental section. The shift of voltage-dependence activation and steady-state inactivation is shown in the two insets in panel *A* and *C*, respectively. *D*, box plot summary of $V_{1/2}$ for voltage-dependence of steady-state inactivation (voltage at which 50% channels are closed) in the indicated experimental groups. Data are mean \pm S.E.; * $p < 0.05$.

Intrinsic Fluorescence Spectroscopy Confirms a Key Role of V160 in the FGF14:Nav1.6 Complex– Our molecular modeling, LCA, and patch-clamp data indicate that the V160 residue in FGF14 plays a unique and crucial role in modulating Nav1.6 currents. A single alanine switch at this site or a concomitant alanine mutation at Y158 and V160 are the only changes that can fully restore Nav1.6 currents to the GFP control level. K74 and I76, on the other hand, might work more synergistically and mutations at these sites cannot completely rescue changes in Nav1.6 currents mediated by FGF14. To provide correlative binding studies to our functional data, we used tryptophan-based fluorescence spectroscopy to probe energy transfer processes occurring in PPI. The tryptophan fluorescence spectra for individual FGF14^{WT}, FGF14^{K74A/I76A}, FGF14^{V160A} or Nav1.6-C tail proteins exhibited a λ_{max} at 332 nm. Combining the FGF14^{WT} and the Nav1.6 C-tail increased the fluorescence emission intensity by more than 2-fold without any shift in the λ_{max} , indicating strong protein complex formation without change in local environment. Both FGF14^{K74A/I76A} and FGF14^{V160A} mutants disrupted the interaction with Nav1.6-C-tail, but FGF14^{V160A} appeared the most impairing (**Fig. 3.12**). All mutant proteins had identical hydrodynamic radii as FGF14 as observed during gel filtration (data not shown). As evident from the emission spectra profiles (**Fig. 3.12**), none of the mutations lead to any major conformational changes in the protein complex indicating that reduction in fluorescence intensity arises from decreased binding affinity (Möller and Denicola, 2002).

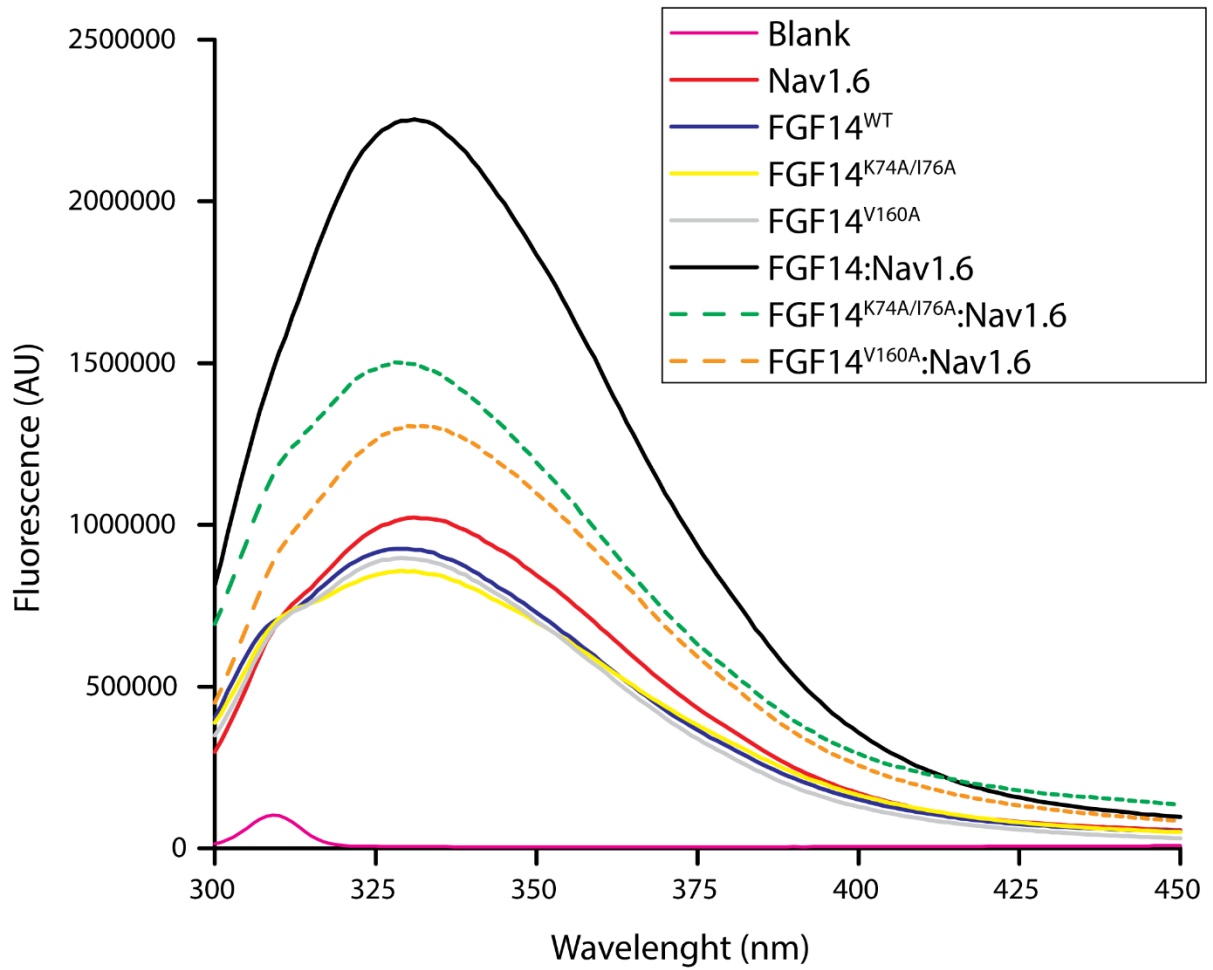


Figure 3.12. Intrinsic fluorescence emission spectra reveal reduced assembly of FGF14^{K74A/I76A} and FGF14^{V160A} to Nav1.6 C-tail. The fluorescence spectra of indicated purified proteins alone or combined; blank, Nav1.6, FGF14^{WT}, FGF14^{K74A/I76A}, FGF14^{V160A}, FGF14^{WT}:Nav1.6, FGF14^{K74A/I76A}:Nav1.6, and FGF14^{V160A}:Nav1.6 are shown as pink, red, blue, yellow, gray, black, green-dotted, and orange-dotted, respectively.

DISCUSSION

Previous studies have proposed that all iFGF might utilize a common interface for PPI with specific Nav isoform C-tail or other iFGFs (iFGF:iFGF dimer complexes); a hypothesis not yet directly tested. Through molecular, cellular, functional and structural studies focused on FGF14, a disease-associated protein (van Swieten et al., 2003; Verbeek et al., 2012; Wang et al., 2002; Xiao et al., 2007) and potent regulator of Nav1.6 channels (Laezza et al., 2009; Lou et al., 2005a), we identified significant structural-function similarity and divergence between the PPI interface within the FGF14:Nav1.6 complex and the FGF14:FGF14 dimer.

Using homology models we compared the FGF14:Nav1.6 and the FGF14:FGF14 complex (**Fig. 3.1, A-C**) and proposed K74, I76, L109, L116, R117, N157, Y158, Y159, L202, P205 and V208 at the FGF14 surface as potential hot-spots shared by the two complexes. These residues are part of the N-terminus, β -5, β -9, and β -12 strand of FGF14 and corresponding residues in FGF13 are already recognized as key structural amino acids (Goetz et al., 2009; Musa et al., 2015; Wang et al., 2012). Yet, our *in silico* models predict potential structural divergence at the FGF14 V160 residue of the β -9.

To provide experimental evidence to our model studies, we designed single, double and quadruple mutations at the *in silico* predicted hot-spots and tested FGF14 mutant activities using LCA to reconstitute PPI complexes in live cells (Ali et al., 2014; Hsu et al., 2015; Shavkunov et al., 2012; Shavkunov et al., 2015). LCA studies confirmed our *in silico* predictions showing that most mutations destabilized both the FGF14:Nav1.6 and the FGF14:FGF14 complex, but that the FGF14^{Y158N/V160N} double mutant led to opposite phenotypes depending on the structural context. The FGF14^{Y158N/V160N} mutant increased the stability of the FGF14:FGF14 dimer, but impaired the FGF14:Nav1.6 complex formation. Other amino acid residues that deserved attention were K74 and I76 in the N-terminus of the FGF14. Mutations at these residues strongly impaired the FGF14:Nav1.6 complex formation, but the effect was preserved in the FGF14 dimer complex, indicating a potential conserved role of the N-terminus at the two PPI interfaces.

This result prompted us to examine the role of Y158, V160, K74 and I76 in the FGF14:Nav1.6 and FGF14:FGF14 dimer complex using targeted alanine scanning mutations in combination with LCA. When

examined in the context of the FGF14:Nav1.6 complex, I76A and Y158A did not lead to any phenotypes (**Fig. 3.4, B** and **Fig. 3.6, B**), while K74A and/or V160A were sufficient to disrupt the FGF14:Nav1.6 complex formation (**Fig. 3.4, B** and **3.6, B**). In the FGF14^{WT}:Nav1.6 homology model we observed that K74 and V160 interact with E1884 and I1886 of Nav1.6, respectively, through salt-bridge and hydrophobic interactions. These findings corroborate the critical role of K74 and V160 residues in holding PPI interfaces through salt-bridge (Wang et al., 2012) and hydrophobic interactions respectively (Ochiai et al., 2011). Replacement of K74 and V160 with a smaller alanine residue might increase the distance between the two neighboring residues, resulting in a less favorable structural environment for PPI (Gregoret and Sauer, 1998). Importantly, we show that FGF14^{Y158A} or FGF14^{V160A} alone are not sufficient to disrupt the FGF14:FGF14 dimer formation. In the FGF14:FGF14 dimer homology model Y158 directly interacts with V208 of the neighboring monomer via hydrogen bonding (Jiang and Lai, 2002). Replacing Y158 with A is not sufficient to interfere structurally with the dimer, but if combined with V160A the stability of the β -9 strand might be weakened and monomer affinity reduced. Simultaneous mutations of Y158 and V160 to alanine can work synergistically to disrupt both the FGF14:Nav1.6 complex and the FGF14:FGF14 dimer, but the single V160A mutant has a different impact on the FGF14:FGF14 dimer versus the FGF14:Nav1.6 complex. Replacing both Y158 and V160 with an N in each FGF14 monomer increases FGF14:FGF14 dimer formation (**Fig. 3.2, D**). Both Y and N are polar residues; however, N is smaller than Y. Replacing both the bulky Y158 and the V160 residues in the two FGF14 monomers with a smaller N residue might facilitate interactions and increase stability of the mutant homodimer (FGF14^{Y158N/V160N}:FGF14^{Y158N/V160N}). These predictions and results are in agreement with previous *in silico* and LCA studies from our group (Ali et al., 2014).

At the N-terminus of FGF14 we found that K74 directly interacts with Y159 through a strong salt-bridge, and replacing K74 with an alanine disrupts this interaction, impairing the FGF14:FGF14 dimer formation. K74 and I76 acted synergistically in the FGF14:Nav1.6 complex formation, but not in the FGF14 dimer (**Fig. 3.6, A, B, E, F**) further supporting structural divergence at the two PPI interfaces.

Our molecular modeling and LCA studies were corroborated by whole cell-patch clamp electrophysiology. We investigated whether mutations at K74 and V160 had any functional impact on the well described effect of FGF14 on Nav1.6-mediated currents. In agreement with previous studies, we found that FGF14 suppresses transient peak I_{Na+} density and affects voltage-dependence of activation and steady-state inactivation compared to control. The single FGF14^{V160A} completely rescued peak current density to the control (GFP) (**Fig. 3.8**, and **Table 3.4**), whereas FGF14^{K74A} was only partially effective (**Fig. 3.10** and **Table 3.5**). I76 worked synergistically with K74 in that the FGF14^{K74A/I76A} mutant fully rescued Nav1.6-mediated currents to the control (GFP), supporting LCA results (**Fig. 3.6, B**). A more thorough analysis of Nav1.6 currents revealed a previously unreported effect of FGF14 on fast inactivation. This phenotype persisted with expression of FGF14^{V160A} and required double mutations at V160 and Y158 (FGF14^{Y158A/V160A} and FGF14^{Y158N/V160N}) to be abolished. Notably, single K74, I76 or double K74/I76 mutations were unable to abolish the changes in tau (**Fig 3.10, C-D**). Intrinsic fluorescence spectroscopy (Chen and Barkley, 1998; Drendall et al., 2010) based on purified proteins confirmed this model indicating that the single V160A mutation was more disruptive than K74A/I76A in impairing the FGF14:Nav1.6 complex formation.

Collectively, our studies demonstrate that amino acid residues located at N-terminal and at the β -9 of FGF14 are crucial for the FGF14:Nav1.6 complex and the FGF14:FGF14 dimer formation. Yet, the V160 residue is a point of divergence between the two complexes and is required for the full FGF14 functional activity toward Nav1.6 channels. Although V160 is conserved in other iFGF, its role varies depending on the structural environment provided by specific iFGF and Nav channel isoforms. In the FGF13:Nav1.5 complex, for instance, the Y98 (the FGF13 residue corresponding to FGF14 Y158) appears to have a more prominent role in the PPI complex formation, suggesting high precision and fidelity at each iFGF:Nav channel complex interface (Wang et al., 2012). Chemical probes that could leverage these unique structure-function features might provide an unprecedented opportunity for targeted interventions against excitability-driven brain and heart pathologies.

Acknowledgments – We thank Dr. Neli Panova for technical support, Dr. Miroslav Nenov for his critical feedback on analyzing patch-clamp data and reviewing the manuscript. The authors acknowledge the Sealy Center for Structural Biology and Molecular Biophysics at the University of Texas Medical Branch at Galveston for providing research resources and Dr. Heather Lander for proof reading the manuscript. This work was supported by R01MH095995 (FL) and the John Sealy Memorial Endowments Funds (FL) and a training fellowship from the Keck Center for Interdisciplinary Bioscience Training of the Gulf Coast Consortia NIGMS Grant No.1 T32 GM089657-04 (SRA).

Conflict of interest – The authors declare no conflict of interest.

Author contributions – Syed Ali designed and performed LCA, western blot, and patch-clamp electrophysiological experiments, analyzed data, built homology models and wrote the manuscript. Aditya Singh purified proteins, performed intrinsic fluorescence experiments and wrote the manuscript. Fernanda Laezza designed and supervised the work and the analysis and interpretation of the data and wrote the manuscript. All authors read and approved the final version of the manuscript.

Chapter 4

The following chapter was published to the CNS & Neurological Disorders - Drug Targets (October, 2014) under the title “**Modulation of the FGF14:FGF14 homodimer interaction through short peptide fragments.**”

Written permission was taken from the CNS & Neurological Disorders - Drug Targets journal to use this article as a chapter in my dissertation.

Modulation of the FGF14:FGF14 homodimer interaction through short peptide fragments

Syed Ali¹, Alexander Shavkunov¹, Neli Panova¹, Svetla Stoilova-McPhie^{2, 3*} and Fernanda Laezza^{1, 3, 4, 5*}

Department of Pharmacology & Toxicology¹, Department of Neuroscience and Cell Biology³, Sealy Center for Structural Biology and Molecular Biophysics³, Center for Neurodegenerative Diseases⁴, Center for Addiction Research⁵, The University of Texas Medical Branch, Galveston, TX 77555, USA

***Corresponding Authors:**

Dr. Fernanda Laezza

Department of Pharmacology & Toxicology

The University of Texas Medical Branch

301 University Boulevard

Galveston, 77555, Texas, USA

Phone: 001:409:772:9672

Fax: 001:409:772:9642

felaezza@utmb.edu

Dr. Svetla Stoilova-McPhie

Department of Neuroscience & Cell Biology

The University of Texas Medical Branch

301 University Boulevard

Galveston, 77555, Texas, USA

Phone: 001:409:747-2159

Fax: 001:409:747-2200

svmcphie@utmb.edu

Abstract

Fibroblast growth factor 14 (FGF14) is a member of the intracellular FGF (iFGFs) family and a functionally relevant component of the neuronal voltage-gated Na⁺ (Nav) channel complex. Through a monomeric interaction with the intracellular C-terminus of neuronal Nav channels, FGF14 modulates Na⁺ currents in an Nav isoform-specific manner serving as a fine-tuning regulator of excitability. Previous studies based on the highly homologous FGF13 homodimer crystal structure have proposed a conserved protein:protein interaction (PPI) interface common to both Nav channel binding and iFGF homodimer formation. This interface could provide a novel target for drug design against neuronal Nav channels. Here, we provide the first in-cell reconstitution of the FGF14:FGF14 protein complex and measure the dimer interaction using the split-luciferase complementation assay (LCA). Based on the FGF14 dimer structure generated *in silico*, we designed short peptide fragments against the FGF14 dimer interface. One of these fragments, FLPK aligns with the pocket defined by the β 12-strand and β 9 loop, reducing the FGF14:FGF14 dimer interaction by 25% as measured by LCA. We further compared the relative interaction strength of FGF14 wild type homodimers with FGF14 hetero- and homodimers carrying double N mutations at the Y158 and V160 residues, located at the β 9 loop. The Y158N/V160N double mutation counteracts the FLPK effect by increasing the strength of the dimer interaction. These data suggest that the β 12 strand of FGF14 might serve as scaffold for drug design against neuronal FGF14 dimers and Nav channels.

Keywords

Fibroblast growth factors, hot-spots, protein:protein interaction, split-luciferase assay, voltage-gated sodium channels, peptides

INTRODUCTION

The pore-forming α subunit of the voltage-gated Na^+ (Nav) channel (Nav1.1-Nav1.9) provides the basis for excitability in neurons and cardiac cells. Upon membrane depolarization, these channels open, inactivate and subsequently close allowing a rapid influx of Na^+ ions that mediate the rising and the initial decay phase of the action potential (Catterall, 2014; Catterall et al., 2005a; Catterall et al., 2005b; Denac et al., 2000; Savio-Galimberti et al., 2012). In the brain, up- or down-regulation of specific Nav channel α isoforms are associated to a plethora of channelopathies and neurological disorders, including epilepsy, neurodegeneration, demyelinating disorders, migraine, post-traumatic brain injury, and mental illnesses (Catterall et al., 2008; Mantegazza et al., 2010; Roberts, 2006; Waxman et al., 2002), diseases that are all in need of targeted therapeutics. Compounds targeting Nav channels are widely used in the clinical setting, but the lack of Nav isoform specificity of these drugs is a source of side effects and remains a significant barrier in neuropharmacology (Nouette-Gaulain et al., 2012; Silos-Santiago, 2008; van Rooij et al., 2013). More specific compounds targeting non-conserved channel domains are therefore highly desirable.

Native Nav channels are found in complex with multiple accessory proteins bound to the intracellular domains of the pore-forming α -subunit (Chahine et al., 2005; Leterrier et al., 2010; Savio-Galimberti et al., 2012). However, only few of these protein-protein interactions (PPI) produce functional outcomes on Na^+ currents and cell firing. Among those are the PPI complexes formed by the iFGFs with the C-terminal tail of Nav channels (Goetz et al., 2009; Laezza et al., 2007; Laezza et al., 2009; Lou et al., 2005b; Shavkunov et al., 2013a; Wang et al., 2012). The iFGFs, including FGF11-FGF14, are highly homologous in sequence (~45%) and fold, consisting of a well-conserved 12-stranded β -trefoil structure (Goetz et al., 2009; Olsen et al., 2003). Despite this degree of homology, though, the iFGF regulatory effect on Na^+ currents is factor-dependent and specific for each Nav channel isoform (Goldfarb, 2005; Olsen et al., 2003). This functional specificity suggests non-conserved structural properties at each iFGF:Nav pair interface placing the iFGFs in a category of promising molecular targets for the development of new Nav isoform specific drugs (Stoilova-McPhie et al., 2014).

In addition to forming high-affinity monomeric complexes with the Nav channel C-tail, iFGFs can exist as homodimers. *In vitro* structure-function studies based on purified proteins have proposed a conserved interface mediating both iFGF:iFGF and iFGF:Nav channel complexes (Goetz et al., 2009). Because of this structural overlap, the iFGF monomer interface reconstituted from full length iFGF proteins could serve as an accurate template for designing peptides and/or small molecules targeting the iFGF:Nav channel complex.

In the central nervous system (CNS), FGF14 is highly abundant and is required for action potential firing and synaptic plasticity of neurons (Xiao et al., 2013). In heterologous expression systems, FGF14 has been shown to control Na⁺ current amplitude and voltage-dependence of activation and/or steady-state inactivation of the neuronal Nav1.1, Nav1.2, and Nav1.6 channels (Laezza et al., 2009; Lou et al., 2005a). In animal models, deletion, mutations or overexpression of FGF14 disrupt Nav channel sub-cellular targeting, modify Na⁺ currents and alter neuronal excitability in the hippocampus and cerebellum (Laezza et al., 2007; Laezza et al., 2009; Lou et al., 2005b; Xiao et al., 2007). In humans, inherited mutations of FGF14 have been linked to spinocerebellar ataxia 27 (SCA27), a complex motor-cognitive disorder (Chen et al., 2012; Coebergh et al., 2013; van Swieten et al., 2003), and SNPs in the FGF14 gene linked to schizophrenia (Jungerius et al., 2008) and depression (Verbeek et al., 2012), indicating a critical role of FGF14 in the brain. FGF14-based interventions modulating the FGF14:Nav channel complex could therefore be of great therapeutic value for diseases of the CNS.

To gain structure-function insights on the FGF14:FGF14 dimer that could guide future interventions against neuronal Nav channels, we have combined the split-luciferase complementation assay (LCA) with molecular modeling and *in silico* studies. We designed FGF14 model-based peptide fragments inhibiting the FGF14:FGF14 dimer interaction and tested the effect of these peptide fragments on the FGF14:FGF14 homodimer interaction when reconstituted in live cells. *In silico* studies predict that one short peptide fragment, FLPK, aligns to the β 12 strand and β 9 loop region at the FGF14 monomer:monomer interface, reducing significantly the dimer interaction. The FLPK effect is abolished upon N double

mutations of the Y158 and V160 from the β 9 loop in both hetero- and homo FGF14 mutant dimers. Previous studies have shown that these same Y158 and V160 residues modulate the FGF14:Nav1.6 complex formation (Shavkunov et al., 2012), confirming structural overlap between iFGF homodimers and iFGF:Nav channel interfaces and suggesting that the β 12 strand and the β 9 loop region of FGF14 might be part of a PPI pocket that could serve as target for drug development against Nav channels.

RESULTS

Reconstitution of the CLuc-FGF14:FGF14-NLuc Homodimer Complex in Live Cells

We applied the split-luciferase complementation assay (LCA) in live cells to reconstitute the FGF14:FGF14 homodimer protein complex in a physiological microenvironment. **Fig. 4.1, A** illustrates the molecular engineering strategy used to generate the two constructs bearing the complementary N-terminus (NLuc) and C-terminus (CLuc) fragments of the *Photinus* Firefly luciferase (Luker and Piwnica-Worms, 2004; Shavkunov et al., 2012) fused to the FGF14 wild type molecule in either 5' or 3' position (CLuc-FGF14 and FGF14-NLuc respectively). In this reporter system, the two luciferase fragments are brought in close proximity by the corresponding FGF14 protein driving full reconstitution of the luciferase enzyme and consequent light production upon addition of the D-luciferin substrate (**Fig. 4.1, B**). The resulting luminescence signal is as a measure of relative binding strength and/or stability of the protein complex. The CLuc-FGF14 and FGF14-NLuc constructs were transiently expressed in HEK293 cells using lipid-based transfection methods. Upon initiation of the assay by addition of the substrate, a strong luminescence signal (RLU), reaching a steady-state maximal value after ~12-15 minutes and persisting to the end of each experiment, was detected indicating a robust assembly of the FGF14:FGF14 dimer complex in live cells (**Fig. 4.1, C**, n=10 independent experiments, black circle). In contrast, the luminescence response produced by cells transfected with CLuc-FGF14 alone was negligible and used as a background reference (**Fig. 4.1, C-D**, open circles). These results indicate that LCA is a suitable method for the reconstitution and characterization of the FGF14:FGF14 homodimer in the physiological microenvironment of living cells.

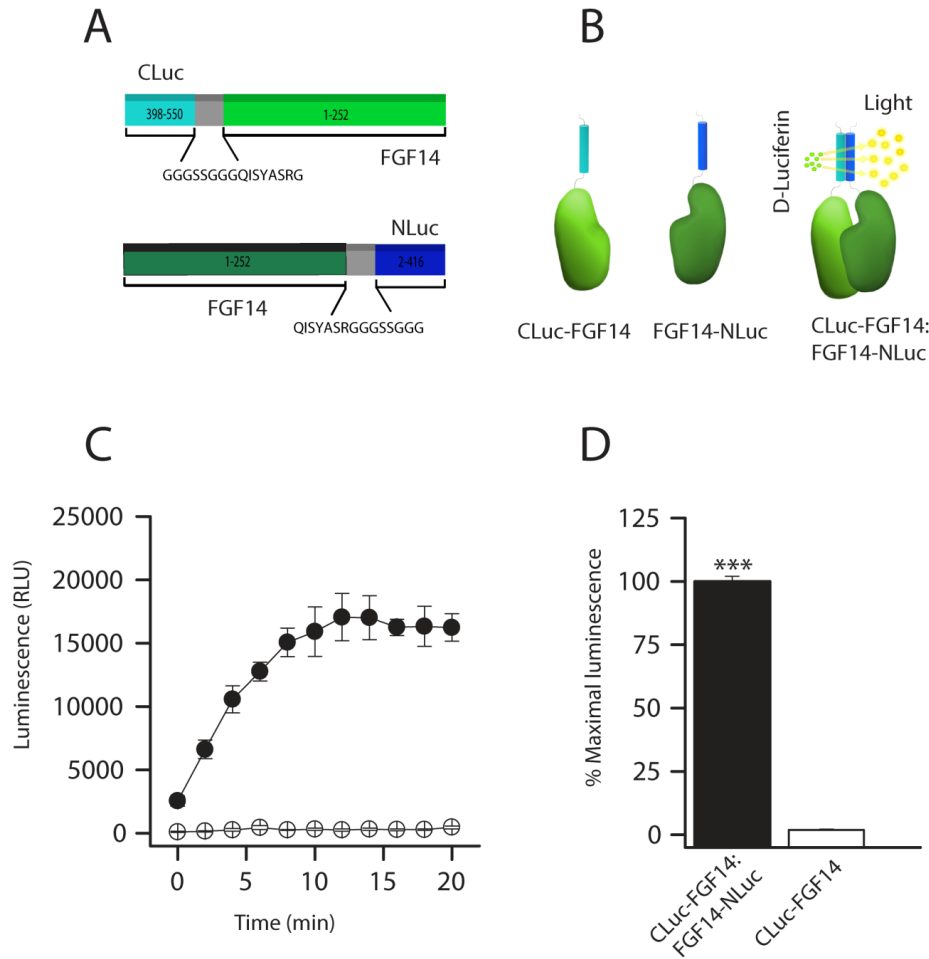
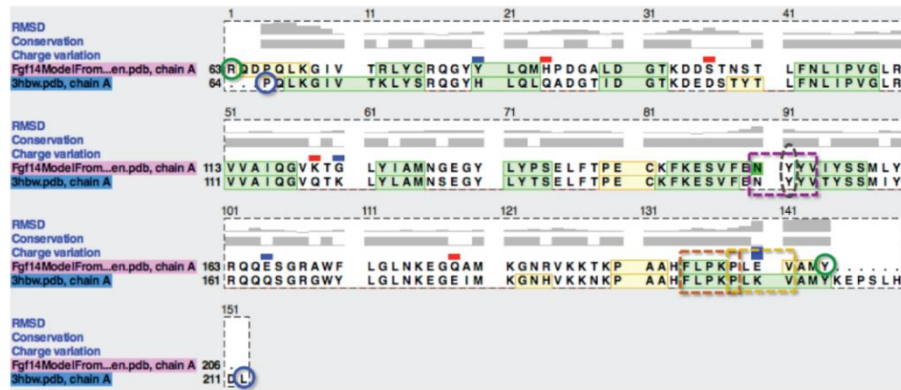


Fig. 4.1. In-cell reconstitution of the FGF14:FGF14 homodimer complex using the split-luciferase complementation assay (LCA). **A.** Schematic representation of FGF14 constructs expressing either the CLuc (398-550) or the NLuc (2-416) fragment of firefly *Photinus pyralis* luciferase. A flexible linker (grey) spaces the FGF14 protein from the luciferase fragments. **B.** Spontaneous association of CLuc-FGF14 and FGF14-NLuc brings in close proximity the two halves of the luciferase fragments, allowing the enzyme to reconstitute and to emit light in the presence of the D-luciferin substrate. **C.** Luminescence (RLU) corresponding to the assembly of CLuc-FGF14 and FGF14-NLuc (black circle) is detected in HEK293 cells upon addition of D-luciferin at time zero (n=10 independent experiments). Cells expressing CLuc-FGF14 alone (open circle) produced negligible luminescence signal. **D.** Summary bar graph represents % maximal luminescence response of the FGF14:FGF14 homodimer versus background. Data are mean \pm SEM. The statistical significance between the two groups was assessed using by Student's *t*-test, n=10, *** p <0.001.

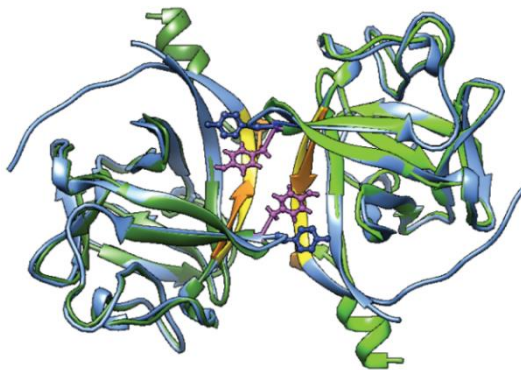
Molecular Model of the FGF14:FGF14 Dimer

To gain structural insights into the FGF14 dimer interface, we generated a homology model of the FGF14 dimer from the FGF14 monomer model proposed by Van Swieten (van Swieten et al., 2003) and the FGF13 homodimer crystal structure as a template (Goetz et al., 2009). Two FGF14 monomers were each aligned by sequence and structure to the FGF13 monomers in the FGF13 dimer crystal structure. The FGF14 dimer structure was further energy minimized to optimize the monomer:monomer interface (**Fig. 4.2, B-C**). From the 146 common amino acid residues resolved in the FGF13 homodimer crystal structure and common for both FGF13 and FGF14 structures only 28 are not conserved, giving an 81% sequence identity between the two molecules (**Fig. 4.2, A**). All the amino acid residues that are part of the β 9 loop holding the Y158 and the V160 residues are conserved, pointing to a stabilizing function of the loop in both the FGF13 and FGF14 homodimer (**Fig. 4.2, B-C**). Comparison of the FGF13 and FGF14 dimer models shows that Y158 in FGF14 and Y151 in FGF13 are extending at the monomer:monomer interface holding the dimers macromolecular organization and structure. The orientation of the amino acid side chain of the FGF14:Y158 and FGF13:Y151 differs, indicating a flexibility element which can cause structural divergence between the two iFGFs (**Fig. 4.2, B**).

A



B



C

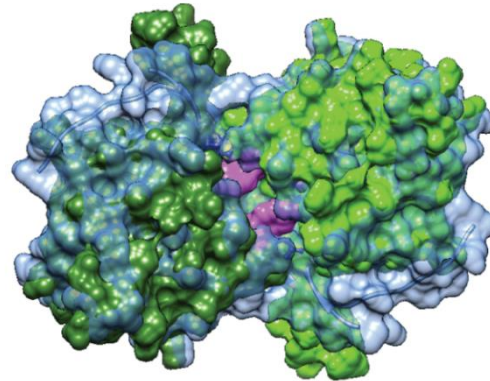


Fig. 4.2. Model of the FGF14 homodimer. **A.** Sequence and structure alignment of the FGF14 homodimer with the FGF13 homodimer crystal structure as a template. The FGF13 N terminal – R64 and C terminal – L212 are indicated with blue circles. The FGF14 N terminal – P63 and C terminal – Y206 are indicated with green circles. The FGF14 and FGF13 sequences FLPK, PLEV and NYV are indicated with dashed boxes in orange, yellow and purple, respectively. The position of FGF14-Y158 and corresponding FGF13-Y151 from the β 9 loop are indicated with a dark grey dashed oval. The conservation and charge variation (red is negative, blue is positive) of the FGF14 and FGF13 amino acid residues, and the root mean square deviation (RMSD) between the C_{α} atoms of the FGF14 and FGF13 polypeptide chains are shown. **B.** Ribbon representation of the FGF14 dimer structure (green) superimposed with the FGF13 dimer crystal structure (3hbw, blue). The FGF14 β 12 strand is indicated in orange and the FGF13 β 12 strand in yellow. The FGF14 Y158 and V160 residues side chains at the monomer:monomer interface are shown in magenta and purple, respectively. The corresponding FGF13 Y151 and V153 residues side chains are shown in blue and magenta, respectively. **C.** Surface representation of the FGF13 homodimer (light blue) superimposed with the surface representation of the FGF14 homodimer in green. The FGF14 - Y158 residue surface, defining the monomer:monomer interface is colored in magenta. Part of the V160 residue side chain exposed at the FGF14 monomer:monomer interface is visible and colored in purple.

Model-Based Peptide Design

To further characterize the FGF14:FGF14 interaction interface we used the molecular model of the FGF14 dimer as a template to design three short peptides (4 amino acids long) against the FGF14 β 12 C-terminal strand and the β 9 loop at the monomer:monomer interface. The FLPK and PLEV peptides correspond to two specific consecutive areas of the β 12 sheet (FLPKPLEV) at the monomer:monomer interface, while the EYYV mimics the exposed YYV sequence of the β 9 loop (**Fig. 4.3, A**). As the FGF14 monomers are organized head-to-toe in the dimer structure (**Fig. 4.2, B**), the designed short peptides are expected to compete with the monomer:monomer interaction by blocking the respective pockets on the FGF14 dimer interface.

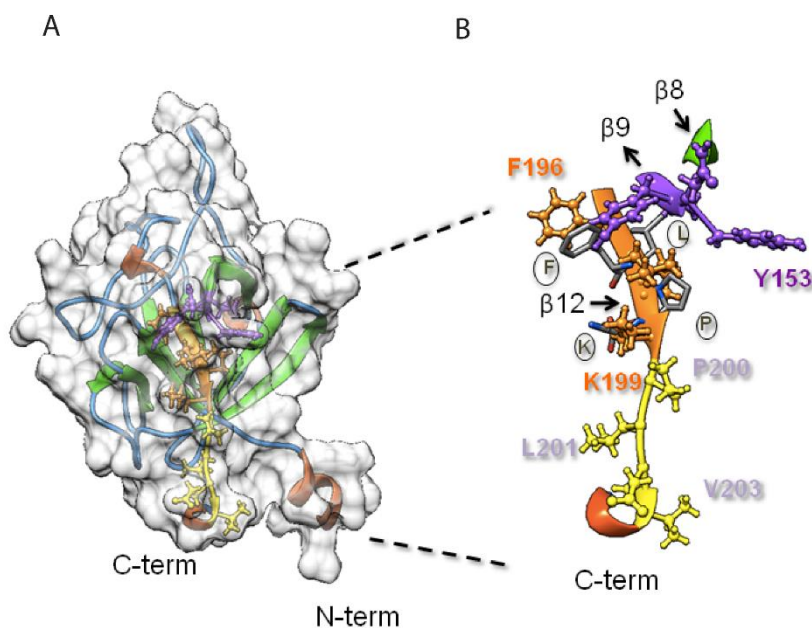


Fig. 4.3. Peptide mapping on the FGF14 surface. **A.** Mapping of the FLPK (orange), PLEV (yellow) and EYYV (purple) sequences on the FGF14 structure. The FGF14 secondary structure is presented as β strands in green, random coils in light blue and α -helices in orange. The N- and C-termini are indicated. The FGF14 surface is shown in light grey. **B.** Alignment of the FLPK peptide (dark grey) to the FGF14 β -12 strand. The position of the FLPK residues is indicated with circled letters. The FLPK (orange), PLEV (yellow) and EYYV (purple) sequence of FGF14 are indicated.

In-cell activity of small peptides against the FGF14:FGF14 dimer

FLPK, PLEV and EYYV were synthesized in their acetylated form and tested for their activity against the FGF14 dimer assembly in cells. To ensure efficient intracellular delivery, peptides were introduced into cells at the time of transfection using lipid-based methods. HEK293 cells expressing CLuc-FGF14 and FGF14-NLuc along with individual peptide fragments were assayed with LCA (**Fig. 4.4, A**). The most significant reduction of the luminescence response occurred in the presence of 10 μ M FLPK (75 ± 3 %, $n=20$, *** $p < 0.001$, one way ANOVA, *post-hoc* Bonferroni), while mild, but non-statistically significant effects were detected with 10 μ M PLEV (87 ± 4 %, $n= 28$ * $p=0.080$), and with 10 μ M EYYV (89 ± 4 %, $n= 24$, $p=0.28$) compared to control cells (**Fig. 4.4, B**). To rule out non-specific interactions of these peptides with the luciferase enzyme, the peptides were tested against full length firefly luciferase. HEK293 cells were transiently transfected with pLG3-CMV-full length firefly luciferase and peptides delivered while performing transfection. None of these peptides had any statistically significant effect on the firefly luciferase activity compared to control (FLPK, 95 ± 18 %, $p=0.804$, **Fig. 4.4, C**; PLEV, 75 ± 8 %, $p=0.0478$; EYYV, 99 ± 14 %, $p=0.96$; for all groups $n=6$, data for PLEV and EYYV are not shown). To further support the notion that FLPK peptide can reduce the FGF14:FGF14 dimer formation, we have performed co-immunoprecipitation from lysates of HEK293 cells transiently transfected with FGF14-GFP and FGF14-6xmyc and treated with either FLPK peptide (10 μ M, dissolved in H₂O) or vehicle (H₂O). The FGF14-6xmyc:FGF14-GFP complex was co-immunoprecipitated using anti-myc agarose beads. As illustrated in **Fig. 4.4 D**, the fraction of FGF14-GFP co-immunoprecipitating with FGF14-6xmyc was significantly lower in cells treated with FLPK peptide compared to vehicle (~44% compared to 100% control). Altogether, these results corroborate the hypothesis that FLPK can interfere with the FGF14 dimer formation.

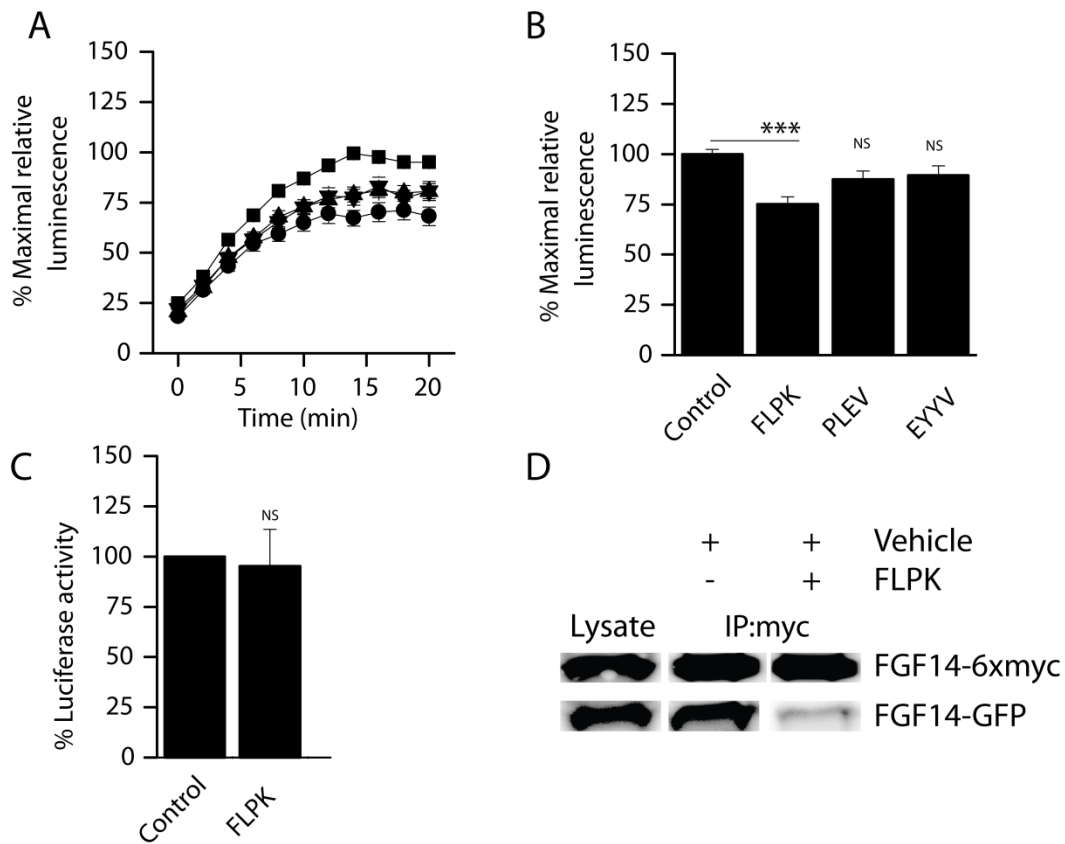


Fig. 4.4. Effect of FGF14 model-based peptides on the FGF14:FGF14 homodimer assembly. **A.** Percent of maximal luminescence response corresponding to the assembly of CLuc-FGF14 and FGF14-NLuc in the presence of FLPK (circle), PLEV (inverted-triangle), EYYV (upward-triangle), and control (square) detected in HEK293 cells upon addition of D-luciferin at time zero. **B.** Summary bar graph represents % maximal luminescence response corresponding to the assembly of CLuc-FGF14 and FGF14-NLuc in the presence of either PBS control ($100 \pm 2\%$), $10\ \mu\text{M}$ FLPK ($75 \pm 3\%$), $10\ \mu\text{M}$ PLEV ($87 \pm 4\%$), $10\ \mu\text{M}$ EYYV ($89 \pm 4\%$). Data are mean \pm SEM. The statistical significance between the three groups was assessed using one-way ANOVA *post-hoc* Bonferroni ($n=20-28$ experiments, $***p<0.001$). **C.** HEK293 cells were transiently transfected with full-length firefly luciferase with FLPK ($10\ \mu\text{M}$) or vehicle (PBS) and expressed as % luciferase activity compared to control (PBS); data are mean \pm SEM representing four replicates from six independent experiments ($n=6$). Statistical significance between the four groups was assessed using student *t*-test; ns=non-significant. **D.** Western blot analysis of cell lysate and co-immunoprecipitated fraction (IP: myc) of FGF14-6xmyc and FGF14-GFP. Treatment with $10\ \mu\text{M}$ FLPK reduced the FGF14-6x-myc : FGF14-GFP complex formation.

***In Silico* Modeling of FLPK**

Of the three designed peptides against the 12 amino acid residues of the β 9 loop and the β 12 strand of the FGF14 dimer interface, FLPK had the most pronounced effect on the monomer:monomer interaction. Therefore, we proceeded to define the pockets at the FGF14 dimer interface adjacent to the β 12 strand FLPK sequence (**Fig. 4.3, A**). To achieve this we aligned the FLPK sequence to the FGF14 dimer interface by creating a script in the Match-align algorithm plug-in of UCSF Chimera (Meng et al., 2006; Pettersen et al., 2004) (**Fig. 4.3, B**). In our model, the FLPK fragment aligned well in the region defined by the β 9 loop and the FLPK sequence of the β 12 strand, which implies that the pocket defined by Y158, Y154, V160 and by F196, L197, P198, K199 might be at the FGF14 dimer interface. Thus, FLPK might act as a competitive inhibitor targeting the β 9 loop and the β 12 strand preventing the FGF14 dimer formation. This prediction is confirmed by our in cell studies showing a significant reduction of ~25% in the monomer:monomer interaction upon FLPK treatment (**Fig. 4.4, A-B**).

Impact of Mutations at Y158 and V160 on FGF14:FGF14 Homodimer Stability

Previous structure-function studies derived from the crystal structure of the FGF13 dimer propose that Y151 and V153 located at FGF13 are part of the surface conserved in the core domain of all iFGFs that mediates PPI at both the iFGF:iFGF and the iFGF:Nav channel interfaces (Goetz et al., 2009). To examine the impact of Y158 and V160 on the FGF14 dimer assembly, CLuc-FGF14 and FGF14-NLuc constructs bearing Y158N/V160N double mutations (**Fig. 4.5, A**) were transiently transfected in HEK293 cells to form either FGF14^{Y158N/V15N}:FGF14^{Y158N/V160N} homodimers or FGF14^{Y158N/V160N}:FGF14 heterodimers (**Fig. 4.5, B**). Both hetero- and homodimer mutants could be reconstituted in live cells giving rise to a strong luminescence signal (**Fig. 4.5, B-C**). One way ANOVA with *post-hoc* Bonferroni comparisons of RLU across the three different pairs of constructs, revealed that the strength of interaction for the FGF14^{Y158N/V160N}:FGF14 heterodimer was not different from the FGF14:FGF14 dimer complex ($109 \pm 8\%$, $n=16$ independent experiments, $p=0.08$), while the one of the FGF14^{Y158N/V160N}:FGF14^{Y158N/V160N} homodimer was significantly increased ($136 \pm 8\%$, $n=11$, *** $p<0.001$, **Fig. 4.5, C**). To rule out that the

observed changes in luminescence across the experimental groups were driven by changes in the protein expression level, Western blot analysis was performed on total cell lysates from cells transfected with either hetero- or homodimer FGF14 mutants. As shown in **Fig. 4.5, D**, an anti-goat luciferase antibody that recognizes both CLuc- and NLuc fragments revealed two bands corresponding to a predicted molecular weight of either ~75 kD for the FGF14 constructs carrying the NLuc- fragment or ~50 kD for the FGF14 constructs carrying the CLuc- fragment. The band intensity corresponding to the two fragments was visually indistinguishable across conditions and quantification of CLuc/NLuc band intensity showed no statistical difference across the three conditions (n=4, p=0.88, one way ANOVA, **Fig. 4.5, D**). These results indicate that Y158 and V160 are “hot-spots” and play a key role in the stability and structural organization of the FGF14:FGF14 dimer interface as shown by increased interaction strength upon mutations of these residues. Furthermore, these data combined with previous results showing that the FGF14^{Y158N/V160N} double mutation affects the FGF14:Nav1.6 complex assembly (Shavkunov et al., 2012), confirm the hypothesis that the FGF14:FGF14 and the FGF14:Nav1.6 interfaces overlap.

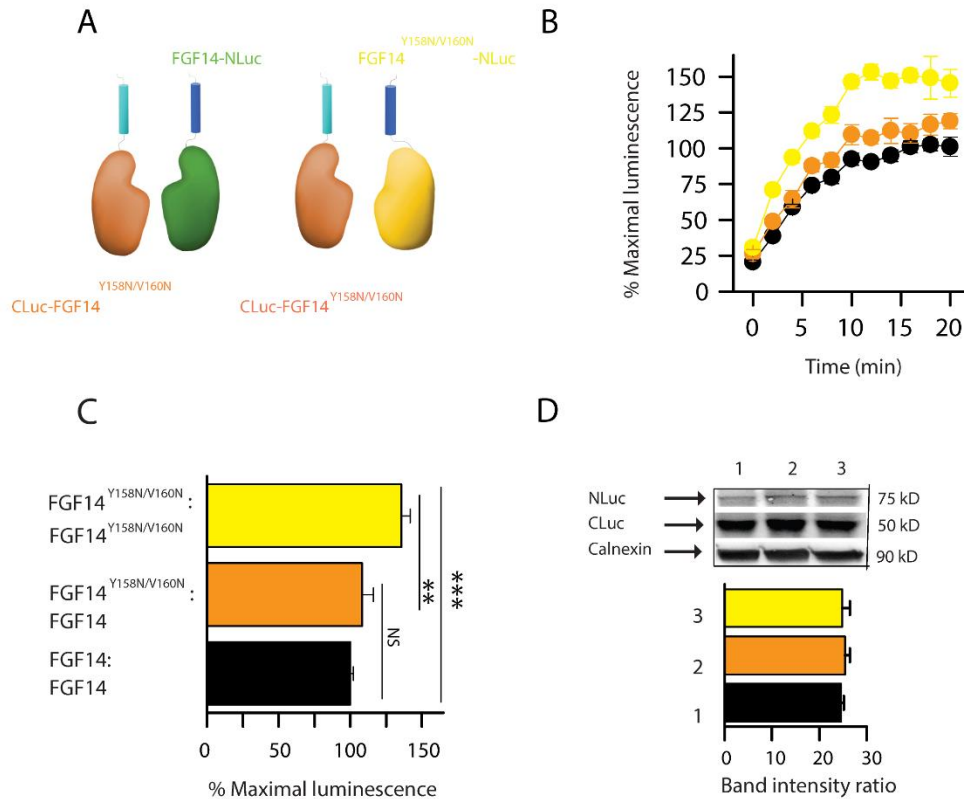


Fig. 4.5. Y158N/V160N mutations modify the FGF14:FGF14 homodimer formation. **A.** A schematic representation of the CLuc- and NLuc- constructs carrying the Y158N/V160N mutations is illustrated. **B.** Luminescence (RLU) corresponding to the assembly of CLuc-FGF14 and FGF14-NLuc (black circles), CLuc-FGF14^{Y158N/V160N} and FGF14-NLuc (orange circles), and CLuc-FGF14^{Y158N/V160N} and FGF14^{Y158N/V160N}-NLuc (yellow circles) is detected in HEK293 cells upon addition of D-luciferin at time zero (n=11-16 independent experiments). **C.** Summary bar graph represents % maximal luminescence response of each pair normalized to the CLuc-FGF14:FGF14-NLuc homodimer response. Data are mean \pm SEM. The statistical significance between the three groups was assessed using Kruskal–Wallis one-way ANOVA on ranks with *post-hoc* Dunn’s method (n=11-17 independent experiments, ** p <0.01; *** p <0.001). **D.** Western blots of whole-cell extracts (equal amount of protein per lane) from cells transfected with CLuc-FGF14 wild type + FGF14-NLuc (lane 1, from left), CLuc-FGF14^{Y158N/V160N} + FGF14-NLuc (lane 2), CLuc-FGF14^{Y158N/V160N} + FGF14^{Y158N/V160N}-NLuc (lane 3). Western blots were probed with a polyclonal anti-luciferase antibody which recognizes different epitopes on the NLuc and CLuc fragments (~75 kD and 50 kD, respectively); immunodetection of calnexin is used as loading control. **E.** Densitometry analysis was determined by taking the ratio of CLuc and NLuc band intensity. Calnexin was used as loading control; the expression level of CLuc-FGF14^{Y158N/V160N} was comparable across conditions one-way ANOVA (n=4, p values = 0.88); data are mean \pm SEM.

Role of the Y158 and V160 residues at the FGF14:FGF14 Dimer Interface

The mechanism of action of the Y158N and V160N mutations at the FGF14 dimer interface was also predicted *in silico* by creating models of the FGF14 hetero- and homodimer mutants. In **Fig. 4.6 A**, the ribbon and surface representation of FGF14 wild type are shown. Y158 and V160 residues are shown as magenta and purple. When the Y158N and V160N mutations are introduced only on one FGF14 monomer, the FGF14^{Y158N/V160N}:FGF14 monomer:monomer interface is not significantly disturbed due to the head-to-toe orientation of the monomers and the presence of the Y158 in the wild type monomer which preserves the heterodimer structure (**Fig. 4.6, B**). On the other hand, mutating Y158 and V160 in both FGF14 monomers heavily affects the dimer stability, resulting in a collapse of the structure seen as a tighter packing of the two monomers in the FGF14^{Y158N/V160N} homodimer (**Fig. 4.6, C**). This ‘tighter packing’ is due to the lack of the bulk tyrosine phenol ring in the Y158N mutation, which stabilizes the homodimer interface in the wild type FGF14. The V160N mutation further “smooths” the surface corresponding to the β 9 loop reinforcing the interaction between the two FGF14^{Y158N/V160N} monomers. The *in silico* model for the FGF14^{Y158N/V160N} homodimer correlates with the ~36% significantly increased interaction between the two monomers compared to the wild type dimer assessed by LCA (**Fig. 4.5, B-C**).

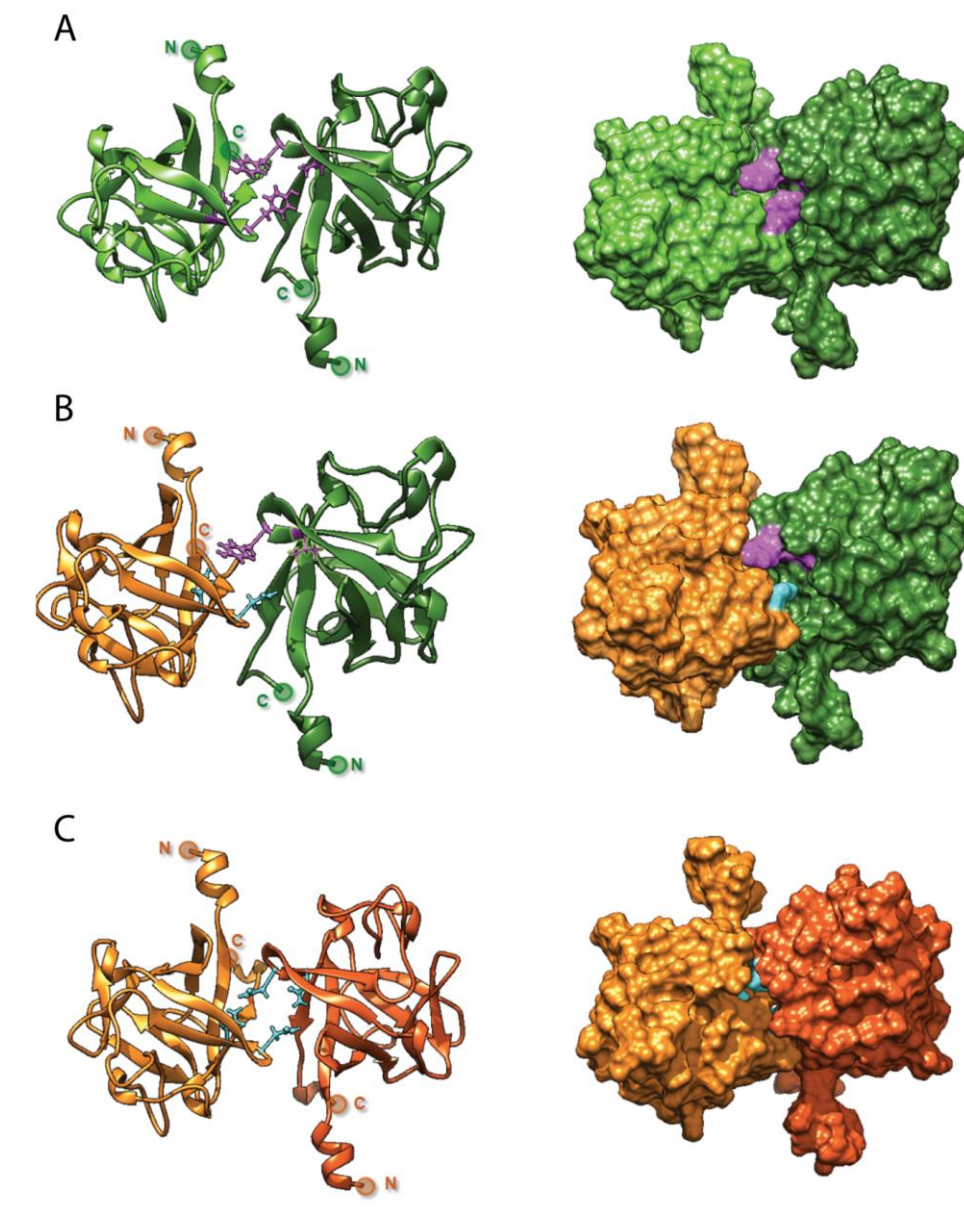


Fig. 4.6. Model of FGF14^{Y158N/V160N} hetero- and homodimer. **A.** Ribbon and surface representation of the FGF14:FGF14 homodimer structure after energy minimization. The two FGF14 wild type monomers are colored light (chain A) and dark green (chain B), respectively. The side chains/surface of the Y158 is colored in magenta and the one of V160 in purple, on both chains. **B.** Ribbon and surface representation of the FGF14^{Y158N/V160N}:FGF14 heterodimer structure. The FGF14^{Y158N/V160N} monomer (chain B) is colored in orange, and the FGF14 wild type monomer (chain A) is colored in light green. The Y158 and V160 on the FGF14 wild type monomer are colored in magenta, respectively. The side chains/surface of Y158N and V160N on the FGF14^{Y158N/V160N} monomer are colored in cyan. **C.** Ribbon and surface representation of the FGF14^{Y158N/V160N} homodimer structure in which the two monomers are colored in orange (chain A) and orange-red (chain B), respectively. The side chains/surface of the mutated Y158N and V160N is colored in cyan on both chains. All FGF14 homo and heterodimers are oriented the same way as in **Fig. 4.2**.

Effect of FLPK on FGF14 Homo- and Heterodimer Mutants

All three peptides were tested in cells for their effect on the FGF14 wild type homodimers, but only FLPK showed a significant activity inhibiting the FGF14 monomer:monomer interaction. Given that FLPK aligns in a pocket adjacent to the $\beta 9$ loop holding the Y158 and V160, one expectation is that the activity of FLPK would be influenced by the same N mutations that disrupt the FGF14 dimer organization (**Fig. 4.5, B-C**). To test this hypothesis, cells expressing the FGF14^{Y158N/V160N}:FGF14 heterodimer or the FGF14^{Y158N/V160N}:FGF14^{Y158N/V160N} homodimer with FLPK were processed for LCA. As illustrated in **Fig. 4.7**, FLPK was inactive against both the hetero- and the homodimer. The luminescence response detected from the FGF14^{Y158N/V160N}-FGF14 heterodimer and the FGF14^{Y158N/V160N}:FGF14^{Y158N/V160N} homodimer in the presence of FLPK was 90.8 ± 5.1 % and 98.3 ± 3.3 %, respectively, and both values were statistically different from the corresponding FGF14:FGF14 homodimer condition in the presence of FLPK (n=20, p<0.05 for FGF14^{Y158N/V160N}:FGF14 vs. n=12, p<0.01 for FGF14^{Y158N/V160N}:FGF14^{Y158N/V160N}). These results were complemented with the *in silico* modeling of the FLPK on the FGF14 interface shown in **Fig. 4.3**. The modeling predicts that FLPK obstructs the interaction of the Y158 from the $\beta 9$ loop of one FGF14 monomer with the opposing FGF14 in the homodimer (**Fig. 4.8**). Mutating the Y158 residue to N might reduce the accessibility of FLPK to this pocket creating a tighter interaction between the two monomers, thus preventing the effect of FLPK on the dimer assembly.

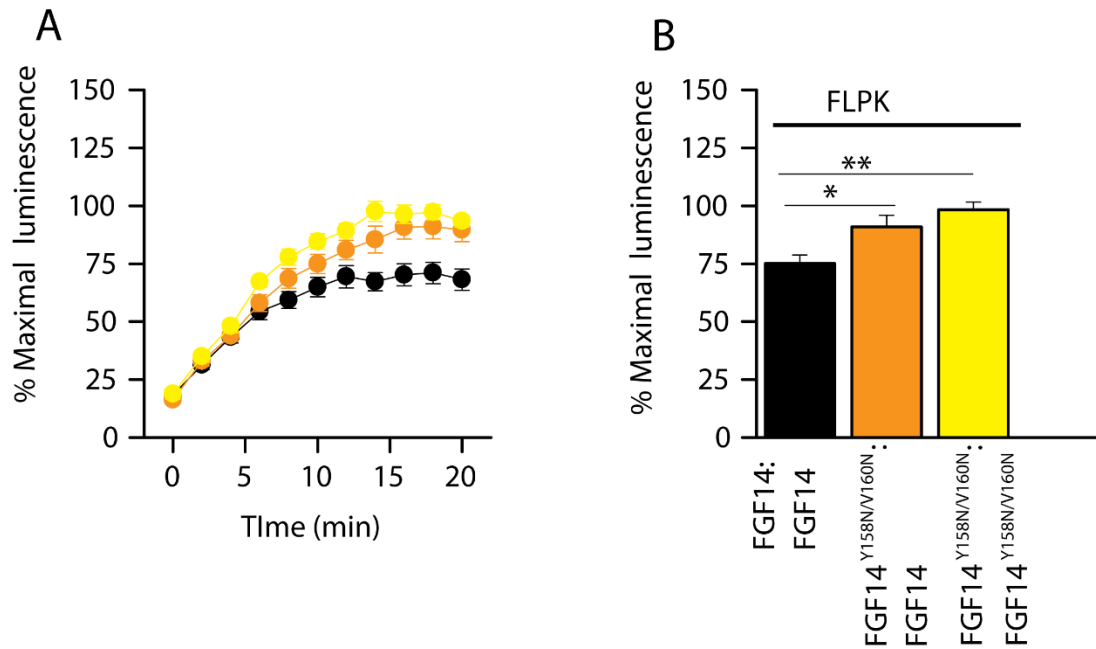


Fig. 4.7. The Y158N and V160N mutations prevent activity of FLPK. **A.** Luminescence (RLU) corresponding to the assembly of CLuc-FGF14 and FGF14-NLuc (black circles), CLuc-FGF14^{Y158N/V160N} and FGF14-NLuc (orange circles), and CLuc-FGF14^{Y158N/V160N} and FGF14^{Y158N/V160N}-NLuc (yellow circles) in the presence of FLPK is detected in HEK293 cells upon addition of D-luciferin at time zero. **B.** Summary bar graph represents % maximal luminescence response of each pair normalized to the corresponding dimer control (PBS) response. Data are mean \pm SEM. The statistical significance between the three groups was assessed using one-way ANOVA with *post-hoc* Bonferroni method (n= 16-20 experiments, * p <0.05; ** p <0.01).

A

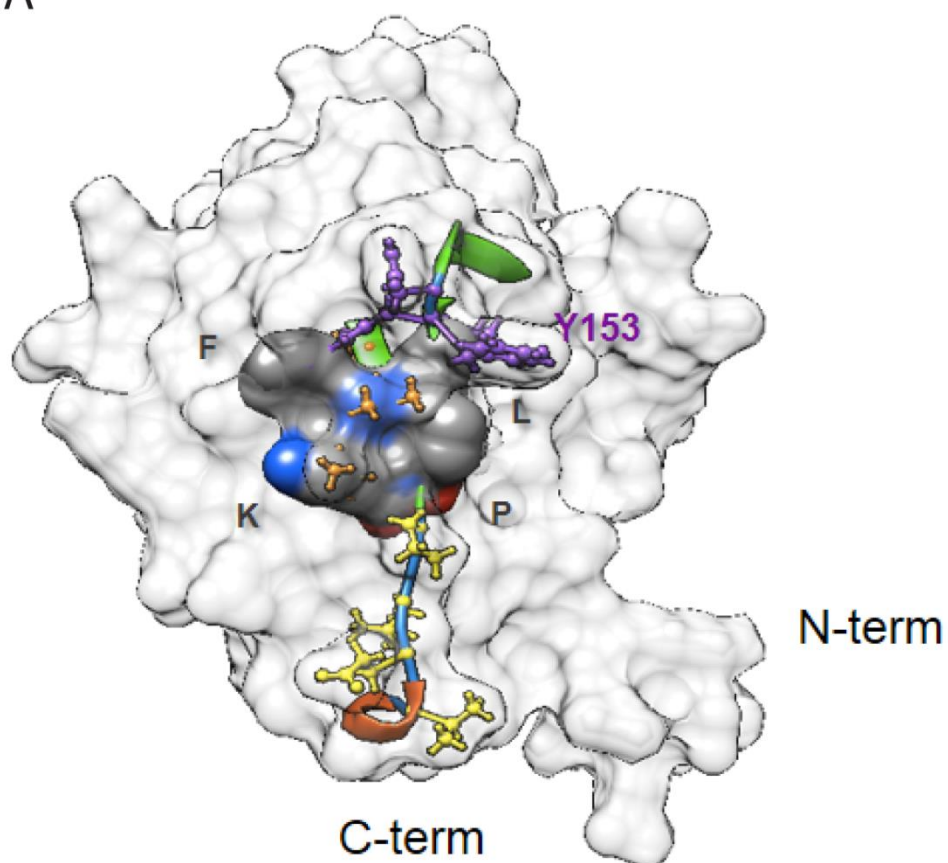


Fig. 4.8. FLPK peptide aligns to the FGF14 monomer interface. The FLPK peptide is presented as an electrostatic surface (positive red, negative–blue, neutral–dark grey). The FGF14 surface is in light grey.

DISCUSSION

In this study we characterize for the first time the FGF14:FGF14 homodimer interface by combining an in-cell approach designed to reconstitute the dimer complex in live cells with an *in silico* approach based on the FGF14 homodimer structure calculated with the FGF13 dimer crystal structure as a template. To identify potential critical regions at the FGF14:FGF14 interface we designed three short peptides, matching two consecutive areas on the β 12 strand (FLPKPLEV) and the adjacent β 9 loop (EYYV), which are located at the homodimer interface. These peptides were tested for in-cell activity with LCA and data showed that the FLPK peptide significantly reduces the formation of the FGF14 homodimer. In our homology model the FLPK β 12-strand mimic fragment aligned well in the region defined by the β 9 loop, which includes Y158 and V160.

To determine whether Y158 and V160 acted as “hot-spots” at the FGF14:FGF14 dimer and whether were required for FLPK activity, we examined the effect of the FGF14^{Y158N/V160N} double mutation on the FGF14:FGF14 homodimer stability and the impact of these mutations on the activity of FLPK. Using LCA we found that the conversion of Y158 and V160 into N increases the stability/relative binding strength of the two monomers presumably by inducing a tighter packed dimer. The role of the two Y158/V160 “hot spots” was further confirmed by comparing the strength of interaction of hetero- and homodimers carrying double Y158N and V160N mutations using *in silico* models and predicting that the β 9 loop encompassing Y158 and V160 and the FLPK sequence of the β 12 strand would be adjacent and critical for the FGF14 monomer:monomer interaction. Mutating both Y158 and V160 to N abolished the FLPK effect in cells indicating that its activity depends on these residues and suggesting a synergy of action between the β 12 area and the β 9 loop.

Introducing short peptide fragments that mimic the modeled FGF14 dimer interface and modulate the monomer:monomer interaction in cells further corroborates the idea that Y158/V160 of the β 9 loop and the β 12 strand of the FGF14 C-terminal tail are critical for the FGF14:FGF14 homodimer assembly and that are integral parts of the dimer interface. Furthermore, these results combined with previous studies

showing that Y158 and V160 affect the FGF14:Nav1.6 channel interaction (Shavkunov et al., 2012) and are “hot-spots” at this interface provide evidence of overlaps between the FGF14:FGF14 and the FGF14:Nav1.6 interfaces, confirming prior structural studies (Goetz et al., 2009; Shavkunov et al., 2012). Overall, these results identify the β 12-strand FLPK sequence and the β 9 loop containing Y158/V160 as modulatory PPI sites and potential druggable targets against the FGF14:FGF14 and the FGF14:Nav1.6 channel interface (Shavkunov et al., 2012).

We also observed a small, but not statistically significant effect of PLEV and EYYV on the FGF14 dimer. The EYYV and the PLEV sequences are structurally adjacent to the FLPK sequence on the FGF14:FGF14 dimer interface. Thus, longer peptides such as FLPKPLEV or YYVFLPKP or cyclic peptide derivatives could act as more potent modulators of the FGF14:FGF14 dimer and/or FGF14:Nav complex. Future medicinal chemistry and pharmacological efforts along with structural resolution of the peptide/s and their conformers in solution and/or docked to various FGF14 protein complexes will be needed to test this hypothesis and will be required to identify peptide variants suited for selective *in vivo* interventions against the dimer versus the FGF14:Nav channel complex.

Despite their high sequence homology and similar 3D fold, iFGFs differ in their binding affinity for Nav channels and the way they modulate Nav channel currents (Goetz et al., 2009; Laezza et al., 2009). Divergence in function typically translates in structural variations at the protein interface responsible for specific macromolecular interactions. From the *in silico* comparison between the two FGF13 and FGF14 dimer structures structural differences in the side chains of residues at the β 12 strand and the β 9 loop region holding the Y158 in FGF14 and the Y151 in FGF13 were evident. These differences might be the basis of specialized functions towards Nav channels and could translate into highly targeted drug-based interventions against each iFGF:Nav channel pair.

CONCLUSION

PPI interfaces are emerging targets for pharmacological interventions especially in the CNS, where selectivity and specificity are vital for developing drugs with limited side effects. PPI are flexible and

structural adaptive (Arkin and Wells, 2004; Luque and Freire, 2000; Ma et al., 2002; Mullard, 2012). However, a general strategy for a rapid characterization of PPI interfaces is still being sought. The combined methodology presented here including a combination of in-cell split-luciferase assays, molecular modeling, and model-based peptide design responds to an urgent need in the field of molecular pharmacology of providing an integrated method for characterizing PPI interfaces. When applied to the study of iFGF:iFGF and iFGF:Nav channel complexes, this methodology will provide a rapid method to predict and screen for “hot-spots”, map interacting surfaces, and identify druggable pockets that can guide drug design against Nav channels with applicability to channelopathies and other Nav channel-related disorders.

CONFLICT OF INTEREST

The authors declare no conflict of interest.

ACKNOWLEDGEMENTS

This work was supported by a research starter grant from the PhRMA Foundation (FL, SSM), R01MH095995 (FL) and training fellowship from Keck Center for Interdisciplinary Bioscience Training of the Gulf Coast Consortia NIGMS Grant No.1 T32 GM089657-04 (SRA). We thank Anesh Prasai for initial experiments.

Author contributions – Syed Ali designed and performed LCA, western blot, analyzed data, and wrote the manuscript. Dr. Neli Panova and Dr. Shavkunov performed western blot. Fernanda Laezza and Svetla Stoilova-McPhie designed and supervised the work and interpreted the data and wrote the manuscript. Svetla Stoilova-McPhie designed the peptides and made homology models. All authors read and approved the final version of the manuscript.

Chapter 5

Modulation of the FGF14:Nav1.6 channel interaction through a short peptidomimetic fragment

Syed R. Ali^{1,2,§}, Zhiqing Liu^{1,§}, Miroslav N. Nenov¹, Federico Scala¹, Thomas James³, Aditya Singh¹, Neli I. Panova-Elektronova¹, Haiying Chen¹, Jia Zhou^{1,5,*}, and Fernanda Laezza^{1,3,4,5,*}

Department of Pharmacology & Toxicology¹, Pharmacology and Toxicology Graduate Program²
Department of Neuroscience and Cell Biology³, Center for Neurodegenerative Diseases⁴, Center for
Addiction Research⁵, University of Texas Medical Branch, Galveston, TX 77555, USA

[§]These two authors contributed equally to this work.

***Corresponding Authors:**

Dr. Fernanda Laezza

Department of Pharmacology & Toxicology

The University of Texas Medical Branch

301 University Boulevard

Galveston, 77555, Texas, USA

Phone: 001:409:772:9672

Fax: 001:409:772:9642

felaezza@utmb.edu

Dr. Jia Zhou, Ph.D.

Department of Pharmacology & Toxicology

The University of Texas Medical Branch

301 University Boulevard

Galveston, 77555, Texas, USA

Phone: 001:409:772:9748

Fax: 001:409:772:9648

jizhou@utmb.edu

Abstract

The pore-forming α -subunit of the voltage-gated Na^+ (Nav) channels (Nav1.1-Nav1.9) provides the basis for neuronal electrical excitability in the brain. These channels are regulated by a number of brain-specific accessory proteins. One of the critical accessory proteins is fibroblast growth factor 14 (FGF14), a member of the intracellular FGFs (iFGFs; FGF11-13) associated with several brain disorders. FGF14 binds directly to the C-tail of Nav channel and regulates neuronal excitability by controlling the channel expression and gating properties. We have identified a short sequence on FGF14 and designed a peptidomimetic fragment as an effective probe for modulating Nav1.6 channels by luciferase-based assay. This peptidomimetic was further evaluated with purified proteins, *in silico* docking, and whole-cell patch clamp electrophysiology in both *in vitro* and *ex vivo* systems. Overall, our data support that the compound ZL181 exerts a more profound effect on Nav1.6 channels compared to Nav1.1 and to Nav1.2 isoforms in the presence of FGF14 and suppresses neuronal firing in medium spiny neurons of nucleus accumbens. The novel knowledge from this study might have a broad impact on the design and development of novel small molecule modulators for the treatment of various brain disorders associated with Nav1.6 channel dysfunction.

Significance

Neuronal voltage-gated sodium (Nav) channels play critical roles in the regulation of neuronal excitability in brain. Most drugs that block Nav channels in the market are proposed to interact with highly conserved transmembrane domain of Nav channel isoforms, as such most of them show lack of selectivity across all Nav channel isoforms. We have identified a short peptidomimetic fragment of FGF14 protein, a physiologically relevant accessory protein of Nav channels, which targets Nav1.6 channels.

Introduction

Voltage-gated sodium (Nav) channels are transmembrane proteins that facilitate the influx of sodium ions (I_{Na} current) in excitable cells, and thus they are involved in the initiation and propagation of action potentials (Hodgkin and Huxley, 1952). Nav channels are composed of a pore-forming α -subunit (220-260

kDa) and an auxiliary β -subunits (32-36 KDa) (Catterall, 2000; Yu and Catterall, 2003; Yu et al., 2005). To date, nine isoforms of Nav channels (Nav1.1-Nav1.9) have been functionally characterized and a tenth (Na_x) has been identified (Catterall, 2012, 2014; Catterall et al., 2005a; Chahine et al., 2008; Cusdin et al., 2008; Denac et al., 2000; Goldin et al., 2000; Letierrier et al., 2010; Marban et al., 1998; Savio-Galimberti et al., 2012; Yu and Catterall, 2003). Nav channel isoforms exhibit differential distributions (Felts et al., 1997), electrophysiological properties (Catterall et al., 2005a), and pharmacological properties (Catterall et al., 2005a; England and de Groot, 2009).

A number of neurological and psychiatric disorders, including Dravet syndrome (15-17), congenital insensitivity to pain (18, 19), primary erythromelalgia (20), paroxysmal extreme pain disorder (21, 22), cardiac arrhythmias (23, 24), Brugada syndrome (25), and autism (26), are linked to Nav1.1, Nav1.2, and Nav1.6 channels (Chahine et al., 2008; Eijkelkamp et al., 2012). Among these three isoforms of Nav channels, Nav1.6 is an emerging target which is expressed throughout soma and axon of different neuronal cells (Schaller and Caldwell, 2003). Nav1.6 has a significant contribution in persistent current, resurgent current, and repetitive neuronal firing (Catterall et al., 2005a). Both loss of function or gain of function from Nav1.6 channel mutations are related to malfunction of neuronal excitability. In animal models, mouse *Scn8a* (med) mutants showed dystonia, tremor, movement disorders, and sleep disorder. Furthermore, a number of de novo mutations have been identified in patients linked to epilepsy, ataxia, and cognitive disorders (McKinney et al., 2008; O'Brien and Meisler, 2013; Savio-Galimberti et al., 2012; Woodruff-Pak et al., 2006). The accumulating evidence suggests that Nav1.6 has a great potential of clinical value, and developing selective pharmacological modulators of Nav1.6 sodium channels is possible and urgently needed

Most drugs targeting Nav channels in the market, including local anesthetic, antiepileptic, and antiarrhythmic agents, are proposed to interact with amino acid residues within the transmembrane S6 segment in Domain 4 (Payandeh et al., 2011). This site is highly conserved across all Nav channel isoforms (Fozzard et al., 2011; Liu et al., 2003b; Ragsdale et al., 1996), as such most Nav channel drugs show lack of selectivity across all Nav channel isoforms (England and de Groot, 2009). The lack of specificity results

in unwanted side effects such as inhibiting cardiac Nav1.5 channel. Therefore, there is an unmet need to develop novel, selective compounds targeting Nav channels. Currently, there is an ongoing effort both in industry and academia to develop isoform-specific inhibitors targeting Nav channels via high-throughput screening (Yu et al., 2016). Although there has been some success in the discovery of subtype specific Nav1.6 channel blockers based on structure–activity relationship (SAR) of Nav1.6 channels (Rivara et al., 2012), novel approaches are required to develop subtype specific compounds targeting Nav1.6 channels.

In search of new strategies to develop novel compounds targeting Nav1.6 channel, we have explored protein-protein interaction (PPI) sites to discover novel compounds. Nav channels are regulated by a number of accessory proteins (Liu et al., 2001; Liu et al., 2003a; Musa et al., 2015; Olsen et al., 2003; Savio-Galimberti et al., 2012; Schoorlemmer and Goldfarb, 2001; Wittmack et al., 2004). This rich macromolecular complex of Nav channels introduces specific PPI sites that could serve as targets for drug development (Stoilova-McPhie et al., 2013). In searching for PPI surfaces that could lead to the development of potential probes and drug-like molecules targeting Nav1.6 channels, we have proposed the interactions between Nav1.6 channels and intracellular fibroblast growth factor (FGF14) as potential novel targets. FGF14 is a physiologically relevant accessory protein of Nav channels that has been associated with neurological disorders such as ataxia (van Swieten et al., 2003), schizophrenia (Rodriguez-Murillo et al., 2014) and depression (Verbeek et al., 2012). Furthermore, FGF14 differentially modulates Nav1.1, Nav1.2 and Nav1.6 channels, and its phenotype is distinct from other iFGFs (Ali et al., 2014; Ali et al., 2016a; Goetz et al., 2009; Liu et al., 2001; Liu et al., 2003a; Rush et al., 2006; Tempia et al., 2015; Wittmack et al., 2004). Therefore, it is promising to develop isoform-specific modulators targeting the FGF14:Nav1.6 complex.

Previously, we have proposed a four-amino acid residue peptide (FLPK), a fragment of FGF14, as a novel modulator of Nav channel (Ali et al., 2014). Here, we have applied chemical biology approach to generate more cell permeable peptidomimetics of FLPK peptide, and we have demonstrated the activity of the peptidomimetic (ZL181) in Nav1.6 channel recombinant cell system and in brain tissue slices. Overall, we identified a novel peptidomimetic based on the PPI of Nav1.6 channel and fibroblast growth factor 14,

and we have validated this peptidomimetic using a combination of bioluminescence assay, surface plasmon resonance, *in silico* docking, and patch clamp electrophysiology using both *in vitro* and *ex vivo* techniques. These results might provide fundamental new knowledge for the design of novel therapeutics targeting the FGF14:Nav1.6 interaction interface as a new therapeutic strategy for the treatment of brain disorders associated with Nav1.6 channel's malfunction.

Result

Synthesis and Identification of Novel Inhibitors Targeting Nav1.6 Channels

We have postulated previously that a fragment of FGF14 (Ac-FLPK-CONH₂) might modulate Nav1.6 channel (Ali et al., 2014). Based on this finding, we have rationally designed multiple analogs of this compound to improve the stability, permeability and potency of the Ac-FLPK-CONH₂ peptide. Two peptidomimetics were synthesized by shortening the parent compound (i.e., ZL141, Cbz-FLP-CONH₂ and ZL148, Ac-FLK(Boc)-CONH₂) while additional two analogs were synthesized by introducing hydrophobic functional groups to improve cell permeability (i.e., ZL181, Cbz-FLPK(Boc)-CONH₂; ZL181, FLPK(Fmoc)-OH).

In Cell Validation of Peptidomimetics

To monitor the role of peptidomimetics in the FGF14:Nav1.6 complex, we screened the peptidomimetics by split-luciferase complementation assay (LCA) where FGF14 and the C-tail of Nav1.6 channels are fused to vectors expressing CLuc and NLuc luciferase reporter. ZL141, ZL148, ZL181, and ZL182 were tested at 50 μ M in HEK293 cells expressing CLuc-FGF14 and CD4:Nav1.6-NLuc. The changes of luminescence response were observed in the presence of ZL141 (103 ± 14 %, $n=5$, $p > 0.05$), ZL148 (132 ± 9 %, $n=9$, $*p < 0.001$, Student's t test), ZL181 (75 ± 6 %, $n=9$, $*p < 0.001$, Student's t test), and ZL182 (129 ± 13 %, $N=9$, $**p < 0.001$, Student's t test) compared to control (DMSO, 0.5X) (**Fig. 5.1 A-B**). None of the compounds interfered with the full-length luciferase enzyme (Fig. 2C). We then performed dose-response studies with ZL148, ZL181, and ZL182 against the FGF14:Nav1.6 complex. Out of these compounds, ZL181 was identified to show dose-response inhibition against the FGF14:Nav1.6 interaction ($IC_{50} = 63$ μ M) (**Fig. 5.1 D**).

The role of ZL181 was further determined by surface plasmon resonance spectroscopy. To determine the affinity of the ZL181 to Nav1.6 and FGF14, fixed amount of individual protein was immobilized to a C5 sensor chip surface, and ZL181 was flowed over the chip surface at different concentration (10- 200 μ M). The sensogram and fitted saturation binding curve of the ZL181 to the Nav1.6 and FGF14 is shown in **Fig 5.1. E-F**. The K_d value for FGF14 is lower (13 μ M) than that for Nav1.6 (212 μ M), indicating that the ZL181 has a higher affinity to FGF14 protein compared to Nav1.6 C-tail. The data is also consistent with *in silico* docking results by Schrödinger Small-Molecule Drug Discovery Suite. By using the peptide docking program, ZL181 can be well docked at the interface of the FGF14:Nav1.6 complex where ZL181 interacts with key residues R83, E156 and T194 of FGF14 and N1833, L1853, R1854, R1892 of Nav1.6 channels (**Fig. 5.1 I-J**).

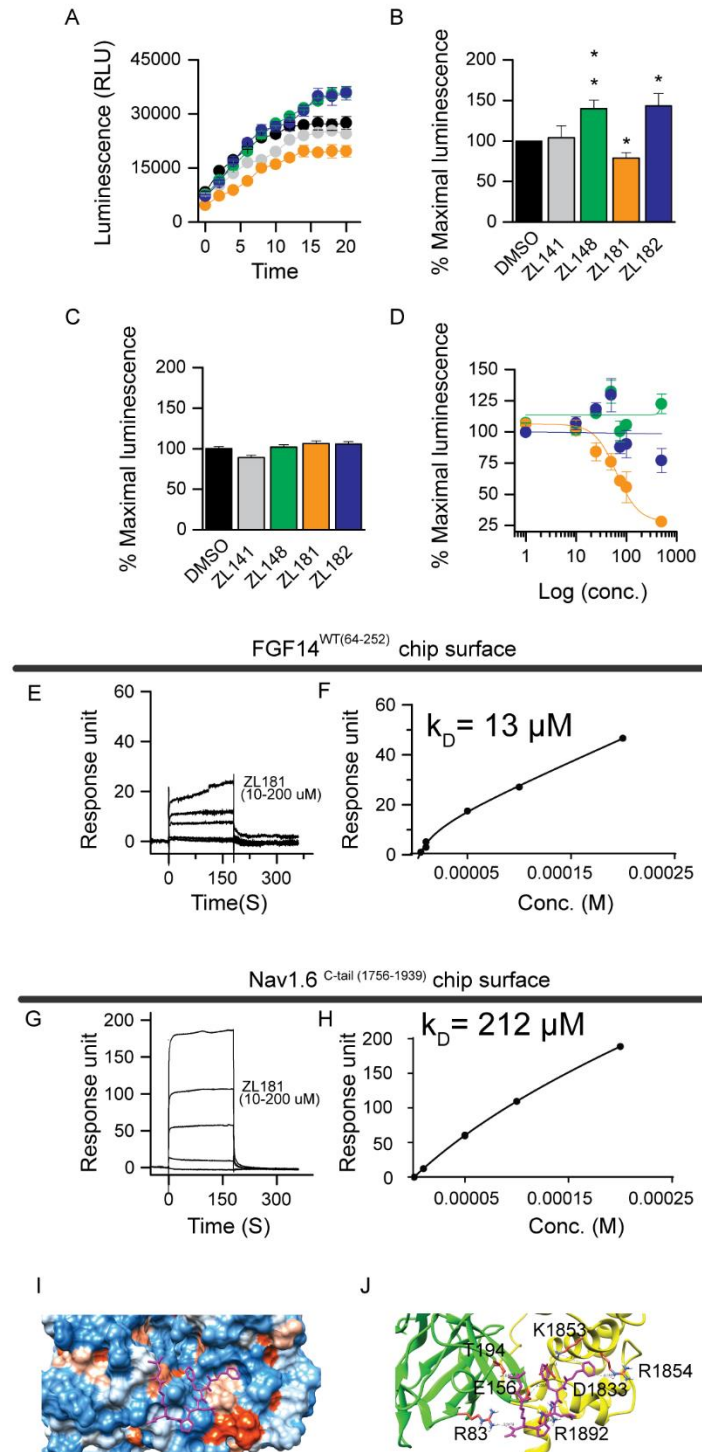


Fig. 5.1. Validation of peptidomimetics against the FGF14:Nav1.6 complex. (A) HEK293 cells were transiently transfected with CLuc-FGF14 and CD4-Nav1.6-NLuc and treated with ZL141 (gray), ZL148 (green), ZL181 (blue), ZL182 (orange) at 50 μ M or DMSO (0.5%, control). The assembly of LCA pair is detected as luminescence response (RLU) upon addition of D-luciferin substrate at time zero; data are mean \pm SEM. (B) Bar graph represents % maximal luminescence of treated compounds (50 μ M), which is normalized to control (0.5% DMSO). The Statistical significance of the treated groups was compared to control using t-test (* $p < 0.01$ or ** $p < 0.01$). (C) The peptidomimetics were tested against full-length luciferase reporter. (D) Dose-response modulation of ZL148, ZL181 and ZL182; data are mean \pm SEM. Panel A shows the SPR sensogram of WT FGF14 binding to Nav1.6. (E) The SPR sensogram of ZL181 (10- 200 μ M) to Nav1.6 C-tail and (F) the fitted saturation binding curves. (G) The SPR sensogram of ZL181 (10-200 μ M) to Nav1.6 C-tail and (H) the fitted saturation binding curves. (I) Electrostatic surface representation of ZL181 peptidomimetic (magenta) was docked at the interface of FGF14:Nav1.6 homology model complex. (J) Ribbon representation of docking pose shows the interactions of ZL181 (magenta) with Nav1.6 channel (yellow ribbon) and FGF14 (green ribbon). ZL181 directly interacts with key residues R83, E156, T194 (FGF14) and D1833, K1853, R1854, R1892 (Nav1.6).

ZL181 Peptidomimetic Modulates Nav1.6 Channels Alone and Works Synergistically With FGF14 to Modulate Nav1.6 Channels

To determine the role of ZL181 peptidomimetic in Nav1.6 channels alone and Nav1.6 channels in the presence of FGF14, we designed 2 x 2 experimental groups. HEK-Nav1.6 cells were transiently transfected with *GFP* or *FGF-GFP* and treated with either DMSO (0.15% final concentration, control group) or ZL181 (20 μ M, final concentration) 20–60 min prior to the experiments. As shown in Fig. 5.2 A, rapid rising and fast decaying transient inward Na^+ currents were evoked in response to depolarizing voltage steps from Nav1.6 channels transfected with GFP. In cells pretreated with ZL181 (20 μ M), the Nav1.6-mediated peak current density was significantly lower (-20.9 ± 3.4 pA/pF, $n = 12$, $p < 0.05$) compared to control (-73.8 ± 13.6 pA/pF, $n = 12$; **Fig. 5.2 B**, and **Table S 5.1**). ZL181 does not change activation and inactivation properties of Nav channel alone (**Fig. 5.2, C-D**). Thus, ZL181 inhibits peak current amplitude of Nav1.6 current.

We then investigated the role of ZL181 in Nav1.6 channel in the presence of FGF14. In agreement with previous studies (Laezza et al., 2009; Shavkunov et al., 2013b), we found that HEK-Nav1.6 cells expressing FGF14-GFP shows significantly lower Na^+ current (I_{Na}) amplitudes than cells expressing GFP (-18.1 ± 3.8 pA/pF, $n = 20$, for FGF14-GFP-expressing cells; -73.8 ± 13.6 pA/pF, $n = 12$, for GFP-

expressing cells, $**p < 0.01$, one-way ANOVA, post hoc Bonferroni, see **Fig. 5.2 , B** and **Table S 5.1**). Notably, ZL181 further decreases in Na^+ current peak amplitude (-7.4 ± 4.4 pA/pF, $n = 19$, for FGF14-GFP-expressing cells treated with ZL181 compared with FGF14-GFP-expressing cells (DMSO), $p < 0.05$, unpaired t test, see **Fig. 5.2, B**). Furthermore, we have also investigated the role of ZL181 to modulate the biophysical properties of Nav1.6 channel in the presence of FGF14. In consistency with previous studies, voltage dependence of activation and steady-state inactivation kinetics changes in the cells expressing FGF14-GFP compared with control (**Fig. 5.2 C-D**, and **Table S 5.1**). Interestingly, treatment with ZL181 rescued the depolarizing shift of the steady-state inactivation induced by FGF14-GFP expression back to control levels ($p > 0.05$, one-way ANOVA, post hoc Dunnett's test; **Fig. 5.2, D**, and **Table S 5.1**). Thus, ZL181 works synergistically with FGF14 to regulate the peak current amplitude as well as the inactivation kinetics.

Furthermore, using a range of doses from 1 μM to 100 μM , we developed a dose-response profile for ZL181 in HEK293-Nav1.6 cells alone and HEK-Nav1.6 cells transfected with FGF14. The inhibitor does exhibit dose-dependent inhibition of Nav1.6 encoded currents that exhibits an IC_{50} of 19.67 ± 5.7 μM (**Fig. 5.2, E**), and the inhibitor exhibits dose-dependent inhibition of Nav1.6 encoded currents in presence of FGF14 ($\text{IC}_{50} = 11.55 \pm 1.3$ μM) (**Fig. 5.2, F**).

We also investigated the role of ZL181 in regulating Nav1.1 and Nav1.2 channels. Although ZL181 also suppresses peak current amplitude in Nav1.1 and Nav1.2 channels like Nav1.6 channel, it does neither act synergistically to further suppress Na^+ current in presence of FGF14 or rescue the voltage-dependence inactivation property ($V_{1/2}$) in presence of FGF14 to the control (GFP, DMSO) (**Fig. S 5.1** and **Fig. S 5.2**).

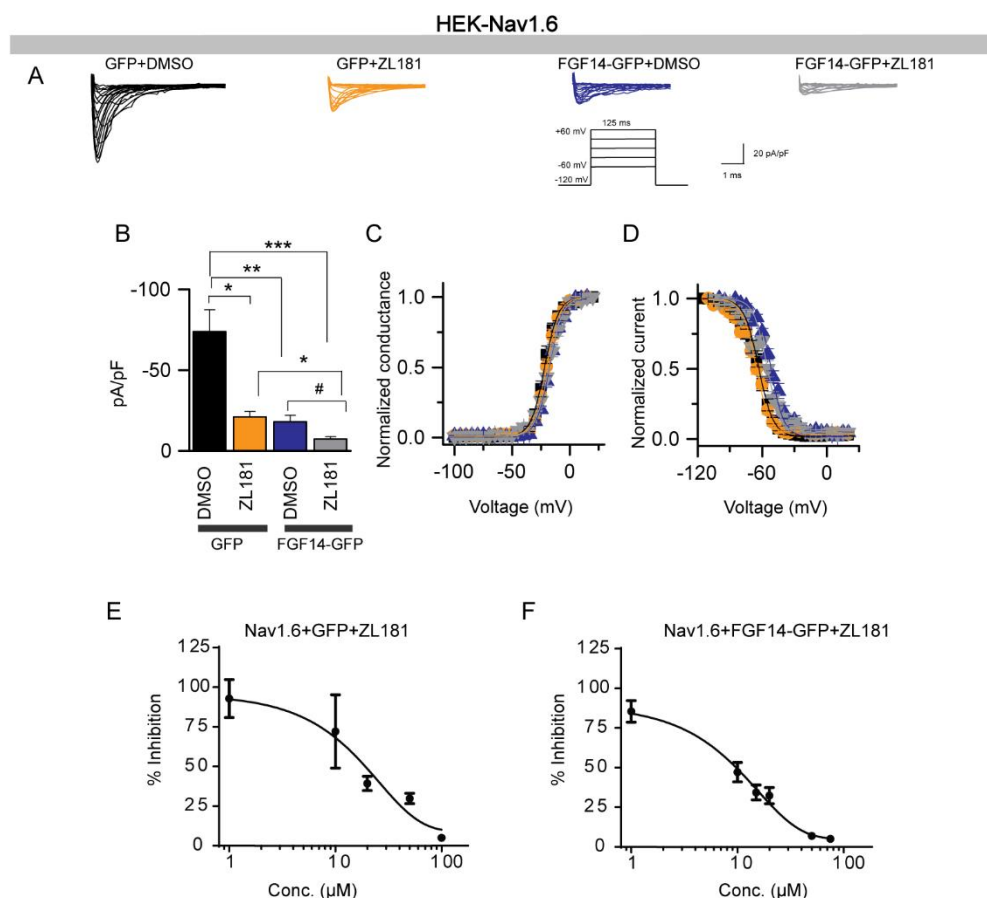


Fig. 5.2. ZL181 modulates Nav1.6 channels alone and works synergistically with FGF14 to further modulate Nav1.6 channels. (A) Representative traces of voltage-gated Na^+ currents (I_{Na}) recorded from HEK-Nav1.6 cells transiently expressing GFP or FGF14-GFP in response to voltage steps from -120 mV to $+60$ mV from a holding potential of -70 mV (inset). Only selected current traces in response to voltage steps are shown. GFP-expressing cells were treated with 0.15% DMSO (black traces) or with $20 \mu\text{M}$ ZL181 (orange traces), whereas FGF14-GFP-expressing cells were treated either with 0.15% DMSO (blue traces) or with $20 \mu\text{M}$ ZL181 (gray traces). (B) Bar graphs representing peak current densities measured in individual HEK-Nav1.6 cells expressing GFP (treated with 0.15% DMSO; black bar), GFP (treated with $20 \mu\text{M}$ ZL181; orange bar), FGF14 (treated with 0.15% DMSO; blue bar), or FGF14 (treated with $20 \mu\text{M}$ ZL181; gray bar). Data are mean \pm S.E. Treatment with ZL181 to cells expressing GFP (orange bar) suppresses peak current densities in comparison with DMSO-treated control ($**p < 0.01$, Kruskal-Wallis, post hoc Dunn test). Treatment of ZL181 to cells expressing FGF14-GFP (gray bar) suppresses peak current densities in comparison with DMSO-treated control ($\#p < 0.05$, unpaired t test). (C) Voltage dependences of I_{Na} activation and (D) steady-state inactivation were measured as described under “Experimental Procedures” and means \pm S.E. Values are plotted as a function of the membrane potential. The activation and inactivation data were fitted with the Boltzmann function as described under “Experimental Procedures.” The fitted parameters are provided in **Table S 5.1**. (E) Treatment with ZL181 inhibits Na^+ current in a dose-response manner in Nav1.6 channels alone. (F) Treatment with ZL181 inhibits Na^+ current in a dose-response manner in Nav1.6 channels with expression of FGF14.

ZL181 Decreases Neuronal Intrinsic Excitability in Nucleus Accumbens (NAc) Medium Spiny Neurons (MSN)

The Nucleus accumbens plays a critical role in reinforcement-associated learning (Papale et al., 2010; Woodruff-Pak et al., 2006) and in addiction-related behavior (McKinney et al., 2008). It has been shown that Nav1.6 channels are expressed at the nucleus accumbens medium spiny neurons (Shah et al., 2001). Thus, knowing that NAc medium spiny neurons express Nav1.6 channels (Shah et al., 2001), and our in vitro studies show that ZL181 exhibits elevated affinity toward Nav1.6 channels compared to other neuronal Nav channels, we decided to test the effect of ZL181 in this region. In order to test the effect of ZL181 on neuronal firing along with active and passive properties, we used whole-cell patch clamp techniques in brain tissue slices. Nucleus accumbens medium spiny neurons (MNS) were treated with either DMSO (0.05X) or ZL181 (50 μ M) for one hour in an incubation chamber before being transferred to submerge experimental chamber perfused with oxygenated artificial cerebrospinal fluid for patch clamp experiments. We found that treatment of MSNs with ZL181 significantly reduced the number of spikes evoked by rectangular current steps of 10 pA increments compared to DMSO control (**Fig. 5.3 A-B**). Input-output curves revealed that the effect of ZL181 persists across wide spectrum of injected currents (**Fig. 5.3 C**). For instance at current step of 150 pA the number of spikes in DMSO treated MSNs was 18.4 ± 1.3 , $n=8$ versus 6.9 ± 2.3 , $n=10$ in ZL181 treated MSNs; $p<0.005$ with Student *t*-test (**Fig. 5.3 C**). To test the mechanisms underlying neuronal firing reduction and related to sodium channels activity, action potential voltage and current thresholds were measured. We found that treatment with ZL181 significantly increases both voltage threshold (-35.9 ± 2.3 mV for DMSO treated MSNs, $n=8$ versus -27.8 ± 2 mV for ZL 181 treated MSNs, $n=10$; $p<0.05$ with Student *t*-test) and current threshold (72.5 ± 11.5 pA for DMSO treated MSNs, $n=8$ versus 135.8 ± 12.5 pA for ZL 181 treated MSNs, $n=10$; $p<0.01$ with Student *t*-test) in MSNs compare to DMSO control (**Fig. 5.3, D-E** and **Table S 5.4**). Further analysis of neuronal active and passive properties revealed no significant changes in MSN treated with ZL181 compare to DMSO control (Table S4). Overall, we found that treatment with ZL181 suppresses intrinsic excitability in medium spiny neurons of nucleus accumbens.

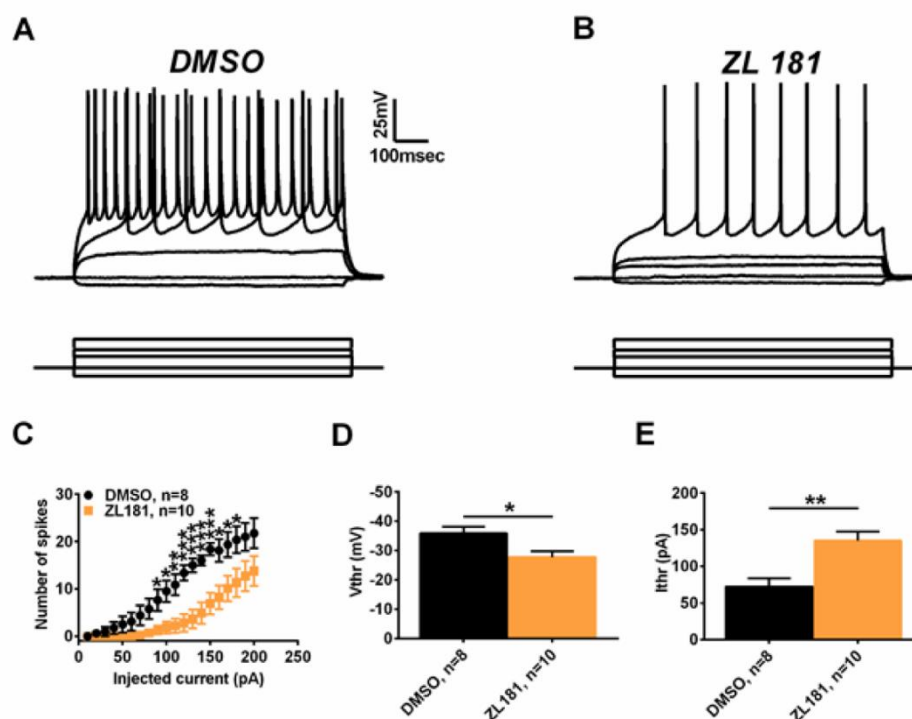


Fig. 5.3. The effect of ZL181 on neuronal firing in medium spiny neurons of nucleus accumbens. (A-B) Representative traces showing trains of action potentials evoked by current steps of fixed increments in MSNs treated with 0.05 % DMSO (A) or 50 μM of ZL181 (B). Representative traces of action potential are shown at -20, 0, 50, 80 and 110 pA current steps of 800 ms duration. (C) Input-output curve showing reduced number of spikes in MSN treated with ZL181 compared to DMSO control. (D-E) Graph bars for voltage and current thresholds showing increased voltage and current thresholds for MSN treated with ZL181 compare to DMSO control. * $p < 0.05$, ** $p < 0.01$, *** $p < 0.005$ with Student t-test.

DISCUSSION

Significant efforts to develop isoform-specific Nav channel modulators do exist (Bagal et al., 2015; Mantegazza et al., 2010; Theile and Cummins, 2011). Unfortunately, most of the approaches to discover new compounds targeting Nav channels are based on high-throughput screening without extensive knowledge of the molecular structure of Nav channels or an understanding of the full complexity of Nav channel isoforms (Birch et al., 2004; Castle et al., 2009). In this study, we targeted PPI as a base to develop Nav1.6 channel specific probes. Previously, we identified a fragment of FGF14 protein (AC-FLPK-CONH₂) as a potential modulator for Nav1.6 channel (Ali et al., 2014). In this study, we have performed

modification of this peptide to generate more cell permeable peptidomimetics and have tested these peptidomimetics against the FGF14:Nav1.6 complex via luciferase assay. Among four peptidomimetics, we have narrowed down our selection to ZL181 based on diverse chemical structures and in cell response from LCA assay. Implementation of a chemical modification approach by introducing hydrophobic carboxybenzyl (Cbz) and *tert*-butyloxycarbonyl (Boc) groups improves cellular permeability, fragment stability, and potency of ZL181 compared to the initial peptide hit (Anger et al., 2001; Jukic et al., 2014).

Our comprehensive electrophysiological studies in a recombinant cell system showed that ZL181 differentially modulates Nav1.1, Nav1.2, and Nav1.6 channels in the presence of FGF14 (**Fig. 5.2, Fig. S 5.1, and Fig. S 5.2**). We observed that ZL181 is more effective in suppressing Na⁺ current in the presence of FGF14 in Nav1.6 channels compared to Nav1.1 and Nav1.2 channels. Most likely ZL181 can synergistically work with both FGF14 and Nav1.6 channels to modulate the peak current density in Nav1.6 channels. Furthermore, ZL181 antagonizes the action of FGF14 only in Nav1.6 channel kinetics, rescuing V_{1/2} of steady-state inactivation back to control level (**Fig. 5.2 D and Table S 5.1**). Such characteristics of ZL181 on different Nav channels in the presence of FGF14 could be explained as structural difference among different Nav channel isoforms. Structurally, Nav1.1 and Nav1.2 are different from Nav1.6 (Catterall, 2012; Catterall et al., 2005a; Yu and Catterall, 2003; Yu et al., 2005), and FGF14 modulates differently from Nav1.1, Nav1.2, and Nav1.6 channels in terms of biophysical properties. Structural divergences among difference isoforms of Nav channels and differential modulations of Nav channels by FGF14 determine the isoform-specificity of ZL181 to Nav1.6 channels. We are proposing that ZL181 has better specificity to Nav1.6 channel compared to Nav1.1, Nav1.2 in the presence of FGF14 because FGF14 might interact with Nav1.6 channels in such a way that the peptidomimetic can interact efficiently with both Nav1.6 channels and FGF14. The simultaneous affinity of ZL181 to Nav1.6 channel and FGF14 is further supported by SPR studies and *in silico* docking (**Fig. 5.1, E-J**).

It is worthwhile to mention we have determined the IC₅₀ for ZL181 is around 63 μM by LCA assay; however, in experiments with whole-cell patch clamp obtained IC₅₀ for ZL181 is around 11 μM. This discrepancy was observed likely because we have measured the disruption of relative affinity of truncated

Nav1.6 channels (C-tail) to FGF14 through LCA, whereas with patch clamp in recombinant system the sodium current was recorded from full-length α -subunit of Nav1.6 channels in presence of FGF14.

Finally, we have extended the functional role of ZL181 to *ex-vivo* studies. Our data show that ZL181 reduces the number of evoked action potentials compared to control group. Furthermore, treatment with ZL181 shifts voltage threshold toward depolarized membrane potential and increases current threshold, supporting that ZL181 decreased neuronal excitability in nucleus accumbens medium spiny neurons.

In conclusion, we have identified ZL181, a novel peptidomimetic, by investigating the interaction between Nav1.6 channel and FGF14. Our study shows that ZL181 compound can selectively target Nav1.6 channels compared to other Nav1.1 and Nav1.2 channels in presence of FGF14, and ZL181 suppresses neuronal excitability in medium spiny neurons of the nucleus accumbens in brain tissue slices. In the future, we will monitor the efficacy of this novel peptidomimetic in kindling mouse model for any behavioral changes. The outcome of our study will contribute significantly for development of Nav1.6 channel isoform specific drugs.

ACKNOWLEDGMENTS

This work was supported by grants R01MH095995 (FL), R01DA038446 (JZ), P30DA028821 (JZ), the John Sealy Memorial Endowments Fund (FL) and training fellowships from the NIEHS T32 Environmental Toxicology Fellowship Grant No. T32-ES007254 and from the Keck Center for Interdisciplinary Bioscience Training of the Gulf Coast Consortia NIGMS Grant No.1 T32 GM089657-04 (SRA).

CONFLICT OF INTEREST

The authors declare no conflict of interest.

AUTHOR CONTRIBUTIONS

F.L., J.Z., S.R.A and Z.L conceived and designed experiments, wrote and revised the manuscript. Z.L. designed and chemically synthesized the peptidomimetics. S.R.A performed LCA and patch clamp experiment. A.S. performed surface plasmon resonance experiments. M.N., F.S., and T.J. performed patch

clamp electrophysiology in brain tissue slices. H.C. performed in silico docking and assisted chemical characterization analysis of the molecules.

SUPPLEMENTARY MATERIAL

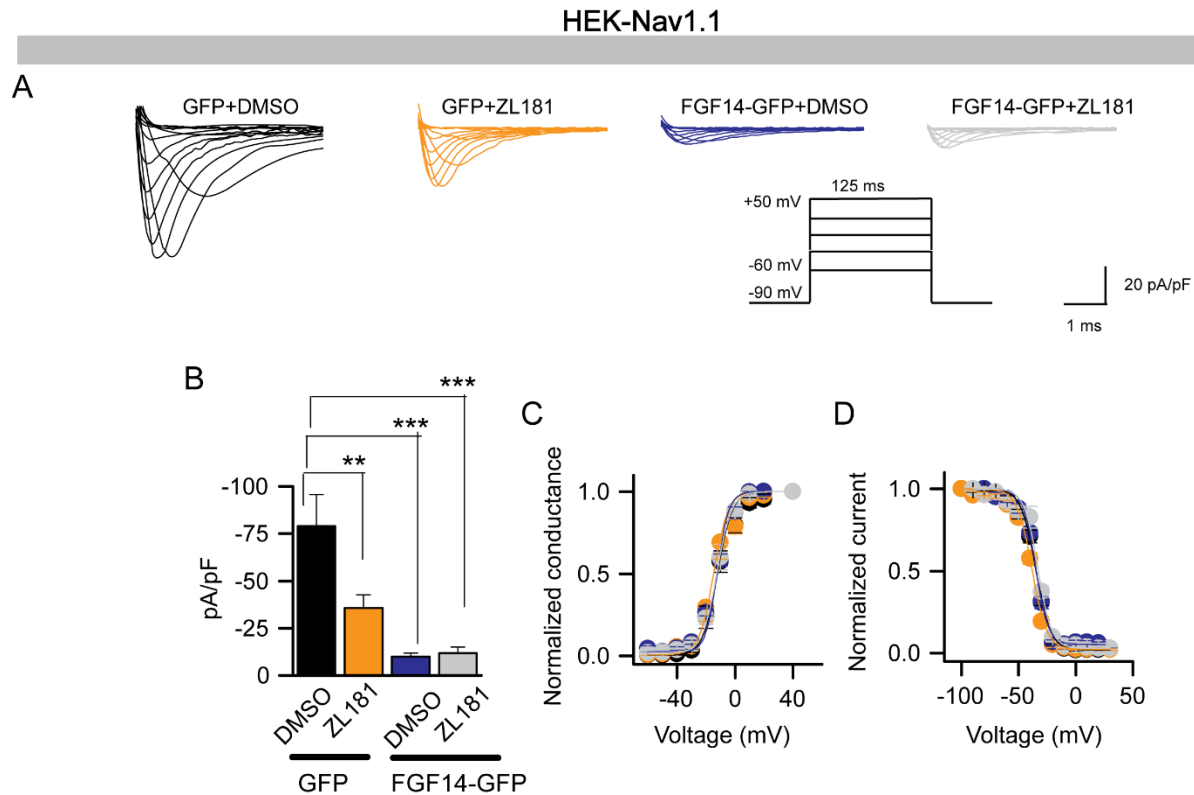


Fig. S 5.1. Pharmacological inhibition of ZL181 modulates the functional properties of Nav1.1 channels by FGF14. (A) Representative traces of voltage-gated Na^+ currents (I_{Na}) recorded from HEK-Nav1.1 cells transiently expressing GFP or FGF14-GFP in response to voltage steps from -60 mV to $+60$ mV from a holding potential of -70 mV (*inset*). Only selected current traces in response to voltage steps are shown. GFP-expressing cells were treated with 0.15% DMSO (*black traces*) or with $20 \mu\text{M}$ ZL181 (*orange traces*), whereas FGF14-GFP-expressing cells were treated either with 0.15% DMSO (*blue traces*) or with $20 \mu\text{M}$ ZL181 (*gray traces*). (B) *bar graphs* representing peak current densities measured in individual HEK-Nav1.1 cells expressing GFP treated with 0.15% DMSO (*black bar*), GFP treated with $20 \mu\text{M}$ ZL181 (*orange bar*), FGF14 treated with 0.15% DMSO (*blue bar*), or FGF14 treated with $20 \mu\text{M}$ (*gray bar*). Data are mean \pm S.E. Cells expressing FGF14-GFP treated with DMSO exhibit significantly lower peak current amplitude than the corresponding cells expressing GFP treated with DMSO (** $p < 0.01$, One-way ANOVA, post hoc Dunnett's multiple comparisons). Treatment with ZL181 to cells expressing GFP (*orange bar*) suppresses peak current densities in comparison with DMSO-treated control (** $p < 0.01$, One-way ANOVA, post hoc Dunnett's multiple comparisons). (C) Voltage dependences of I_{Na} activation, and (D) steady-state inactivation were measured as described under “Experimental Procedures,” and means \pm S.E. values are plotted as a function of the membrane potential. The activation and inactivation data were fitted with the Boltzmann function as described under “Experimental Procedures.” The fitted parameters are provided in **Table S 5.2**.

A

HEK-Nav1.2

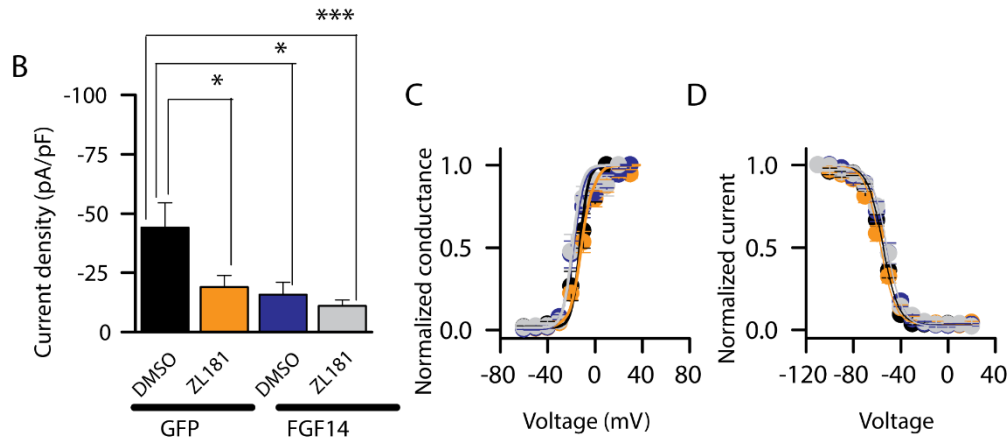
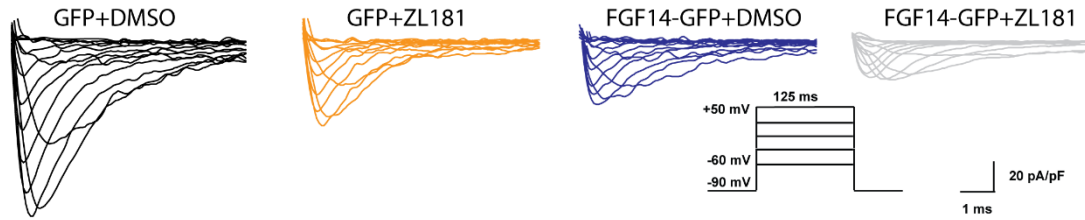


Fig. S 5.2. Pharmacological inhibition of ZL181 modulates the functional properties of Nav1.2 channels by FGF14. (A) Representative traces of voltage-gated Na^+ currents (I_{Na}) recorded from HEK-Nav1.2 cells transiently expressing GFP or FGF14-GFP in response to voltage steps from -60 mV to $+60$ mV from a holding potential of -70 mV (*inset*). Only selected current traces in response to voltage steps are shown. GFP-expressing cells were treated with 0.15% DMSO (*black traces*) or with $20 \mu\text{M}$ ZL181 (*orange traces*), whereas FGF14-GFP-expressing cells were treated either with 0.15% DMSO (*blue traces*) or with $20 \mu\text{M}$ ZL181 (*gray traces*). (B) Bar graphs representing peak current densities measured in individual HEK-Nav1.2 cells expressing GFP treated with 0.15% DMSO (*black bar*), GFP treated with $20 \mu\text{M}$ ZL181 (*orange bar*), FGF14 treated with 0.15% DMSO (*blue bar*), or FGF14 treated with $20 \mu\text{M}$ (*gray bar*). Data are mean \pm S.E. Cells expressing FGF14-GFP treated with DMSO exhibit significantly lower peak current amplitude than the corresponding cells expressing GFP treated with DMSO ($***p < 0.01$, One-way ANOVA, post hoc Dunn's multiple comparisons test). Treatment with ZL181 to cells expressing GFP (*orange bar*) suppresses peak current densities in comparison with DMSO-treated control ($***p < 0.01$, One-way ANOVA, post hoc Dunn's multiple comparisons test). (C) Voltage dependences of I_{Na} activation, and (D) steady-state inactivation were measured as described under “Experimental Procedures,” and means \pm S.E. values are plotted as a function of the membrane potential. The activation and inactivation data were fitted with the Boltzmann function as described under “Experimental Procedures.” The fitted parameters are provided in **Table S3**.

TABLE S 5.1. Voltage-gated Na⁺ currents in HEK-Nav1.6

Condition for Nav1.6	Peak density	Activation	K _{act}	Inactivation	K _{inact}	tau
	pA/pF	mV	mV	mV	mV	ms
GFP (DMSO)	-73.8 ± 13.6 (12)	-21.5 ± 1.3 (11)	4.8 ± 0.4 (10)	-64.1 ± 1.6 (12)	6.9 ± 0.5 (12)	0.9±0.05(12)
GFP (ZL181)	-20.9 ± 3.4 (15) ^a	-19.4±0.9 (12)	4.8±0.4 (12)	-66.3 ± 1.6 (14)	7.2±0.4 (14)	1.0±0.08(10)
FGF14-GFP (DMSO)	-18.1 ± 3.8 (20) ^b	-16.9±0.9 (19) ^d	5.3 ± 0.4 (19)	-50.7 ± 1.6 (14) ^e	7.2±0.6 (14)	1.5±0.1(12) ^g
FGF14-GFP (ZL181)	-7.4 ± 4.4 (19) ^c	-16.6±1.4 (11)	6.6 ± 0.5 (11)	-57.6 ± 1.6 (14) ^f	7.9±1.2 (14)	2.15±0.4(8)

^a $p < 0.05$, Kruskal-Wallis, post hoc Dunn test compared with GFP (DMSO); data are mean ± S.E.

^b $p < 0.01$, Kruskal-Wallis, post hoc Dunn test compared with GFP (ZL181); data are mean ± S.E.

^c $p < 0.01$, unpaired t tests compared to FGF14-GFP (DMSO); data are mean ± S.E.

^d $p < 0.05$, one-way ANOVA, post hoc Bonferroni's multiple comparisons test compared with GFP (DMSO); data are mean ± S.E.

^e $p < 0.05$, Kruskal-Wallis, , post hoc Dunn test compared to GFP (DMSO); data are mean ± S.E.

^f $p < 0.05$, Mann-Whitney test compared to FGF14-GFP (DMSO)

^g $p < 0.05$, one-way ANOVA, post hoc Dunn test compared with GFP (DMSO); data are mean ± S.E.

TABLE S 5.2. Voltage-gated Na⁺ currents in HEK-Nav1.1

Condition for Nav1.1	Peak density	Activation	K _{act}	Inactivation	K _{inact}	tau
	pA/pF	mV	mV	mV	mV	ms
GFP (DMSO)	-79.08 ± 16.5 (12)	-10.9 ± 1.8 (12)	6.0 ± 0.6 (12)	-45.5 ± 1.1 (11)	6.1 ± 0.6 (11)	1.3±0.1(11)
GFP (ZL181)	-35.6 ± 7.1 (12) ^a	-9.5±3.6 (11)	7.6±1 (11)	-47.9 ± 0.8 (12)	6.2±0.3 (12)	1.3±0.1(12)
FGF14-GFP (DMSO)	-9.83 ± 1.9 (12) ^b	-10.1±1.2 (11)	6.1 ± 0.6 (11)	-44.6 ± 0.6 (10)	5.6±1.1 (10)	2.6±0.5(10)
FGF14-GFP (ZL181)	-11.8 ± 3.1 (11) ^c	-8.5±1.8 (11)	6.8 ± 0.7 (11)	-43.3 ± 0.6 (10)	5.9±1.0 (10)	1.5±0.2(10)

^a $p < 0.01$, One-way ANOVA, post hoc Dunnett's multiple comparisons test compared with GFP (DMSO); data are mean ± S.E.

^b $p < 0.01$, One-way ANOVA, post hoc Dunnett's multiple comparisons test compared with GFP (DMSO); data are mean ± S.E.

^c $p < 0.01$, One-way ANOVA, post hoc Dunnett's multiple comparisons test compared with GFP (DMSO); data are mean ± S.E.

TABLE S 5.3. Voltage-gated Na⁺ currents in HEK-Nav1.2

Condition for Nav1.2	Peak density	Activation	K _{act}	Inactivation	K _{inact}
	pA/pF	mV	mV	mV	mV
GFP (DMSO)	-44.0 ± 10.4 (15)	-15.3 ± 1.6 (11)	6.1 ± 0.4 (11)	-54.7 ± 1.1 (16)	6.4 ± 0.3 (16)
GFP (ZL181)	-18.9 ± 4.8 (19) ^a	-11.3 ± 1.9 (12)	7.0 ± 0.3 (12)	-59.4 ± 2.7 (17)	7.7 ± 0.7 (17)
FGF14-GFP (DMSO)	-17.7 ± 5.2 (11) ^b	-16.9 ± 1.7 (11)	5.6 ± 0.7 (11)	-51.4 ± 1.7 (11)	6.3 ± 0.8 (11)
FGF14-GFP (ZL181)	-11.0 ± 2.4 (15) ^c	-17.0 ± 1.8 (10)	4.1 ± 0. (10)	-54.2 ± 1.8 (15)	7.3 ± 0.7 (15)

^a $p < 0.01$, One-way ANOVA, post hoc Dunn's multiple comparisons test compared with GFP (DMSO); data are mean ± S.E.

^b $p < 0.01$, One-way ANOVA, post hoc Dunn's multiple comparisons test compared with GFP (DMSO); data are mean ± S.E.

^c $p < 0.01$, One-way ANOVA, post hoc Dunn's multiple comparisons test compared with GFP (DMSO); data are mean ± S.E.

Table S 5.4. Active and passive properties of medium spiny neurons.

	MRP (mV)	V _{trh} (mV)	I _{trh} (pA)	max rise (mV/msec)	max decay (mV/msec)	C _m (pF)	R _{in} (mΩ)	Tau (msec)	Latency to first AP (msec)	half-width (msec)
DMSO (control)	-79.6 ± 1.83	-35.89 ± 2.25	72.5 ± 1.46	243.66 ± 2.073	-70.41 ± 6.81	61.6 ± 5.6	137.2 ± 5.18	8.34 ± 1.02	253.18 ± 39	1.04 ± 0.07
ZL181	-78.1 ± 2.19	-27.75 ± 1.99	135 ± 12.5	211.39 ± 18.04	-74.15 ± 4.05	67.04 ± 7.78	115.75 ± 8.21	7.82 ± 1.12	392.5 ± 8.46	0.95 ± 0.05
<i>p</i> value	0.62	0.016	0.002	0.26	0.65	0.58	0.24	0.73	0.09	0.32

MRP – membrane resting potential, V_{trh} – voltage threshold, I_{trh} – current threshold, max rise – action potential repolarization maximal speed, max decay – action potential depolarization maximal speed, C_m – membrane capacitance, R_{in} – input resistance, Tau – membrane constant, latency to first AP – latency to first spike induced with I_{trh}, half-width – action potential half-width. All *p*-values obtained with Student *t*-test.

Chapter 6

CONCLUSION

A number of approved sodium channel modulators are in the market for the treatment of clinical conditions associated with abnormal neuronal excitability (Bagal et al., 2013). Unfortunately, isoform selective Nav channel modulators are not available in the market due to high degree of amino acids sequence similarity across all Nav channel isoforms. In this regard, there is a significant interest both in industry and academia to develop subtype specific Nav channel modulators. However, most of the Nav channel drugs are discovered via high-throughput screening without extensive structural and functional studies of Nav channels. Therefore, new approaches are required to develop selective Nav channel modulators. Targeting the protein:protein interaction (PPI) sites of Nav channels in macromolecular complex is a novel approach for drug development. Although targeting PPI sites for drug development is very challenging due to the nature of flat, featureless, and large interacting surfaces of PPI complex. Targeting PPI can be further complicated if high-resolution crystal structures and suitable assays are not available. Nevertheless, potential “hot-spots” at the interface of Nav channel macromolecular complexes could introduce new enthusiasm to discover highly selective Nav channel modulators.

In our study, we have focused particularly on Nav1.6 channels because Nav1.6 has a significant contribution to persistent current, resurgent current, and repetitive neuronal firing. Both loss of function or gain of function mutations in the Nav1.6 channel are related to malfunction of neuronal excitability in the brain. Additionally, this isoform of Nav channels has been expressed in the nucleus accumbens medium spiny neurons. This part of the brain region related to brain rewards pathway plays a critical role in reinforcement-associated learning, depression, and in addiction-related behavior. All this information inspires us to select Nav1.6 channels as a new molecular target to discover isoform-specific small molecules.

Instead of using high-throughput screening to discover novel molecules targeting Nav1.6 channels, we have targeted hot-spots at the interface of FGF14:Nav1.6 complex to design new molecules. Although

FGF14 is an accessory protein of Nav1.6 channels, FGF14 not only regulates the functional properties of Nav1.6 channels in an isoform specific manner, but this protein also has been associated with neurological disorders such as ataxia, schizophrenia, and depression. The FGF14 protein directly interacts with C-tail of the Nav1.6 channels with high-affinity, and not all residues at the interface of PPI complex have functional roles in the regulation of the FGF14:Nav1.6 complex. We have identified a number of critical amino acid residues at the interface of the FGF14:Nav1.6 complex. Among all these amino acids, we discover that either a single alanine mutation at V160 or a double alanine mutation at K74/I76 is sufficient to abolish functional modulations of Nav1.6 currents by FGF14 (**Chapter 3**).

After we identified a number of hot-spots, we were interested in designing short peptides that could modulate the FGF14:Nav1.6 complex. To do this, we have focused on the structural properties of the FGF14 (**Chapter 3**). Based on the information of FGF14 hot-spots, we have designed three short peptides. These peptides aligned with two consecutive areas on the β 12 strand (FLPKPLEV) and the adjacent β 9 loop (EYYV). As mentioned earlier that FGF14 can also exist as homodimers, and it is expected from our molecular model that these peptides would act as modulators of the FGF14:FGF14 dimer. Indeed, our LCA data showed that one peptide, FLPK, significantly reduces the FGF14 homodimer formation. Furthermore, our homology model predicts that the FLPK targets V160 and adjacent Y158 of FGF14 which was subsequently validated by in cell assay (**Chapter 4**).

We also showed in chapter 3 that there are some similarities between the FGF14:Nav1.6 and the FGF14 dimer complexes. Because of this structural overlap, the FGF14 monomer could serve as an accurate template for designing peptides that would target the FGF14:Nav1.6 channel complex. We then implemented a chemical biology approach to generate peptidomimetic of FLPK peptide for better stability, permeability, and potency. In collaboration with Dr. Zhou's group, we have synthesized peptidomimetics of FLPK peptide. The peptidomimetics were tested against the FGF14:Nav1.6 complex, and we have identified ZL181 as a potential lead. We then showed the specificity of ZL181 to Nav1.6 channel compared to other Nav channels (Nav1.1 and Nav1.2). Furthermore, this compound reduced the number of action

potentials and maximum firing frequency in the nucleus accumbens medium spiny neurons in brain tissue slices, an indication that ZL181 can suppress neuronal excitability (**Chapter 5**).

Overall, our drug discovery campaign incorporates molecular modeling, LCA assay, *in silico* docking, intrinsic fluorescence spectroscopy, surface-plasmon studies, and patch-clamp electrophysiology both *in vitro* and *in vivo* to investigate the FGF14:Nav1.6 PPI as a new molecular target for drug development. From this study, we have discovered that ZL181 targets the FGF14:Nav1.6 complex and modulates the steady-state inactivation property of the Nav1.6 channels in presence of FGF14. These studies might usher in a new direction for developing novel therapies to treat brain disorders associated with malfunction of Nav1.6 channels. These results will also provide fundamental new knowledge for further modification of novel therapeutics targeting the FGF14:Nav1.6 complex. Extending these studies from basic biomedical research to translational research should create an opportunity to develop novel drugs to treat a number of brain disorders such as depression, epilepsy, spinocerebellar ataxia and schizophrenia.

FUTURE DIRECTION

To discover small molecules targeting the FGF14:Nav1.6 complex, we have focused on ZL181 which is an analog of the FLPK peptide. Our molecular model also predicts that PLEV (correspond to β -12 sheet) and EYYV (correspond to β 9 sheet) fragments of FGF14 might also play a critical role in modulating the FGF14:Nav1.6 complex. Our preliminary data collected from LCA and patch-clamp showed that PLEV and EYYV might regulate the FGF14:Nav1.6 complex. Additional experiments are required to confirm this result. In future, we like to do the following experiments:

- 1) Synthesize analogs of PLEV and EYYV in collaboration with Dr. Jia Zhou.
- 2) Test analogs of PLEV and EYYV against the FGF14:Nav1.6 complex by LCA
- 3) Performed patch-clamp studies with the selected compound in recombinant systems (Nav1.1, Nav1.2, and Nav1.6 with or without FGF14)
- 4) Perform patch-clamp studies in brain tissue slices with the selected compound.

REFERENCES

- Ali, S., Shavkunov, A., Panova, N., Stoilova-McPhie, S., Laezza, F., 2014. Modulation of the FGF14:FGF14 homodimer interaction through short peptide fragments. *CNS Neurol Disord Drug Targets* 13, 1559-1570.
- Ali, S. R., Singh, A. K., Laezza, F., 2016a. Identification of Amino Acid Residues in the Fibroblast Growth Factor 14 (FGF14) Required For Structure-Function interactions with the Voltage-Gated Sodium Channel Nav1.6. *Journal of Biological Chemistry*.
- Anger, T., Madge, D. J., Mulla, M., Riddall, D., 2001. Medicinal chemistry of neuronal voltage-gated sodium channel blockers. *J Med Chem* 44, 115-137.
- Arkin, M. R., Wells, J. A., 2004. Small-molecule inhibitors of protein-protein interactions: progressing towards the dream. *Nat Rev Drug Discov* 3, 301-317.
- Bagal, S. K., Brown, A. D., Cox, P. J., Omoto, K., Owen, R. M., Pryde, D. C., Sidders, B., Skerratt, S. E., Stevens, E. B., Storer, R. I., Swain, N. A., 2013. Ion channels as therapeutic targets: a drug discovery perspective. *J Med Chem* 56, 593-624.
- Bagal, S. K., Marron, B. E., Owen, R. M., Storer, R. I., Swain, N. A., 2015. Voltage gated sodium channels as drug discovery targets. *Channels (Austin)* 9, 360-366.
- Bath, K. G., Scharfman, H. E., 2013. Impact of early life exposure to antiepileptic drugs on neurobehavioral outcomes based on laboratory animal and clinical research. *Epilepsy Behav* 26, 427-439.
- Birch, P. J., Dekker, L. V., James, I. F., Southan, A., Cronk, D., 2004. Strategies to identify ion channel modulators: current and novel approaches to target neuropathic pain. *Drug Discov Today* 9, 410-418.
- Blumenfeld, H., Lampert, A., Klein, J. P., Mission, J., Chen, M. C., Rivera, M., Dib-Hajj, S., Brennan, A. R., Hains, B. C., Waxman, S. G., 2009. Role of hippocampal sodium channel Nav1.6 in kindling epileptogenesis. *Epilepsia* 50, 44-55.
- Bosmans, F., Martin-Eauclaire, M. F., Swartz, K. J., 2008. Deconstructing voltage sensor function and pharmacology in sodium channels. *Nature* 456, 202-208.
- Castle, N., Printzenhoff, D., Zellmer, S., Antonio, B., Wickenden, A., Silvia, C., 2009. Sodium channel inhibitor drug discovery using automated high throughput electrophysiology platforms. *Comb Chem High Throughput Screen* 12, 107-122.
- Catterall, W. A., 2000. From ionic currents to molecular mechanisms: the structure and function of voltage-gated sodium channels. *Neuron* 26, 13-25.
- Catterall, W. A., 2012. Voltage-gated sodium channels at 60: structure, function and pathophysiology. *J Physiol* 590, 2577-2589.
- Catterall, W. A., 2014. Structure and function of voltage-gated sodium channels at atomic resolution. *Exp Physiol* 99, 35-51.
- Catterall, W. A., Dib-Hajj, S., Meisler, M. H., Pietrobon, D., 2008. Inherited neuronal ion channelopathies: new windows on complex neurological diseases. *J Neurosci* 28, 11768-11777.

Catterall, W. A., Goldin, A. L., Waxman, S. G., 2005a. International Union of Pharmacology. XLVII. Nomenclature and structure-function relationships of voltage-gated sodium channels. *Pharmacol Rev* 57, 397-409.

Catterall, W. A., Kalume, F., Oakley, J. C., 2010. Nav1.1 channels and epilepsy. *J Physiol* 588, 1849-1859.

Catterall, W. A., Perez-Reyes, E., Snutch, T. P., Striessnig, J., 2005b. International Union of Pharmacology. XLVIII. Nomenclature and structure-function relationships of voltage-gated calcium channels. *Pharmacol Rev* 57, 411-425.

Chahine, M., Chatelier, A., Babich, O., Krupp, J. J., 2008. Voltage-gated sodium channels in neurological disorders. *CNS Neurol Disord Drug Targets* 7, 144-158.

Chahine, M., Ziane, R., Vijayaragavan, K., Okamura, Y., 2005. Regulation of Nav channels in sensory neurons. *Trends Pharmacol Sci* 26, 496-502.

Chanda, B., Bezanilla, F., 2002. Tracking voltage-dependent conformational changes in skeletal muscle sodium channel during activation. *J Gen Physiol* 120, 629-645.

Chen, V. B., Arendall, W. B., 3rd, Headd, J. J., Keedy, D. A., Immormino, R. M., Kapral, G. J., Murray, L. W., Richardson, J. S., Richardson, D. C., 2010. MolProbity: all-atom structure validation for macromolecular crystallography. *Acta Crystallogr D Biol Crystallogr* 66, 12-21.

Chen, Y., Barkley, M. D., 1998. Toward understanding tryptophan fluorescence in proteins. *Biochemistry* 37, 9976-9982.

Chen, Z., Li, X., Tang, B., Wang, J., Shi, Y., Sun, Z., Zhang, L., Pan, Q., Xia, K., Jiang, H., 2012. Spinocerebellar ataxia type 27 (SCA27) is an uncommon cause of dominant ataxia among Chinese Han population. *Neurosci Lett* 520, 16-19.

Claes, L., Del-Favero, J., Ceulemans, B., Lagae, L., Van Broeckhoven, C., De Jonghe, P., 2001. De novo mutations in the sodium-channel gene SCN1A cause severe myoclonic epilepsy of infancy. *Am J Hum Genet* 68, 1327-1332.

Clare, J. J., Tate, S. N., Nobbs, M., Romanos, M. A., 2000. Voltage-gated sodium channels as therapeutic targets. *Drug Discov Today* 5, 506-520.

Coebergh, J. A., van de Putte, D. E., Snoeck, I. N., Ruivenkamp, C., van Haeringen, A., Smit, L. M., 2013. A new variable phenotype in spinocerebellar ataxia 27 (SCA 27) caused by a deletion in the FGF14 gene. *Eur J Paediatr Neurol*.

Cohen, M., Potapov, V., Schreiber, G., 2009. Four distances between pairs of amino acids provide a precise description of their interaction. *PLoS Comput Biol* 5, e1000470.

Crestey, F., Frederiksen, K., Jensen, H. S., Dekermendjian, K., Larsen, P. H., Bastlund, J. F., Lu, D., Liu, H., Yang, C. R., Grunnet, M., Svenstrup, N., 2015. Identification and electrophysiological evaluation of 2-methylbenzamide derivatives as Nav1.1 modulators. *ACS Chem Neurosci* 6, 1302-1308.

Cusdin, F. S., Clare, J. J., Jackson, A. P., 2008. Trafficking and cellular distribution of voltage-gated sodium channels. *Traffic* 9, 17-26.

- Denac, H., Mevissen, M., Scholtysik, G., 2000. Structure, function and pharmacology of voltage-gated sodium channels. *Naunyn Schmiedeberg's Arch Pharmacol* 362, 453-479.
- Dib-Hajj, S. D., Binshtok, A. M., Cummins, T. R., Jarvis, M. F., Samad, T., Zimmermann, K., 2009a. Voltage-gated sodium channels in pain states: role in pathophysiology and targets for treatment. *Brain Res Rev* 60, 65-83.
- Dib-Hajj, S. D., Black, J. A., Waxman, S. G., 2009b. Voltage-gated sodium channels: therapeutic targets for pain. *Pain Med* 10, 1260-1269.
- Drendall, C. I., Pham, Q. H., Dietze, E. C., 2010. Purification and characterization of recombinant CH3 domain fragment of the CREB-binding protein. *Protein Expr Purif* 70, 196-205.
- Eijkelkamp, N., Linley, J. E., Baker, M. D., Minett, M. S., Cregg, R., Werdehausen, R., Rugiero, F., Wood, J. N., 2012. Neurological perspectives on voltage-gated sodium channels. *Brain* 135, 2585-2612.
- Emmett, M. R., Kroes, R. A., Moskal, J. R., Conrad, C. A., Priebe, W., Laezza, F., Meyer-Baese, A., Nilsson, C. L., 2014. Integrative biological analysis for neuropsychopharmacology. *Neuropsychopharmacology* 39, 5-23.
- England, S., de Groot, M. J., 2009. Subtype-selective targeting of voltage-gated sodium channels. *Br J Pharmacol* 158, 1413-1425.
- Farber, N. B., Jiang, X. P., Heinkel, C., Nemmers, B., 2002. Antiepileptic drugs and agents that inhibit voltage-gated sodium channels prevent NMDA antagonist neurotoxicity. *Mol Psychiatry* 7, 726-733.
- Felts, P. A., Yokoyama, S., Dib-Hajj, S., Black, J. A., Waxman, S. G., 1997. Sodium channel alpha-subunit mRNAs I, II, III, NaG, Na6 and hNE (PN1): different expression patterns in developing rat nervous system. *Brain Res Mol Brain Res* 45, 71-82.
- Fozzard, H. A., Sheets, M. F., Hanck, D. A., 2011. The sodium channel as a target for local anesthetic drugs. *Front Pharmacol* 2, 68.
- Goetz, R., Dover, K., Laezza, F., Shtraizent, N., Huang, X., Tchetchik, D., Eliseenkova, A. V., Xu, C. F., Neubert, T. A., Ornitz, D. M., Goldfarb, M., Mohammadi, M., 2009. Crystal structure of a fibroblast growth factor homologous factor (FHF) defines a conserved surface on FHF for binding and modulation of voltage-gated sodium channels. *J Biol Chem* 284, 17883-17896.
- Goldfarb, M., 2005. Fibroblast growth factor homologous factors: evolution, structure, and function. *Cytokine Growth Factor Rev* 16, 215-220.
- Goldin, A. L., Barchi, R. L., Caldwell, J. H., Hofmann, F., Howe, J. R., Hunter, J. C., Kallen, R. G., Mandel, G., Meisler, M. H., Netter, Y. B., Noda, M., Tamkun, M. M., Waxman, S. G., Wood, J. N., Catterall, W. A., 2000. Nomenclature of voltage-gated sodium channels. *Neuron* 28, 365-368.
- Gregoret, L. M., Sauer, R. T., 1998. Tolerance of a protein helix to multiple alanine and valine substitutions. *Fold Des* 3, 119-126.
- Guex, N., Peitsch, M. C., Schwede, T., 2009. Automated comparative protein structure modeling with SWISS-MODEL and Swiss-PdbViewer: a historical perspective. *Electrophoresis* 30 Suppl 1, S162-173.

Guo, W., Wisniewski, J. A., Ji, H., 2014. Hot spot-based design of small-molecule inhibitors for protein-protein interactions. *Bioorg Med Chem Lett* 24, 2546-2554.

Hodgkin, A. L., Huxley, A. F., 1952. A quantitative description of membrane current and its application to conduction and excitation in nerve. *J Physiol* 117, 500-544.

Hsu, W. C., Nenov, M. N., Shavkunov, A., Panova, N., Zhan, M., Laezza, F., 2015. Identifying a kinase network regulating FGF14:Nav1.6 complex assembly using split-luciferase complementation. *PLoS ONE* 10, e0117246.

Jiang, L., Lai, L., 2002. CH...O hydrogen bonds at protein-protein interfaces. *J Biol Chem* 277, 37732-37740.

Jukic, M., Kikelj, D., Anderluh, M., 2014. Isoform selective voltage-gated sodium channel modulators and the therapy of pain. *Curr Med Chem* 21, 164-186.

Jungerius, B. J., Hoogendoorn, M. L., Bakker, S. C., Van't Slot, R., Bardoel, A. F., Ophoff, R. A., Wijmenga, C., Kahn, R. S., Sinke, R. J., 2008. An association screen of myelin-related genes implicates the chromosome 22q11 PIK4CA gene in schizophrenia. *Mol Psychiatry* 13, 1060-1068.

Kaplan, M. R., Cho, M.-H., Ullian, E. M., Isom, L. L., Levinson, S. R., Barres, B. A., 2001. Differential Control of Clustering of the Sodium Channels Nav1.2 and Nav1.6 at Developing CNS Nodes of Ranvier. *Neuron* 30, 105-119.

Laedermann, C. J., Pertin, M., Suter, M. R., Decosterd, I., 2014. Voltage-gated sodium channel expression in mouse DRG after SNI leads to re-evaluation of projections of injured fibers. *Mol Pain* 10, 19.

Laezza, F., Gerber, B. R., Lou, J. Y., Kozel, M. A., Hartman, H., Craig, A. M., Ornitz, D. M., Nerbonne, J. M., 2007. The FGF14(F145S) mutation disrupts the interaction of FGF14 with voltage-gated Na⁺ channels and impairs neuronal excitability. *J Neurosci* 27, 12033-12044.

Laezza, F., Lampert, A., Kozel, M. A., Gerber, B. R., Rush, A. M., Nerbonne, J. M., Waxman, S. G., Dib-Hajj, S. D., Ornitz, D. M., 2009. FGF14 N-terminal splice variants differentially modulate Nav1.2 and Nav1.6-encoded sodium channels. *Mol Cell Neurosci* 42, 90-101.

Lai, H. C., Jan, L. Y., 2006. The distribution and targeting of neuronal voltage-gated ion channels. *Nat Rev Neurosci* 7, 548-562.

Lampert, A., O'Reilly, A. O., Reeh, P., Leffler, A., 2010. Sodium channelopathies and pain. *Pflugers Arch* 460, 249-263.

Lang, P. T., Brozell, S. R., Mukherjee, S., Pettersen, E. F., Meng, E. C., Thomas, V., Rizzo, R. C., Case, D. A., James, T. L., Kuntz, I. D., 2009. DOCK 6: combining techniques to model RNA-small molecule complexes. *RNA* 15, 1219-1230.

Large, C. H., Bison, S., Sartori, I., Read, K. D., Gozzi, A., Quarta, D., Antolini, M., Hollands, E., Gill, C. H., Gunthorpe, M. J., Idris, N., Neill, J. C., Alvaro, G. S., 2011. The efficacy of sodium channel blockers to prevent phencyclidine-induced cognitive dysfunction in the rat: potential for novel treatments for schizophrenia. *J Pharmacol Exp Ther* 338, 100-113.

- Leterrier, C., Brachet, A., Fache, M. P., Dargent, B., 2010. Voltage-gated sodium channel organization in neurons: protein interactions and trafficking pathways. *Neurosci Lett* 486, 92-100.
- Liu, C., Dib-Hajj, S. D., Waxman, S. G., 2001. Fibroblast growth factor homologous factor 1B binds to the C terminus of the tetrodotoxin-resistant sodium channel rNav1.9a (NaN). *J Biol Chem* 276, 18925-18933.
- Liu, C. J., Dib-Hajj, S. D., Renganathan, M., Cummins, T. R., Waxman, S. G., 2003a. Modulation of the cardiac sodium channel Nav1.5 by fibroblast growth factor homologous factor 1B. *J Biol Chem* 278, 1029-1036.
- Liu, G., Yarov-Yarovoy, V., Nobbs, M., Clare, J. J., Scheuer, T., Catterall, W. A., 2003b. Differential interactions of lamotrigine and related drugs with transmembrane segment IVS6 of voltage-gated sodium channels. *Neuropharmacology* 44, 413-422.
- Lou, J. Y., Laezza, F., Gerber, B. R., Xiao, M., Yamada, K. A., Hartmann, H., Craig, A. M., Nerbonne, J. M., Ornitz, D. M., 2005a. Fibroblast growth factor 14 is an intracellular modulator of voltage-gated sodium channels. *J Physiol* 569, 179-193.
- Lou, J. Y., Laezza, F., Gerber, B. R., Xiao, M., Yamada, K. A., Hartmann, H., Craig, A. M., Nerbonne, J. M., Ornitz, D. M., 2005b. Fibroblast Growth Factor 14 is an Intracellular Modulator of Voltage-Gated Sodium Channels. *J Physiol* 569, 179-193.
- Luker, K. E., Piwnicka-Worms, D., 2004. Optimizing luciferase protein fragment complementation for bioluminescent imaging of protein-protein interactions in live cells and animals. *Methods Enzymol* 385, 349-360.
- Luque, I., Freire, E., 2000. Structural stability of binding sites: consequences for binding affinity and allosteric effects. *Proteins Suppl* 4, 63-71.
- Ma, B., Shatsky, M., Wolfson, H. J., Nussinov, R., 2002. Multiple diverse ligands binding at a single protein site: a matter of pre-existing populations. *Protein Sci* 11, 184-197.
- Mantegazza, M., Curia, G., Biagini, G., Ragsdale, D. S., Avoli, M., 2010. Voltage-gated sodium channels as therapeutic targets in epilepsy and other neurological disorders. *Lancet Neurol* 9, 413-424.
- Mantegazza, M., Gambardella, A., Rusconi, R., Schiavon, E., Annesi, F., Cassulini, R. R., Labate, A., Carrideo, S., Chifari, R., Canevini, M. P., Canger, R., Franceschetti, S., Annesi, G., Wanke, E., Quattrone, A., 2005. Identification of an Nav1.1 sodium channel (SCN1A) loss-of-function mutation associated with familial simple febrile seizures. *Proc Natl Acad Sci U S A* 102, 18177-18182.
- Mao, Q., Jia, F., Zhang, X. H., Qiu, Y. M., Ge, J. W., Bao, W. J., Luo, Q. Z., Jiang, J. Y., 2010. The up-regulation of voltage-gated sodium channel Nav1.6 expression following fluid percussion traumatic brain injury in rats. *Neurosurgery* 66, 1134-1139; discussion 1139.
- Marban, E., Yamagishi, T., Tomaselli, G. F., 1998. Structure and function of voltage-gated sodium channels. *J Physiol* 508 (Pt 3), 647-657.
- McKinney, B. C., Chow, C. Y., Meisler, M. H., Murphy, G. G., 2008. Exaggerated emotional behavior in mice heterozygous null for the sodium channel Scn8a (Nav1.6). *Genes Brain Behav* 7, 629-638.

- Meisler, M. H., Kearney, J. A., 2005. Sodium channel mutations in epilepsy and other neurological disorders. *J Clin Invest* 115, 2010-2017.
- Meng, E. C., Pettersen, E. F., Couch, G. S., Huang, C. C., Ferrin, T. E., 2006. Tools for integrated sequence-structure analysis with UCSF Chimera. *BMC Bioinformatics* 7, 339.
- Möller, M., Denicola, A., 2002. Protein tryptophan accessibility studied by fluorescence quenching. *Biochemistry and Molecular Biology Education* 30, 175-178.
- Moustakas, D. T., Lang, P. T., Pegg, S., Pettersen, E., Kuntz, I. D., Brooijmans, N., Rizzo, R. C., 2006. Development and validation of a modular, extensible docking program: DOCK 5. *J Comput Aided Mol Des* 20, 601-619.
- Mullard, A., 2012. 2011 FDA drug approvals. *Nat Rev Drug Discov* 11, 91-94.
- Mullen, S. A., Scheffer, I. E., 2009. Translational research in epilepsy genetics: sodium channels in man to interneuronopathy in mouse. *Arch Neurol* 66, 21-26.
- Musa, H., Kline, C. F., Sturm, A. C., Murphy, N., Adelman, S., Wang, C., Yan, H., Johnson, B. L., Csepe, T. A., Kilic, A., Higgins, R. S., Janssen, P. M., Fedorov, V. V., Weiss, R., Salazar, C., Hund, T. J., Pitt, G. S., Mohler, P. J., 2015. SCN5A variant that blocks fibroblast growth factor homologous factor regulation causes human arrhythmia. *Proc Natl Acad Sci U S A*.
- Nouette-Gaulain, K., Capdevila, X., Rossignol, R., 2012. Local anesthetic 'in-situ' toxicity during peripheral nerve blocks: update on mechanisms and prevention. *Curr Opin Anaesthesiol* 25, 589-595.
- O'Brien, J. E., Meisler, M. H., 2013. Sodium channel SCN8A (Nav1.6): properties and de novo mutations in epileptic encephalopathy and intellectual disability. *Front Genet* 4, 213.
- Ochiai, K., Yoshikawa, Y., Yoshimatsu, K., Oonuma, T., Tomioka, Y., Takeda, E., Arikawa, J., Mominoki, K., Omi, T., Hashizume, K., Morimatsu, M., 2011. Valine 1532 of human BRC repeat 4 plays an important role in the interaction between BRCA2 and RAD51. *FEBS Lett* 585, 1771-1777.
- Olsen, S. K., Garbi, M., Zampieri, N., Eliseenkova, A. V., Ornitz, D. M., Goldfarb, M., Mohammadi, M., 2003. Fibroblast growth factor (FGF) homologous factors share structural but not functional homology with FGFs. *J Biol Chem* 278, 34226-34236.
- Papale, L. A., Paul, K. N., Sawyer, N. T., Manns, J. R., Tufik, S., Escayg, A., 2010. Dysfunction of the Scn8a voltage-gated sodium channel alters sleep architecture, reduces diurnal corticosterone levels, and enhances spatial memory. *J Biol Chem* 285, 16553-16561.
- Payandeh, J., Scheuer, T., Zheng, N., Catterall, W. A., 2011. The crystal structure of a voltage-gated sodium channel. *Nature* 475, 353-358.
- Pettersen, E. F., Goddard, T. D., Huang, C. C., Couch, G. S., Greenblatt, D. M., Meng, E. C., Ferrin, T. E., 2004. UCSF Chimera--a visualization system for exploratory research and analysis. *J Comput Chem* 25, 1605-1612.
- Pitteri, S., Hanash, S., 2010. A systems approach to the proteomic identification of novel cancer biomarkers. *Dis Markers* 28, 233-239.

Post, R. M., Frye, M. A., Denicoff, K. D., Leverich, G. S., Kimbrell, T. A., Dunn, R. T., 1998. Beyond lithium in the treatment of bipolar illness. *Neuropsychopharmacology* 19, 206-219.

Prakriya, M., Mennerick, S., 2000. Selective depression of low-release probability excitatory synapses by sodium channel blockers. *Neuron* 26, 671-682.

Probst, V., Kyndt, F., Potet, F., Trochu, J. N., Mialet, G., Demolombe, S., Schott, J. J., Baro, I., Escande, D., Le Marec, H., 2003. Haploinsufficiency in combination with aging causes SCN5A-linked hereditary Lenegre disease. *J Am Coll Cardiol* 41, 643-652.

Ragsdale, D. S., McPhee, J. C., Scheuer, T., Catterall, W. A., 1996. Common molecular determinants of local anesthetic, antiarrhythmic, and anticonvulsant block of voltage-gated Na⁺ channels. *Proc Natl Acad Sci U S A* 93, 9270-9275.

Ramachandran, S., Kota, P., Ding, F., Dokholyan, N. V., 2011. Automated minimization of steric clashes in protein structures. *Proteins* 79, 261-270.

Rivara, M., Baheti, A. R., Fantini, M., Cocconcelli, G., Ghiron, C., Kalmar, C. L., Singh, N., Merrick, E. C., Patel, M. K., Zuliani, V., 2008. 2,4(5)-Diarylimidazoles: synthesis and biological evaluation of a new class of sodium channel blockers against hNa(v)1.2. *Bioorg Med Chem Lett* 18, 5460-5462.

Rivara, M., Patel, M. K., Amori, L., Zuliani, V., 2012. Inhibition of NaV1.6 sodium channel currents by a novel series of 1,4-disubstituted-triazole derivatives obtained via copper-catalyzed click chemistry. *Bioorg Med Chem Lett* 22, 6401-6404.

Roberts, E., 2006. GABAergic malfunction in the limbic system resulting from an aboriginal genetic defect in voltage-gated Na⁺-channel SCN5A is proposed to give rise to susceptibility to schizophrenia. *Adv Pharmacol* 54, 119-145.

Rodriguez-Murillo, L., Xu, B., Roos, J. L., Abecasis, G. R., Gogos, J. A., Karayiorgou, M., 2014. Fine mapping on chromosome 13q32-34 and brain expression analysis implicates MYO16 in schizophrenia. *Neuropsychopharmacology* 39, 934-943.

Rush, A. M., Wittmack, E. K., Tyrrell, L., Black, J. A., Dib-Hajj, S. D., Waxman, S. G., 2006. Differential modulation of sodium channel Na(v)1.6 by two members of the fibroblast growth factor homologous factor 2 subfamily. *Eur J Neurosci* 23, 2551-2562.

Savio-Galimberti, E., Gollob, M. H., Darbar, D., 2012. Voltage-gated sodium channels: biophysics, pharmacology, and related channelopathies. *Front Pharmacol* 3, 124.

Schaller, K. L., Caldwell, J. H., 2003. Expression and distribution of voltage-gated sodium channels in the cerebellum. *Cerebellum* 2, 2-9.

Schoorlemmer, J., Goldfarb, M., 2001. Fibroblast growth factor homologous factors are intracellular signaling proteins. *Curr Biol* 11, 793-797.

Shah, B. S., Stevens, E. B., Pinnock, R. D., Dixon, A. K., Lee, K., 2001. Developmental expression of the novel voltage-gated sodium channel auxiliary subunit beta3, in rat CNS. *J Physiol* 534, 763-776.

Shavkunov, A., Panova, N., Prasai, A., Veselenak, R., Bourne, N., Stoilova-McPhie, S., Laezza, F., 2012. Bioluminescence methodology for the detection of protein-protein interactions within the voltage-gated sodium channel macromolecular complex. *Assay Drug Dev Technol* 10, 148-160.

Shavkunov, A. S., Ali, S. R., Panova-Elektronova, N. I., Laezza, F., 2015. Split-luciferase complementation assay to detect channel-protein interactions in live cells. *Methods Mol Biol* 1278, 497-514.

Shavkunov, A. S., Wildburger, N. C., Nenov, M. N., James, T. F., Buzhdygan, T. P., Panova-Elektronova, N. I., Green, T. A., Veselenak, R. L., Bourne, N., Laezza, F., 2013a. The fibroblast growth factor 14 (FGF14)/Voltage-Gated Sodium Channel Complex is a new target of glycogen synthase kinase 3 (GSK3). *J Biol Chem*.

Shavkunov, A. S., Wildburger, N. C., Nenov, M. N., James, T. F., Buzhdygan, T. P., Panova-Elektronova, N. I., Green, T. A., Veselenak, R. L., Bourne, N., Laezza, F., 2013b. The fibroblast growth factor 14.voltage-gated sodium channel complex is a new target of glycogen synthase kinase 3 (GSK3). *J Biol Chem* 288, 19370-19385.

Sheets, M. F., Kyle, J. W., Kallen, R. G., Hanck, D. A., 1999. The Na channel voltage sensor associated with inactivation is localized to the external charged residues of domain IV, S4. *Biophys J* 77, 747-757.

Silos-Santiago, I., 2008. The role of tetrodotoxin-resistant sodium channels in pain states: are they the next target for analgesic drugs? *Curr Opin Investig Drugs* 9, 83-89.

Stoilova-McPhie, S., Ali, S., Laezza, F., 2013. Protein-Protein Interactions as New Targets for Ion Channel Drug Discovery. *Austin J Pharmacol Ther* 1.

Stoilova-McPhie, S., Ali, S., Laezza, F., 2014. Protein-protein interaction for drug discovery against ion channels. *Austin J Pharmacol Ther* 1.

Tang, Z., Chen, Z., Tang, B., Jiang, H., 2015. Primary erythromelalgia: a review. *Orphanet J Rare Dis* 10, 127.

Teiwees, J., Toto, R. D., 2007. Epithelial sodium channel inhibition in cardiovascular disease. A potential role for amiloride. *Am J Hypertens* 20, 109-117.

Tempia, F., Hoxha, E., Negro, G., Alshammari, M. A., Alshammari, T. K., Panova-Elektronova, N., Laezza, F., 2015. Parallel fiber to Purkinje cell synaptic impairment in a mouse model of spinocerebellar ataxia type 27. *Front Cell Neurosci* 9, 205.

Theile, J. W., Cummins, T. R., 2011. Recent developments regarding voltage-gated sodium channel blockers for the treatment of inherited and acquired neuropathic pain syndromes. *Front Pharmacol* 2, 54.

Tobi, D., Elber, R., 2000. Distance-dependent, pair potential for protein folding: results from linear optimization. *Proteins* 41, 40-46.

van Rooij, L. G., Hellstrom-Westas, L., de Vries, L. S., 2013. Treatment of neonatal seizures. *Semin Fetal Neonatal Med* 18, 209-215.

van Swieten, J. C., Brussee, E., de Graaf, B. M., Krieger, E., van de Graaf, R., de Koning, I., Maat-Kievit, A., Leegwater, P., Dooijes, D., Oostra, B. A., Heutink, P., 2003. A mutation in the fibroblast growth factor

14 gene is associated with autosomal dominant cerebellar ataxia [corrected]. *Am J Hum Genet* 72, 191-199.

Verbeek, E. C., Bakker, I. M., Bevoa, M. R., Bochdanovits, Z., Rizzu, P., Sondervan, D., Willemsen, G., de Geus, E. J., Smit, J. H., Penninx, B. W., Boomsma, D. I., Hoogendijk, W. J., Heutink, P., 2012. A fine-mapping study of 7 top scoring genes from a GWAS for major depressive disorder. *PLoS ONE* 7, e37384.

Wakeling, E. N., Atchison, W. D., Neal, A. P., 2012. Pyrethroids and Their Effects on Ion Channels.

Wang, C., Chung, B. C., Yan, H., Lee, S. Y., Pitt, G. S., 2012. Crystal structure of the ternary complex of a NaV C-terminal domain, a fibroblast growth factor homologous factor, and calmodulin. *Structure* 20, 1167-1176.

Wang, J., Wang, W., Kollman, P. A., Case, D. A., 2006. Automatic atom type and bond type perception in molecular mechanical calculations. *J Mol Graph Model* 25, 247-260.

Wang, J., Wolf, R. M., Caldwell, J. W., Kollman, P. A., Case, D. A., 2004. Development and testing of a general amber force field. *J Comput Chem* 25, 1157-1174.

Wang, Q., Bardgett, M. E., Wong, M., Wozniak, D. F., Lou, J., McNeil, B. D., Chen, C., Nardi, A., Reid, D. C., Yamada, K., Ornitz, D. M., 2002. Ataxia and paroxysmal dyskinesia in mice lacking axonally transported FGF14. *Neuron* 35, 25-38.

Wang, Q., Shen, J., Splawski, I., Atkinson, D., Li, Z., Robinson, J. L., Moss, A. J., Towbin, J. A., Keating, M. T., 1995. SCN5A mutations associated with an inherited cardiac arrhythmia, long QT syndrome. *Cell* 80, 805-811.

Waxman, S. G., Cummins, T. R., Black, J. A., Dib-Hajj, S., 2002. Diverse functions and dynamic expression of neuronal sodium channels. *Novartis Found Symp* 241, 34-51; discussion 51-60.

Wildburger, N. C., Ali, S. R., Hsu, W. C., Shavkunov, A. S., Nenov, M. N., Lichti, C. F., LeDuc, R. D., Mostovenko, E., Panova-Elektronova, N. I., Emmett, M. R., Nilsson, C. L., Laezza, F., 2015. Quantitative proteomics reveals protein-protein interactions with fibroblast growth factor 12 as a component of the voltage-gated sodium channel 1.2 (nav1.2) macromolecular complex in Mammalian brain. *Mol Cell Proteomics* 14, 1288-1300.

Wittmack, E. K., Rush, A. M., Craner, M. J., Goldfarb, M., Waxman, S. G., Dib-Hajj, S. D., 2004. Fibroblast growth factor homologous factor 2B: association with Nav1.6 and selective colocalization at nodes of Ranvier of dorsal root axons. *J Neurosci* 24, 6765-6775.

Woodruff-Pak, D. S., Green, J. T., Levin, S. I., Meisler, M. H., 2006. Inactivation of sodium channel Scn8A (Na-sub(v)1.6) in Purkinje neurons impairs learning in Morris water maze and delay but not trace eyeblink classical conditioning. *Behav Neurosci* 120, 229-240.

Woods, C. G., Babiker, M. O., Horrocks, I., Tolmie, J., Kurth, I., 2015. The phenotype of congenital insensitivity to pain due to the NaV1.9 variant p.L811P. *Eur J Hum Genet* 23, 1434.

Wright, G. E., 2015. Genomic study of congenital insensitivity to pain provides new avenues for the development of analgesics. *Clin Genet* 88, 342-343.

- Xiao, M., Bosch, M. K., Nerbonne, J. M., Ornitz, D. M., 2013. FGF14 localization and organization of the axon initial segment. *Mol Cell Neurosci* 56, 393-403.
- Xiao, M., Xu, L., Laezza, F., Yamada, K., Feng, S., Ornitz, D. M., 2007. Impaired hippocampal synaptic transmission and plasticity in mice lacking fibroblast growth factor 14. *Mol Cell Neurosci* 34, 366-377.
- Xie, W., Strong, J. A., Zhang, J. M., 2015. Local knockdown of the NaV1.6 sodium channel reduces pain behaviors, sensory neuron excitability, and sympathetic sprouting in rat models of neuropathic pain. *Neuroscience* 291, 317-330.
- Yang, Y. C., Huang, C. S., Kuo, C. C., 2010. Lidocaine, carbamazepine, and imipramine have partially overlapping binding sites and additive inhibitory effect on neuronal Na⁺ channels. *Anesthesiology* 113, 160-174.
- Yu, F. H., Catterall, W. A., 2003. Overview of the voltage-gated sodium channel family. *Genome Biol* 4, 207.
- Yu, F. H., Yarov-Yarovoy, V., Gutman, G. A., Catterall, W. A., 2005. Overview of molecular relationships in the voltage-gated ion channel superfamily. *Pharmacol Rev* 57, 387-395.
- Yu, H. B., Li, M., Wang, W. P., Wang, X. L., 2016. High throughput screening technologies for ion channels. *Acta Pharmacol Sin* 37, 34-43.

Vita

Syed Rydwan Ali was born on October 25, 1984 in Dhaka, Bangladesh. He is the son of Syed Mansur Ali and Hasina Begum. He has two brothers and one sister named Syed Ashek Ahmed, Syed Tanjib Ali, and Syeda Tashrifa. Syed Rydwan Ali earned his high school diploma from Notre Dame College, Dhaka, Bangladesh in 2004, and he then enrolled in pharmacy program at Dhaka University, Bangladesh in 2005. In 2006, Syed along with family moved to Queens, New York. He then enrolled in the department of Chemistry at Queens College. He then earned his B.A. in Chemistry from Queens College with honors in chemistry. Subsequently, he took graduate level courses at Long Island University at Brooklyn, NY where he found pharmacology is an interest area to advance his career. He soon switched to the Ph.D. program in the department of Pharmacology and Toxicology in August, 2011. After a couple of lab rotations, he joined to Dr. Fernanda Laezza's laboratory in June, 2012. During graduate training at UTMB, Syed received several prestigious scholarships for excellence in both academics and research. He was awarded the George Palmer Saunders II Memorial Student Scholarship in 2015, and the GSBS Associates Scholarship in 2015. He also obtained a competitive pharmacological fellowship from the Gulf Coast Consortia in 2009 for his outstanding research in the field of pharmacology. Further, he was awarded prestigious "The Biophysical Society Travel Award" in 2015 from BPS for attending the 60th BPS conference, and he also received the UT Austin Trainee Travel Scholarship in 2015 for attending Learning and Memory Conference. Beside academic activities, he served as a Pharmacology & Toxicology program representative at the Graduate Student organization at UTMB since 2013. He also participated as a judge at multiple local schools science fair since 2014.

Education

INSTITUTION AND LOCATION	DEGREE	YEAR(s)	FIELD OF STUDY
University of Dhaka, Dhaka	n/a	2005-2006	Pharmacy
The City U. of New York, Queens College, NY	B.A.	2007-2010	Chemistry
Long Island University, NY	n/a	2010-2011	Pharmaceutical Science
University of Texas Medical Branch, Galveston, TX	Ph.D.	2011-2016	Pharmacology & Toxicology

Permanent address: 4370 Kissena Blvd, Apt 2H, Flushing, NY-11355

This dissertation was typed by Syed Ali.

Publications

Research Articles:

1. **Ali S.**, Singh A., Laezza F. (2016) Identification of Amino Acid Residues in the Fibroblast Growth Factor 14 (FGF14) Required for Structure-Function interactions with the Voltage-Gated Sodium Channel Nav1.6. *The journal of biological chemistry*, *jbc.M115.703868*.
2. Wildburger, N. C., **Ali, S. R.**, Hsu, W. C., Shavkunov, A. S., Nenov, M. N., et al. (2015) Quantitative proteomics reveals protein-protein interactions with fibroblast growth factor 12 as a component of the voltage-gated sodium channel 1.2 (nav1.2) macromolecular complex in Mammalian brain. *Molecular & cellular proteomics* : MCP 14, 1288-1300.
3. **Ali S.**, Shavkunov A., Panova-Elektronova N., Stoilova-McPhie S., Laezza F. (2014) Modulation of the FGF14:FGF14 homodimer interaction through short peptide fragments. *CNS Neurol Disord Drug Targets* 13(9): 1559-1570.
4. Shavkunov A., **Ali S.**, Panova-Elektronova N., Laezza F. (2015) Split-luciferase complementation assay to detect channel-protein interactions in live cells. *Methods in molecular biology* 1278:497-514. doi:10.1007/978-1-4939-2425-7_33.
5. Stoilova-McPhie, S., **Ali S.**, Laezza F. (2013) "Protein-Protein Interactions as New Targets for Ion Channel Drug Discovery." *Austin J Pharmacol Ther* 1(2).
6. **Ali S.**, Liu Z., Nenov M., Scala F., James T, Singh A., Panova-Elektronova N., Chen H., Zhou J., and Laezza F. Modulation of the FGF14: Nav channels interaction through short peptide fragments (*in preparation*).
7. Hsu W., Wold E., **Ali S.**, Panova N., Haidacher J., Denner L. and Laezza F. PPAR-gamma agonists rescue increased phosphorylation of FGF14 at S231 in the Tg2576 mouse model of Alzheimer's disease (*in preparation*).